OPEN ACCESS

University of BRISTOL

This electronic thesis or dissertation has been downloaded from Explore Bristol Research, http://research-information.bristol.ac.uk

Author:
Byrne, Louis

Title:
The Southern Ocean seasonal cycle of N 2 O, an atmospheric modelling study.

General rights
Access to the thesis is subject to the Creative Commons Attribution - NonCommercial-No Derivatives 4.0 International Public License. A copy of this may be found at https://creativecommons.org/licenses/by-nc-nd/4.0/legalcode This license sets out your rights and the restrictions that apply to your access to the thesis so it is important you read this before proceeding.

Take down policy
Some pages of this thesis may have been removed for copyright restrictions prior to having it been deposited in Explore Bristol Research. However, if you have discovered material within the thesis that you consider to be unlawful e.g. breaches of copyright (either yours or that of a third party) or any other law, including but not limited to those relating to patent, trademark, confidentiality, data protection, obscenity, defamation, libel, then please contact collections-metadata@bristol.ac.uk and include the following information in your message:

• Your contact details
• Bibliographic details for the item, including a URL
• An outline nature of the complaint

Your claim will be investigated and, where appropriate, the item in question will be removed from public view as soon as possible.

The Southern Ocean seasonal cycle of N_2O, an atmospheric modelling study.

Louis Byrne

A dissertation submitted to the University of Bristol in accordance with the requirements for award of the degree of Masters of Research in the Faculty of Chemistry

Abstract

The seasonal cycle of N_2O in the Southern Ocean is produced by the thermal in and out-gassing of N_2O driven by changes in temperature and the wind driven ventilation of surface waters due to vertical mixing processes. Previous studies have used atmospheric data from an AGAGE (Advanced Global Atmospheric Gases Experiment) site in Cape Grim, Tasmania, to investigate how these processes affect the seasonal N_2O source in the Southern Ocean, however, the impact of land fluxes on the N_2O signal at Cape Grim remains unaccounted for.

This study utilises a global biogeochemical model of the marine N_2O source as well as the NAME (Numerical Atmospheric Modelling Enivronment) atmospheric particle dispersion model to evaluate the ocean model's prediction of atmospheric concentration changes due to oceanic fluxes of N_2O near Cape Grim. Data are filtered to remove periods of high land influence using the NAME model output. Scaling factors are calculated for each month of data between 2008 and 2013 *via* an orthogonal distance regression analysis. Additionally, the biogeochemical model has been run using two gas exchange parameterisations, to investigate how varying parameterisations of gas exchange affects the results of the analysis.

On average, this analysis found a good agreement between the predicted marine N_2O source and measured atmospheric mole-fractions during periods of high marine influence, although there were large inter-annual variations that remain unexplained. Neither the Wanninkhov 92 or Krakaur gas exchange parameterisations produced a significant difference in the results, although the uncertainty was slightly lower using the Krakaur parameterisation. These results support the view of Nevison et al. (2005), that Southern Ocean ventilation is largely responsible for the seasonal cycle in the marine N_2O source in the Southern Ocean, and that this process is one component of the seasonal N_2O cycle at Cape Grim, however, significant discrepancies in the inter-annual variations suggest that more work is needed to have a complete understanding the Southern Ocean N_2O source.

Acknowledgements

I'd like to thank Dr Matt Rigby and Dr Anita Ganesan for all their support in conducting my analysis and in writing my thesis. I'd also like to thank Dr Manfredi Manizza of Scripps Institute of Oceanography for providing the biogeochemical model used in this analysis, and the Met Office for supplying the atmospheric model runs used in this analysis. I'd also like to thank my colleagues at Bristol University, especially Dr Mark Lunt, for providing the MOZART model runs used to calculate the boundary conditions for this analysis.

I declare that the work in this dissertation was carried out in accordance with the requirements of the University's *Regulations and Code of Practice for Research Degree Programmes* and that it has not been submitted for any other academic award. Except where indicated by specific reference in the text, the work is the candidate's own work. Work done in collaboration with, or with the assistance of, others, is indicated as such. Any views expressed in the dissertation are those of the author.

SIGNED: .....Louis Byrne..... DATE:...10/01/2018.....

Contents

Tables and illustrations

Section 1.1

Section 1.2

Section 1.3

Section 1.4

Section 2.1

Section 3

Chapter 1 – Introduction

1.1 Nitrous oxide in the atmosphere

Scientific interest in the biological pathways and industrial processes which affect the atmospheric concentration of nitrous oxide (N_2O) has increased in recent years, due to increasing awareness of the impact N_2O has on stratospheric ozone concentrations and climate change. Owing to the success of the Montreal protocol in reducing the use of CFCs and other ozone depleting substances, N_2O is now recognised as the leading ozone-depleting substance emitted by humans and is predicted to remain so throughout the 21st century (Ravishankara et al., 2009). N_2O present in the lower atmosphere is also very effective at absorbing solar radiation and thus it plays an important role in modulating the Earth's climate. The importance of N_2O as a greenhouse gas has made it necessary for a greater understanding of the processes that affect the atmospheric concentration of N_2O.

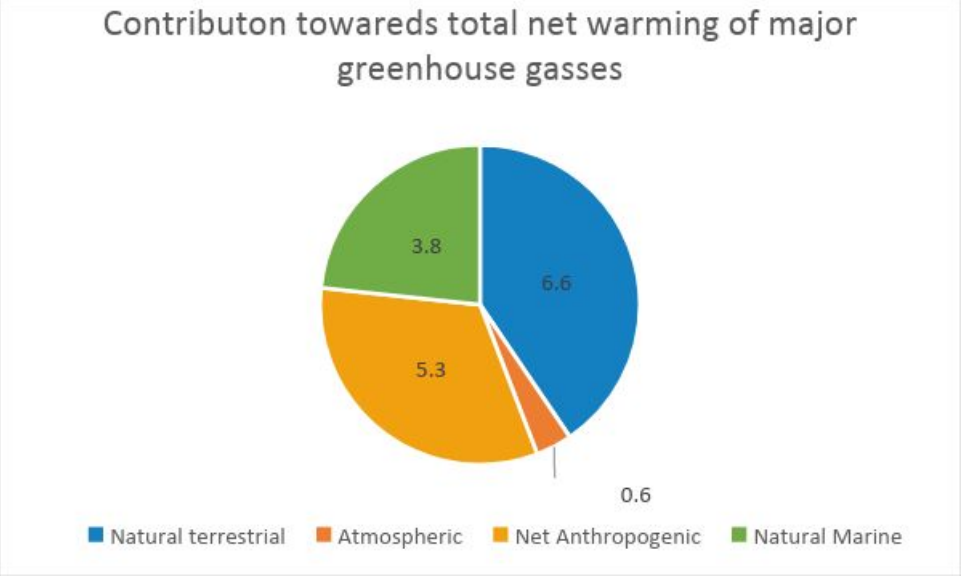

Figure 1A: The relative contribution of different greenhouse gases to climate change (IPCC, 2014)

N_2O is the third most important greenhouse gas (GHG) behind carbon dioxide (CO_2) and methane (CH_4), and anthropogenic N_2O emissions are believed to be responsible for approximately 6% of the total GHG emissions due to anthropogenic activities. Although the impact of anthropogenic emissions of N_2O are not as significant as with CO_2 or CH_4, improving our understanding of the processes that impact atmospheric concentrations of N_2O is important for several reasons. Firstly, because current global estimates of N_2O emissions are more uncertain than with any other greenhouse gas, with N_2O often being the most large source of uncertainty in regional GHG estimates (IPCC, 2013). Additionally, as N_2O has a long lifetime in the atmosphere, increases in the atmospheric concentration of N_2O today will have long-lasting impacts on global temperatures for generations.

An estimated 23% of the annual N_2O source is comprised of fluxes from the marine environment. However, as with anthropogenic emissions the exact figure is subject to significant uncertainty. As marine fluxes comprise a significant percentage of the global N_2O budget, a good understanding of this source is important, both because it will enable us to better understand how anthropogenic activities are increasing atmospheric N_2O concentrations, and also so that we are better able to predict how this important source of N_2O to the atmosphere will change into the future.

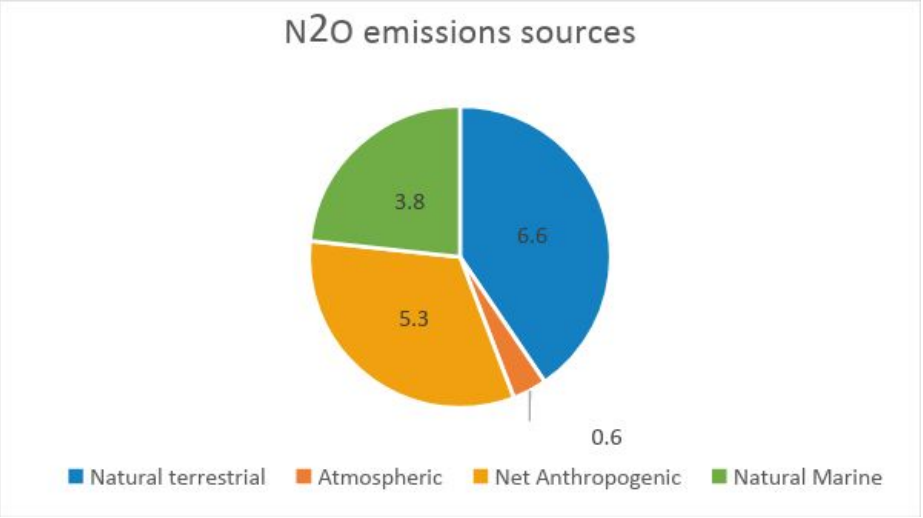

Figure 1B: Estimated sources of N_2O into the atmosphere (IPCC, 2014).

Aside from its importance in understanding the natural nitrogen cycle, an understanding of the mechanisms behind the production of N_2O in the water column, and how these processes are regulated by the environment, also has important implications for assessing the suitability of iron fertilization as a method of sequestering CO_2 from the atmosphere (Fuhrman and Capone, 1991; Jin and Grueber, 2003). Jin and Grueber's 2003 study found fertilizing the oceans with Iron in order to stimulate CO_2 uptake could also result in large N_2O emissions, which could in some areas offset the benefit of CO_2 uptake due to the global warming potential of N_2O as a greenhouse gas. The extent to which iron fertilization increases N_2O production was shown to be highly location and duration dependent, and the study concluded that it was essential to consider the mechanisms behind the marine N_2O with regards to the net benefit of iron fertilization programs.

The relative contribution of nitrous oxide to climate change and the ozone layer

The extent of the influence of N_2O on global temperatures is in-part due to its relative strength as a global warming agent. IPCC (2013) uses two emissions metrics to quantify the relative strength of different greenhouse gases as global warming agents, called the global warming potential (GWP) and global temperature potential (GTP), both of which measure the contribution of various greenhouse gases to global warming over time in relation to a reference gas, CO_2 (Smith, 2010). The difference between the two is outside the scope of this thesis, and all discussion henceforth will refer to the GWP. The global warming potentials of the three most significant greenhouse gases, CO_2, CH_4 and N_2O are provided in Table 1A.

Table 1A: Global warming potentials for three most significant greenhouse gases, CO_2, CH_4, N_2O (IPCC Chapter 8,2014).

Greenhouse gas	Lifetime in the atmosphere (years)	Radiative efficiency (W M^{-2} ppb^{-1})	Radiative forcing (W m^{-2})	GWP for each time horizon (per unit mass)	
				20 years	100 years
CO_2	N/A[1]	1.37 e^{-5}	1.82 ± 0.19	1	1
CH_4	12.4	3.64 e^{-4}	0.48 ± 0.05	84	28
N_2O	121	3.00 e^{-3}	0.17 ± 0.03	268	298

[1] For CO_2 no single lifetime can be given. In their calculations, IPCC (2014) used the impulse response function calculated by Joos et al., 2013.

One gram of N_2O is almost 300 times stronger as a global warming agent when compared against CO_2 over a 100-year life-span. There are essentially two elements which affect the GWPs of different greenhouse gases; how much solar radiation the absorb (their radiative efficiency) and how long they stay in the atmosphere (their lifetime). N_2O has a high GWP because per unit mass, N_2O has a radiative efficiency approximately 200 times greater than CO_2, and it also has a high lifetime in the atmosphere as N_2O is chemically unreactive in the troposphere. N_2O is only effectively removed from the atmosphere once it reaches the stratosphere, where it is broken down through photolysis and oxidation reactions.

The estimated perturbation lifetime of N_2O is 121 ± 10 years (Prather et al., 2012). The perturbation lifetime describes the time taken for a one-off pulse emission of N_2O to be removed from the atmosphere. The perturbation lifetime of a greenhouse gas differs from the global lifetime of a gas as it takes into account how the loss rate of that gas from the atmosphere is affected by its atmospheric concentration. Studies have shown that the lifetime of N_2O in the troposphere decreases as its concentration increases (Prather, 1998), and current best estimates suggest a decline in the lifetime of 0.5% for every 10% increase in the atmospheric concentration of N_2O.

Once in the stratosphere, N_2O is broken down both *via* direct photolysis (reaction one) and by reacting with the excited oxygen atoms produced by ozone photolysis (reactions two and three). Approximately 90% of the N_2O that reaches the stratosphere is broken down *via* direct photolysis (Garcia and Solomon, 1994), 4% is broken down *via* reaction two, and 6% is broken down *via* equation three.

$$N_2O + hv \;\; yields\rightarrow \;\; N_2 + O(^1D) \; (1)$$

$$N_2O + \;\; O(^1D) \; yields\rightarrow N_2 + O_2 \; (2)$$

$$N_2O + \;\; O(^1D) \; yields\rightarrow 2NO \qquad (3)$$

The production of NO *via* equation 3 is a cause for further environmental concern, as NO_x (NO and NO_2) is known to destroy ozone in the stratosphere *via* reactions four and five. As the Montreal protocol has resulted in the gradual decline in anthropogenic emissions of ozone-depleting substances, the importance of N_2O, emissions of which are not regulated by the Montreal protocol, in removing stratospheric ozone is of renewed importance. N_2O is the main source of NO_x into the stratosphere, and NO_x is predicted to be the leading ozone-depleting substance throughout the 21st century (Ravishankara et al., 2009; Portmann et al., 2012).

$$NO + \;\; O_3 \; yields\rightarrow NO_2 + \;\; O_2 \; (4)$$

$$O + NO_2 \; yields\rightarrow \;\; NO + \;\; O_2 \quad (5)$$

Historical changes in N_2O emissions

The natural atmospheric mixing ratio of nitrous oxide (the concentration of N_2O in dry air) prior to the industrial revolution was approximately 270 ppb, a value at which it had been more or less stable at for the previous four millennia (Smith, 2010). Ice core data from the Law Dome Ice Sheet in Antarctica (MacFarling Meure et al., 2006; Wolf and Spahni, 2007) shows that since 1850 AD there has been an increase of approximately 20% in the N_2O mixing ratio, with atmospheric N_2O

concentrations now exceeding 320 ppb. The rate of change in the N_2O mixing ratio has increased from a value of about 0.15 ppb yr^{-1} between 1900 and 1955 to its current linear rate of approximately 0.7 ppb yr^{-1}. Atmospheric N_2O concentrations are now greater than at any point over the past 650,000 years (Spahni et al., 2005).

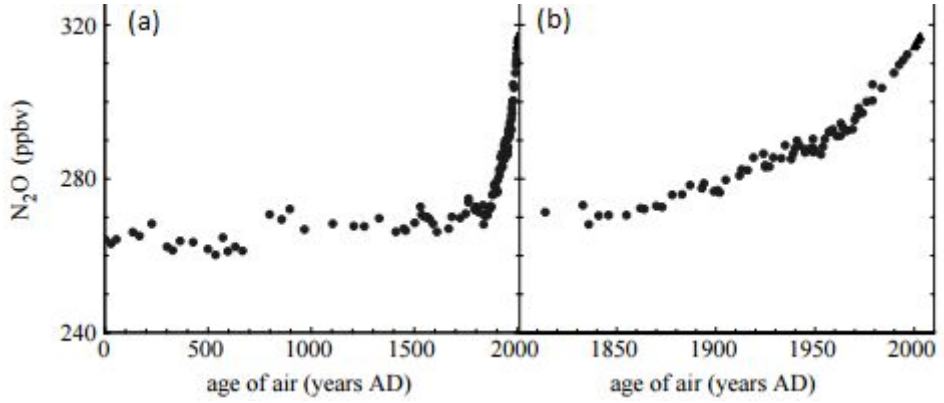

Figure 1C: Atmospheric N_2O concentrations over the last 2000 years (a) and 200 years (b) taken from Wolff and Spahni (2007), using firn air and ice core data from Law Dome, Antarctica and annual averages of flasks from Cape Grim, Tasmania.

Current N_2O budget estimates

Table 1B provides the estimated anthropogenic and natural sources and sinks for N_2O as provided in the most recent IPCC report. The total natural sources of N_2O are estimated at 11 TgN yr^{-1}, with marine emissions making up 3.8 TgN yr^{-1} of that total. Both of these estimates are subject to large uncertainties, with the uncertainty in marine emissions being approximately 200% of the best guess estimate.

Table 1B Global N_2O budget (IPCC Chapter 6, 2014).

	2005 to 2011 (TgN yr^{-1})	mid-1990s (TgN yr^{-1})
Anthropogenic sources		
Fossil fuel combustion and industry	0.7 (0.2 to 1.8)	0.7 (0.2 - 1.8)
Agriculture	4.1 (1.7 - 4.8)	3.7 (1.7 - 4.8)
Biomass and biofuel burning	0.7 (0.2 - 1.0)	0.7 (0.2 - 1.0)
Human excreta	0.2 (0.1 - 0.3)	0.2 (0.1 - 0.3)
Rivers, estuaries, coastal zones	0.6 (0.1 - 2.9)	0.6 (0.1 - 2.9)
Atmospheric deposition on land	0.4 (0.3 - 0.9)	0.6 (0.3 - 0.9)
Atmospheric deposition on ocean	0.2 (0.1 - 0.4)	0.2 (0.1 - 0.4)
Surface sink	-0.01 (0 to -1)	-0.01 (0 to -1)
Total anthropogenic sources	6.9 (2.7 - 11.1)	6.5 (2.7 - 11.1)
Natural sources		
Soils under natural vegetation	6.6 (3.3 - 9.0)	6.6 (3.3 - 9.0)
Oceans	3.8 (1.8 - 9.4)	3.8 (1.8 - 9.4)
Lightning	-	-
Atmospheric chemistry	0.6 (0.3 - 1.2)	0.6 (0.3 - 1.2)
Total natural sources	11.0 (5.4 - 19.6)	11.0 (5.4 - 19.6)
Total natural + anthropogenic sources	17.9 (8.1 - 30.7)	17.5 (8.1 - 30.7)
Stratospheric sink	14.3 (4.3 - 27.2)	-
Net source	3.61 (3.5 - 3.8)	-
Global top-down (year 2011)		
Burden (Tg N)	1553	-

Atmospheric loss	11.9 ± 0.9	-
Atmospheric increase	4.0 ± 0.5	-
Total source	15.8 ± 1.0	-
Natural source	9.1 ± 1.0	-
Anthropogenic source	6.7 ± 1.3	-

The current best estimate of the anthropogenic source is 6.9 TgN yr^{-1}, with the most significant anthropogenic source of N_2O being agriculture, which, when you include the leeching of fertiliser into aquatic environments, is responsible for almost 70% of the anthropogenic N_2O budget. This is supported by N_2O isotope studies (Röckmann and Levin, 2005; Ishijima et al., 2007) which have concluded that the majority of the increase in the N_2O mixing ratio post industrialisation has been through soil emissions. Added together the natural and anthropogenic sources make 17.9 TgN yr^{-1}, which when subtracted from an estimated stratospheric sink of 14.3 TgN yr^{-1} gives the observed annual growth rate of 3.61 TgN yr^{-1}. When looking at the uncertainties for the individual N_2O sources, total N_2O source and the stratospheric sink, it is clear that there is still much work to be done in understanding the contributions of each process to the atmospheric N_2O cycle.

Uncertainties in marine N_2O emissions

Estimates of the marine source of N_2O range from 23% to 38% of the total N_2O budget (Thompson et al., 2014). There are various reasons for the high uncertainty in the marine N_2O budget including methodological differences (e.g. extrapolating flux estimates using the existing data or by using biogeochemical models), the application of different gas exchange parameterisations, spatial and seasonal biases in datasets and because there is no consistent approach to the classification of coastal areas (Nevison et al., 1995; Bange, 2008).

The average marine N_2O source in all studies conducted between 1978 and 2006 is 6.6 ± 3.6 TgN^{-1} yr^{-1} (Bange, 2006a). Studies using biogeochemical models have predicted a total marine source of 3.8 TgN yr^{-1} (Suntharalingam and Sarmiento, 2000) and 4.5 TgN yr^{-1} (Manizza et al., 2012), compared to estimates of 4 ± 2.8 Tg N yr^{-1} (Nevison et al., 1995) and 5 ± 2 TgN yr^{-1} (Nevison et al., 2003) in studies using marine observations. Global inversion modelling studies[2] have calculated the marine source of N_2O to be 3.68 TgN yr^{-1} (Huang et al., 2008) and 5.5 TgN yr^{-1} (Thompson et al., 2014).

In her 1995 study, Nevison identified uncertainties in the air-sea gas exchange coefficients and in the seasonal bias of the available data on N_2O surface concentrations as the primary causes of uncertainty in estimates derived from marine observations. This paucity of data in the marine environment is a problem when estimating global or regional N_2O fluxes, as they show large spatial and seasonal variability. Until a more comprehensive dataset of marine N_2O concentrations becomes available, global modelling studies using atmospheric data are the most reliable methods of determining the marine N_2O source, due to the long timeseries that these methods are able utilise.

1.2 Marine N_20 emissions

Whether the oceans are a source of N_2O to the atmosphere depends on how saturated a body of surface water is with N_2O. N_2O saturation (units of percent) itself describes the ratio of the N_2O concentration in water when compared with a theoretical equilibrium concentration, which depends on the temperature, salinity, ambient air temperature and atmospheric N_2O dry air mole fraction. Water that has a saturation of 100% is in perfect equilibrium with the overlying atmosphere.

[2] These use atmospheric data and atmospheric transport models to scale emissions estimates using the available data.

Under-saturated water (saturation values less than 100%) is a net sink of N_2O to the atmosphere, while supersaturation (saturation values over 100%) indicates that a body of water is a net source of N_2O to the atmosphere.

A study conducted by Nevison et al. (1995) calculated a global mean N_2O saturation of 103.5%, thus demonstrating that, at the global scale, the oceans are supersaturated with N_2O and act as a source of N_2O to the atmosphere. The N_2O anomaly (ΔN_2O) describes the difference between the N_2O concentration of a water body and its theoretical equilibrium concentration (at 100% saturation). Despite the problems associated with estimating the global flux of N_2O to the atmosphere, global maps of the N_2O anomaly have been calculated using the available data (Nevison et al., 1995) as well as in modelling studies (Sunatharalingam and Sarmiento, 2000; Manizza et al., 2012). These generally show N_2O saturation is greatest in coastal regions, especially in locations which experience significant coastal upwelling, and lowest in large areas of the Atlantic, Pacific and Indian oceans where N_2O is close to equilibrium with the overlying atmosphere.

N_2O production in the marine environment

The biogeochemical pathways for the production of N_2O in the marine environment are believed to be dominated by nitrification and denitrification. Nitrification is an important biological process whereby ammonia is oxidised first to nitrite and then to nitrate, replenishing the amount of biologically available nitrogen compounds available to other organisms. Denitrification is almost the opposite process to nitrification, whereby certain types of bacteria reduce nitrates to nitrogen, under anaerobic conditions where NO_3^- is used as an alternative to oxygen during respiration.

During nitrification, ammonia is converted to nitrate, producing nitrous oxide as a by-product. This is a two-step process with each step carried out by different bacteria. In the first step ammonia is first converted to nitrite by ammonia-oxidising bacteria (AOB) and archaea (AOA) with hydroxylamine as an intermediate (Colliver and Stephenson, 2000). Nitrite oxidisers then oxidise the nitrite producing nitrate, releasing nitrous oxide in the process.

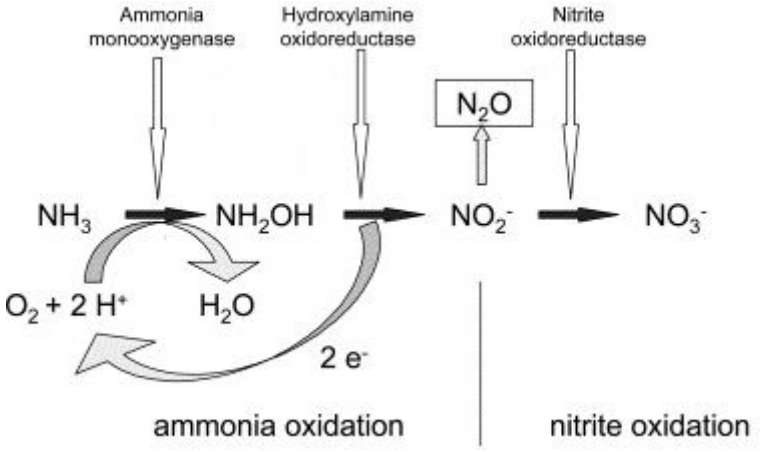

Figure 1E: Nitrification pathway and the enzymes involved (Wrage et al., 2001).

Denitrification is a process whereby ionic nitrogen oxides (NO_2^- and NO_3^-) are reduced to gaseous nitrogen oxides (NO and N_2O), which may then be reduced further to N_2. Denitrification is primarily an anaerobic process, occurring when bacteria choose to use the nitrogen oxides as an electron receptor during respiration instead of oxygen, under low oxygen conditions (Knowles, 1982). Denitrification differs from nitrification in that a single bacterium is responsible for the entire process.

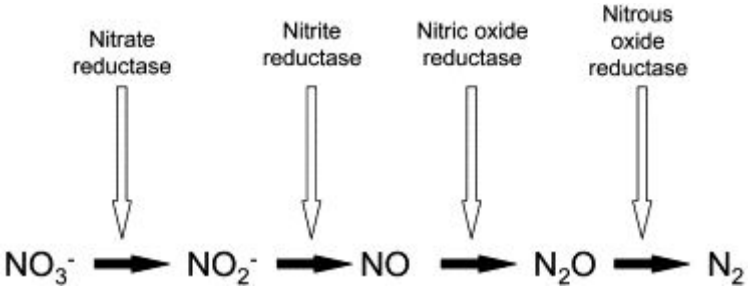

Figure 1F: Denitrification pathway and the enzymes involved (Wrage et al., 2001).

Both nitrification and denitrification are inhibited by light, and thus there is little production of N_2O in surface waters (Horrigan et al, 1981). Aside from surface waters, N_2O is believed to be produced in most other marine environments. Although there is some debate about the relative contribution of nitrification and denitrification to N_2O production in the water column, nitrification is believed to be the dominant process.

Bange and Andreae (1999) have also found relatively small levels of nitrification in the deep ocean, with the majority of nitrification believed to take place in the subsurface regions of the worlds oceans between the surface layer and the deep ocean. N_2O production is highest in coastal seas, and especially in areas with high nutrient loading such as in coastal upwelling regions (Lueker et al., 2003, Nevison et al., 2004) and estuaries (Bange et al., 2006b). Estuaries are important sources of N_2O production due to their high concentrations of biologically available nitrogen, while coastal upwelling regions are important because they are also highly productive and bring large quantities of nutrient rich water (with high N_2O saturation) from depth and into contact with the atmosphere.

Denitrification is believed to be spatially limited to a few oxygen poor areas in the eastern tropical Pacific and the Arabian Sea (Schropp and Schwarz 1983; Naqvi et al., 1998), and in the sediments of estuaries (Laws et al., 1991; Middleburg et al., 1995) and continental regions (Seitzinger, 1988), where both denitrification and nitrification occur. Whether nitrification or denitrification is the dominant process producing N_2O depends largely on the oxygen saturation of the water. In water that is significantly depleted in oxygen, denitrification is the dominant process producing N_2O, as it is fundamentally a biological mechanism for bacteria and archaea to cope with low O_2 conditions. As the oxygen concentration in a body of water increases, nitrification becomes the dominant process.

Aside from the relationship between denitrification and O_2 concentration, oxygen also affects the amount of N_2O produced *via* nitrification. Laboratory studies (Goreau et al., 1980; Joergensen et al., 1984) have shown that the amount of N_2O produced by nitrification increases with decreasing O_2 concentrations, although the exact mechanism by which this occurs is unclear (Smith, 2010).

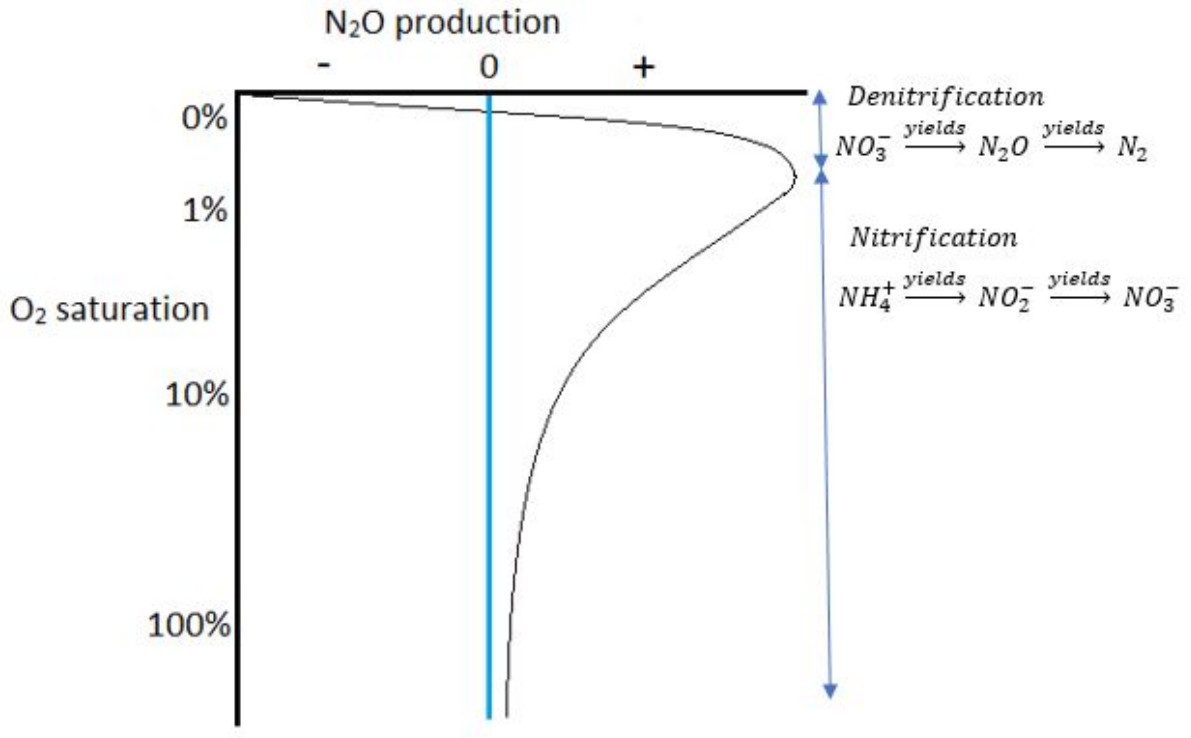

Figure 1G: The approximate regimes of nitrification and denitrification in the water column. The right arrows indicate the dominant process, there is no clear boundary between the two processes and both are often taking place simultaneously in the water column. Left of the turquoise line indicates biological processes in the water column are a net N_2O sink. Right indicates net N_2O source. Adapted from Smith (2010), which was based on Copdispoti et al. (1992).

Apparent Oxygen Utilisation

Apparent Oxygen Utilisation (AOU) is a measure of the amount of O_2 consumed by remineralization of organic matter[3] in a water body since its last contact with the surface. The majority of vertical water profiles show a clear correlation between AOU and water column production of N_2O (ΔN_2O). As nitrification is part of this process, the link between AOU and ΔN_2O is often used as evidence of the dominance of nitrification as the primary process producing N_2O in the water column, which is supported by the linear relationship between N_2O and NO_3^-, which is the final product of the nitrification process (Smith, 2010). However, some debate remains. Yamagashi et al. (2005) concluded that it was possible to have N_2O production *via* denitrification to produce an AOU/ΔN_2O relationship similar to those observed, while Nevison et al. (2003) showed that isopycnal (density driven) mixing of different water masses could also produce a similar relationship. As concentrations of O_2 in the water column are quite high, the mechanisms by which denitrification could take place are unclear, although Yoshida et al. (1989) argued that localised denitrification in low oxygen pockets around suspended particles could be responsible.

The relationship between AOU and ΔN_2O is often used in modelling studies (Sunatharalingam and Sarmiento, 2000; Manizza et al., 2012) as a method to estimate the production N_2O as a function of O_2 consumption. When the data from these studies is presented together (Sunatharalingam and

[3] The breakdown of organic matter into more simple inorganic forms by microorganisms

Sarmiento, 2000; Nevison et al., 2003), it is apparent that significant regional differences in the ΔN_2O/AOU ratio exist. Values for ΔN_2O/AOU ratio calculated by using the regression slopes of the different studies range from 0.076-0.31 nmol N_2O / mmol O_2 (figure 1H). Both Sunatharalingam and Sarmiento (2000) and Manizza et al., (2012) use a linear relationship of 0.1211 nmol N_2O / mmol O_2 in their parameterisation of ΔN_2O, which was estimated as a low average of the observed values. In both modelling studies, an extra term was added to account for N_2O production due to denitrification in low oxygen environments. The spatial differences in the ΔN_2O/AOU ratio is likely to be a major source of uncertainty in these studies. The situation is further complicated as the models both assume a linear relationship between ΔN_2O and AOU, however there is a nonlinearity to the relationship between ΔN_2O and AOU in some regions (Nevison et al., 2003). As mentioned previously N_2O yields from nitrification increase with decreasing O_2 concentrations, and this is believed to be the main cause of the nonlinearity in the ΔN_2O/AOU ratio.

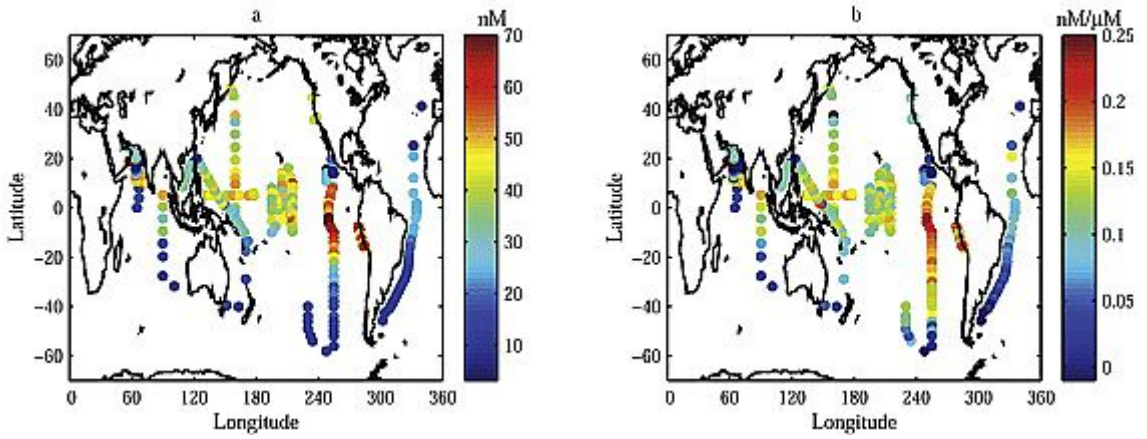

Figure 1H: a) Compilation of the data from various studies showing N_2O concentration at approx. 400-500m. b) ΔN2O/AOU ratio calculated from the same data at the same depth as (a). Figure taken from Nevison et al., 2003.

In the largest global review of the AOU-ΔN_2O relationship to date, Nevison et al, (2003) came up with a better parameterisation of the relationship between N_2O and O_2 for use in biogeochemical modelling studies. This parameterisation is provided in equation 6??, and now estimates the concentration of N_2O produced per mole of O_2 consumed (ΔN_2O/-ΔO_2), as a function of O_2 and depth. Instead of using a fixed value for the ΔN_2O/AOU ratio, it now takes into account the nonlinearity in the relationship between N_2O produced *via* nitrification and AOU.

$$\frac{\Delta N_2O}{-\Delta O_2} = R_{(N:O2)}\left(\frac{a_0}{O_2+a_1}\right) \times \exp exp\left(\frac{-Z}{Z_{scale}}\right) \quad where\ O_2 > O_{2,crit}\ and\ Z > Z_{euph} \quad (6)$$

Here, $R_{(N:O2)}$ is the Redfield ratio (see below) for N:O_2, a_0 and a_1 are the intercept and slope of the ratio of N_2O produced (in moles) per mole of NO_3^- produced (see below), Z is the water depth, Z_{scale} = 3000 m ± 1000 m, $O_{2,crit}$ is a threshold for low oxygen zones dominated by denitrification and Z_{euph} is a threshold for the euphotic zone of the water column, where no nitrification occurs. The values for the constants were estimated to be:

- $R_{(N:O2)}$ = 16:170
- a_o= 0.26 ± 0.06 (mol N_2O / mol N) x (µmol O_2/L)
- a_1= -0.0004 ± 0.0001 (mol N_2O / mol N) x (µmol O_2/L)
- $O_{2,\ crit}$ = 4 ± 3 µmol/L
- Z_{euph} was not specified in Nevison et al. (2003), but is likely to be ~100 m. It is possible this parameter is location dependent.

This parameterisation makes use of the fact that the ΔN_2O/AOU ratio can be considered as the product of two terms, the nitrifier N_2O yield ($\Delta N_2O/\Delta NO_3^-$) which describes the amount of N_2O produced per mole of NO_3^- during nitrification and the Redfield ratio ΔNO_3^-/AOU. Redfield ratios describe the ratios that different elements are found within phytoplankton throughout the world's oceans, and are generally regarded as constants, and the ΔNO_3^-/AOU Redfield ratio describes the concentration (in moles) of NO_3^- released into the water column per mole of O_2 consumed (Anderson and Sarmiento, 1994).

During nitrification, N_2O is produced as NH_3 is oxidised to form NO_2^-, which is then oxidised again to form NO_3^-. Currently there is no evidence of N_2O production during the second reaction in this process, so the $\Delta N_2O/\Delta NO_2^-$ ratio can be seen as equivalent to the $\Delta N_2O/\Delta NO_3^-$ ratio. To estimate the $\Delta N_2O/-\Delta O_2$, the concentration of N_2O produced per mole of NO_3^- produced via nitrification is first calculated following Goreau (1980), and this is then converted to $\Delta N_2O/-\Delta O_2$ using the ΔNO_3^-/AOU Redfield ratio.

While this parameterisation should improve current methods of estimating ΔN_2O as a function of AOU and depth, this study concluded that the biological production of N_2O cannot be estimated with great confidence using the available data, due to the spatial variability in the abundances of nitrifying bacteria and the availability and composition of oxidizable organic matter, isopycnal mixing of water masses and N_2O transport from regions of high production into the wider ocean. All of these processes are partially responsible for the varying ΔN_2O/AOU ratios observed in different studies.

N_2O solubility in seawater

Aside from the biological factors which affect the production of N_2O in the marine environment, changes in surface temperature and salinity affect the solubility of N_2O in seawater, and thus cause outgassing or ingassing of N_2O. Changes in solubility due to temperature are more significant, and these are taken into account by modelling studies such as Manizza et al. (2012) by adding an extra term to the model called thermal N_2O. The net annual flux due to thermal effects is 0, however it can have quite a large impact on the seasonal N_2O emissions cycle so it is important that it is taken into account by ocean models and atmospheric studies.

1.3 Physical factors affecting the distribution of N_2O fluxes in the marine environment

The scientific literature produced to date suggests that there is little N_2O produced in the surface layers of the water column, due to the processes responsible for N_2O production being light inhibited. Therefore, to understand the spatial distribution of global N_2O fluxes, it is important to understand the physical processes which drive ocean circulation, and especially those that promote the vertical mixing of deeper water, supersaturated with N_2O, into surface waters. Secondly, it is important to understand the physical mechanisms that drive air-sea gas exchange. This section will discuss the core physical marine processes responsible for ocean circulation, vertical mixing and air-sea gas exchange.

Ocean circulation

One important feature of the marine environment is that the ocean is not a homogenous body of water, but is composed of many distinct water masses, with little mixing occurring between them. These bodies of water can be clearly identified by their individual density fingerprints, with each having characteristic temperature, salinity and pressure values that can be clearly observed in horizontal transects and vertical profiles in the marine environment. The density profile of each water mass is a consequence of the formation and subsequent history of that body of water. It is the density driven transport of water masses across the world's oceans, and their interaction with wind driven surface currents, that produces the major global ocean circulation patterns, in a process known as Meridional Overturning Circulation (MOC) (Open University, 2001).

Water columns where the density increases with depth are stable, as the lighter, more-buoyant water is sitting above the heavy, less-buoyant water. If there is a situation whereby dense water overlies less-dense, more-buoyant water, then this denser water will sink in a process known as downwelling. The major downwelling regions occur at both poles, where cold salty water is formed due to polar temperatures and sea ice formation. As it sinks, the water also spreads out along the ocean floor, and is replaced with water from surface currents flowing poleward. This sinking polar water forms the deep and intermediate[4] water masses found in the Atlantic and Pacific Oceans, and once it has sunk, it may not come into contact with the atmosphere for tens or even hundreds of years. This allows for a steady build-up of N_2O in the subsurface waters, as it is produced through the processes of nitrification (mainly) and denitrification.

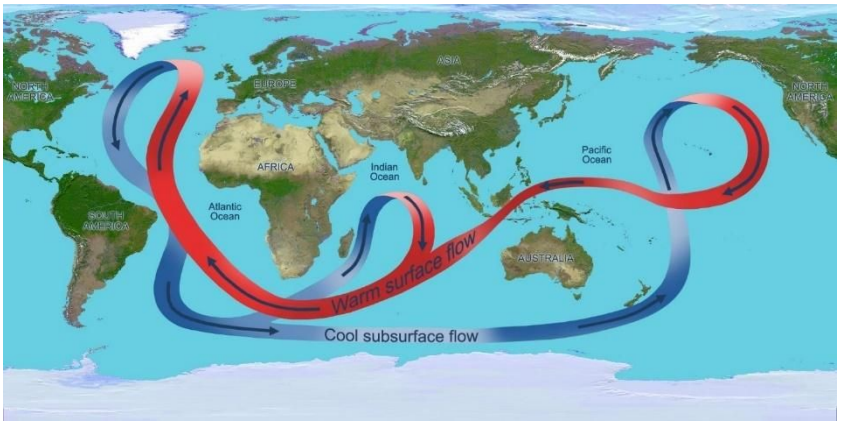

Figure 1l: Thermohaline Circulation (density driven component of Meridional Overturning Circulation). Taken from www.nasa.gov (https://www.nasa.gov/topics/earth/features/atlantic20100325.html)

[4] Water masses which lie above deep water masses, typically with a depth of 500 to 1500 m.

The deep and intermediate waters will eventually be cycled back into contact with the atmosphere, where the N_2O which has accumulated in them can outgas into the atmosphere. There are several specific locations around the world that experience significant upwelling, where deep water supersaturated with N_2O is brought up into the surface layers of the water column. Strong upwelling regions exist in the Pacific Ocean off the coasts of South America and North America, as well as in the Southern Ocean. To understand why this occurs, it is necessary to understand the vertical structure of the upper few hundred metres of the water column, and the factors that affect vertical mixing within this region.

The upper layer of the water column in many locations forms an individual body of water known as the surface mixed layer (SML). The surface mixed layer is characterised by very small vertical density gradients, as wind blowing across the surface inputs kinetic energy into the layer, mixing the water within so that the temperature and salinity of the layer are remarkably uniform. At the bottom of the surface mixed layer exists the pycnocline[5], a shallow area with sharp density gradients which marks the barrier between the surface mixed layer and the layer below. The SML depth ranges from a few metres to over 500 metres, depending on the localised environmental conditions. Although buoyancy driven mixing does have a role in the surface layer, the processes which can affect the depth of the SML and bring water from below the pycnocline into the surface layer are primarily driven by wind.

Vertical mixing

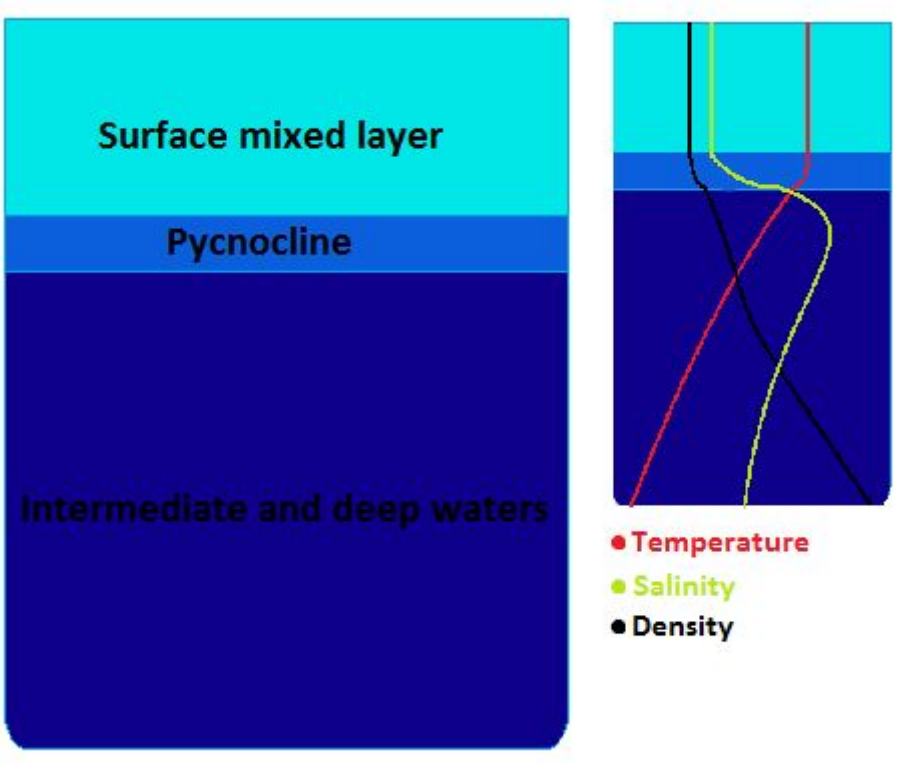

Figure 1J: Vertical structure of the water column in the open ocean alongside a typical vertical profile showing temperature, salinity and density.

[5] The term pycnocline refers to a sharp vertical density gradient, indicating the barrier between two vertically separated water masses. A halocline refers to a sharp density gradient, whereas a thermocline refers to a sharp temperature gradient. Often the term thermocline is used in preference to pycnocline as it is more often the case that vertical density gradients are primarily driven by temperature in the marine environment.

There are various physical mechanisms by which wind energy can propagate through the water column to mix deeper high-N_2O waters into the surface layers. Wind energy can be transferred into the water column both through generating wind-driven currents, which can then affect vertical mixing through mechanisms such as vertical shear instability, Langmuir circulation and Ekman transport, and through injecting turbulence into the water column *via* surface waves.

Vertical shear instability

Wind forcing is a major factor determining the depth of the SML. Variations in the depth of the SML result in mixing between the water lying above and below the pycnocline, with important consequences for a variety of marine processes including carbon sequestering, nutrient transport and outgassing of N_2O into the atmosphere. Wind can affect mixing processes in the SML through the generation of wind driven surface currents, wave induced turbulence and Langmuir circulation which is caused by the interaction between the two.

Surface currents produced by wind blowing across the surface of the ocean eventually propagate down the water column where they can erode the thermocline, by producing shear stress at the base of the thermocline. The shear stress generates Kelvin-Helmholtz instabilities[6] which gradually erode the thermocline, deepening the surface mixed layer (Mellor and Durbin, 1975).

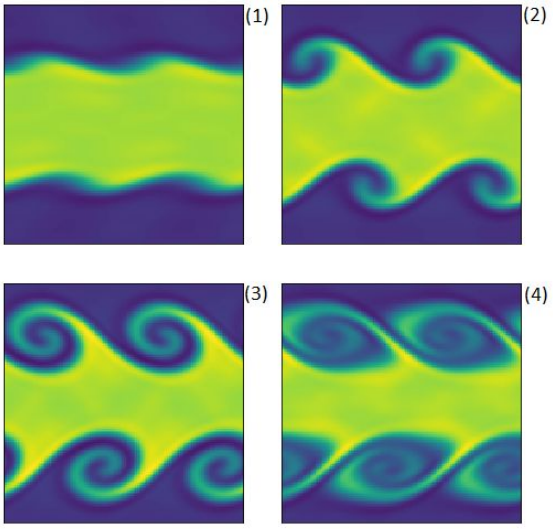

Figure 1K: Kelvin-Helmholtz instability diagram showing the generation of turbulent shear induced flows over time. Model Kelvin-Helmholtz instabilities produced using python code provided by Mocz (2016).

The structure of a vertically stratified water column in the absence of wind is stable, with cold dense water underlying warmer less dense water. Studies have shown (Miles 1961; 1963; Mack and Schoeberlein, 2004) that the vertical shear produced by wind driven currents can eventually become enough to overcome the stable buoyancy structure of stratification, once the gradient Richardson number[7] is less than the critical Richardson (R_{cr}) number[8]. As the R_{cr} is passed the fluid enters a turbulent flow regime and the stability of the water column is overcome, resulting in water from below the thermocline entraining into the SML, causing the thermocline to deepen.

[6] Turbulent flows generated when there is a velocity difference at the interface of two different fluids.
[7] The gradient Richardson number (N_2/S_2) is a ratio of the buoyancy production or consumption of turbulence (N_2) over the vertical shear production of turbulence (S_2).
[8] Often given as 0.25 (Miles 1961; 1963), although other studies (Mack and Schoeberlein, 2004) have found the exact number to vary.

Popular parameterisations of vertical mixing such as the KPP parameterisation (Large et al., 1994) used in ocean modelling use vertical shear instability computed from the gradient Richardson number to estimate vertical mixing in the water column. Although the KPP parametrisation's popularity is due to its ability to reproduce a variety of observed marine phenomena (Large and Crawford, 1995; Large et al., 1997; Gent et al., 1998; Large and Gent; 1999), studies such as Chang et al. (2005) and Zaron and Moum (2009) have argued against modelling vertical mixing as a function of the Richardson number alone, while reviews of turbulent mixing processes in the upper ocean (D'Asaro, 2014) have emphasised processes such as Langmuir circulation and wave induced turbulence may produce additional mixing missing from many current parameterisations.

Breaking wave and none-breaking wave induced turbulence

Aside from the generation of the surface currents involved in vertical shear instability, the action of wind on the ocean surface also imparts energy into the water column by forming waves. The turbulence introduced by breaking waves declines quickly with depth, with its effect on vertical mixing only significant to a depth comparable to the significant wave height (10-20 m) (Terray et al., 1996), thus it is believed to have dissipated long before it has had the chance to impact mixing of the SML (Huang et al., 2011) in many regions.

Turbulence introduced by none-breaking waves has been suggested as an additional source of mixing that may penetrate much deeper than conventional breaking wave induced turbulence by recent laboratory experiments (Babanin and Haus, 2009; Dai et al., 2010) and field studies (Pleskachevsky et al., 2011; Toffoli et al., 2012). One modelling study by Qiao et al. (2004) suggested surface-wave-driven turbulent mixing may contribute to vertical mixing within the SML in some locations including in the Southern Ocean. Unlike wave-breaking, which has a very slow vertical diffusion rate, turbulence introduced by none breaking waves propagates rapidly into the lower water column, and thus may provide and immediate source of turbulence and additional mixing at the base of the SML.

However, the results and conclusions of these studies have been called into doubt by several studies. Beya et al. (2012) was not able to reproduce the results of Babnin and Haus (2009), although Ghantous and Babanin (2014) argues that the results of Beya et al., (2012) are consistent with the earlier experiments. Other studies have argued (Gerbi et al., 2008; D'Asaro; 2014) that the results of field experiments can be satisfactorily explained by measurement error and other vertical mixing theories. However, studies have shown that including none-breaking wave induced turbulence in the KPP vertical mixing parameterisations (Wang et al., 2010; Shu et al., 2011) can improve their performance in calculating the depth of the SML.

Langmuir circulation

The actions of wind-driven shear currents and wave turbulence interact to produce a series of wind-aligned rotating vortices, in a process called Langmuir circulation. Langmuir circulation is a process first described by Irving Langmuir in 1938 (Langmuir, 1938), who noticed lines of seaweed spaced at regular intervals of approximately 100 m during a cruise in the North Atlantic. The phenomenon is produced by counter-rotating cells of water, which are rotating in a direction perpendicular to the wind direction. Because adjacent cells are rotating in opposite directions, they interact to produce convergence and divergence zones parallel to the direction of wind travels. Water downwells in convergence zones and upwells in the divergence zones.

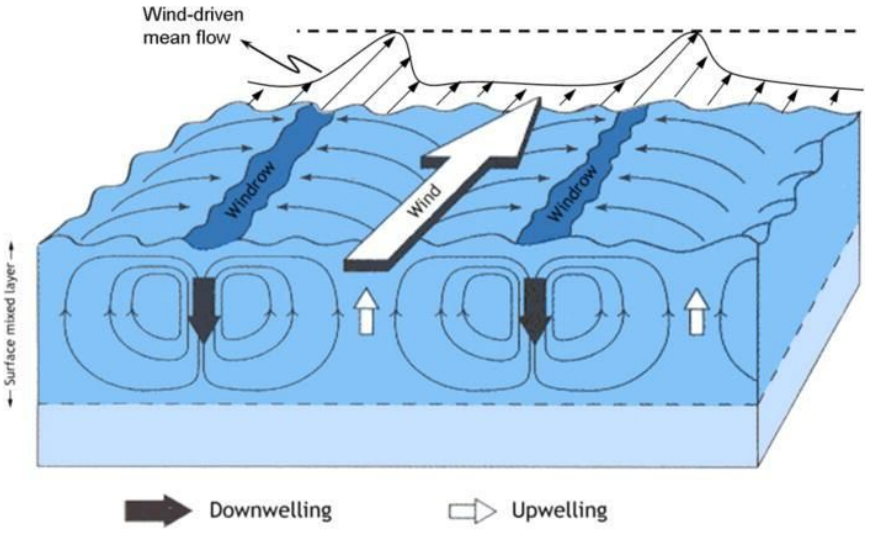

Figure 1L: Plot showing Langmuir circulation with two pairs of counter-rotating water cells driving upwelling and downwelling zones in a direction parallel to that of the wind direction. Figure taken from Tejada-Martínez et al. (2012).

A physical model describing the process was proposed by Craik and Leibovich (1976), which proposed that the cells were produced by the interaction of wind induced shear and wave turbulence processes, through the processes of Stokes drift and the orbital wave motions of particles in the surface layers of the water column.

An individual particle of water at the surface of the ocean will move up and down in a circular manner in the presence of the wave, as it moves up the crest of the wave and down the trough. These orbits are not just occurring at the surface, but down through the water column particles are moving in orbital motions, although these orbital motions decrease with depth. There is a shear stress at the base of these rotations, and small fluctuations in the wind forcing produces a variable shear stress, which creates rotating cells of water. Additionally, because the wave-induced particle velocity is slightly higher at the peak of the wave, than at the trough, the particle will gradually move in the direction of wave propagation, in a phenomenon known as Stokes drift. Stokes drift therefore begins to gradually rotate the cells so that they are perpendicular to the wind direction, due to the processes outlined in the Ekman transport section earlier.

Due to observational constraints, direct scientific measurements of Langmuir circulation are rare. Faller (1978) first demonstrated the phenomenon can be created in a laboratory, and since then field studies such as Smith (1992) and D'Asaro and Dairiki (1997) have observed the circulation in field studies. Although it is believed that Langmuir circulation contributes to mixing within the SML, it is not known whether it causes mixing between the SML and overlying waters. Modelling studies such as Li et al. (2016) have found that including Langmuir turbulence in KPP parameterisations of vertical mixing can improve their estimation of mixed layer depth in some regions, including the Southern Ocean, however there are currently not enough data to assert how significant the effects of Langmuir circulation are on vertical mixing at the base of the SML.

Coastal upwelling in the Southern Ocean

Due to the absence of any significant continental landmass in the region, the Southern Ocean is an area which experiences significant wind speeds. Indeed, annually averaged the wind speeds over the Southern Ocean are the strongest on Earth (Young, 1999). There is a strong seasonal cycle in the wind strength, with the lowest yearly averaged wind speeds occurring in the Southern Hemisphere

summer between December and February, at which point wind strength steadily increases to its peak in May, where it remains at a similar strength through the Southern Hemisphere winter until October, when spring takes over and the annually averaged wind speeds begin to decrease back towards their summer lull (Yuan, 2004). This seasonal pattern in wind speeds is what drives the seasonal oceanic N_2O flux signal, and the following pages are dedicated to explaining how changes in wind patterns drive seasonal N_2O fluxes in the Southern Ocean.

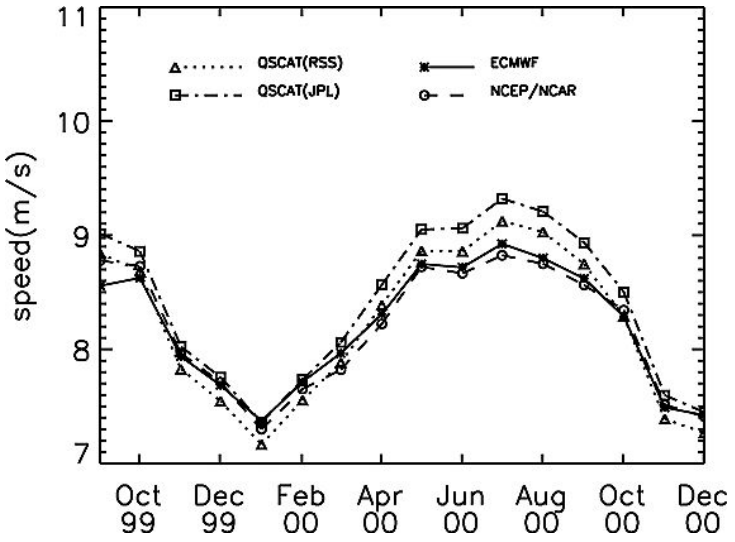

Figure 1M: Monthly wind speeds averaged over the Southern Ocean using data ollected by four different instruments between September 1999 and December 2002. Graph taken from Yuan (2004).

N_2O fluxes in the Southern Ocean largely occur in the Subantarctic Zone, a body of water that lies off the south coast of Australia between the Subtropical Front and the Subpolar Front (Rintoul and Trull, 2001). The vertical structure of the water column in this region is under a regime of constant stratification, whereby a layer of well mixed, less dense water, separated by a pycnocline. During the Australian summer between December and April, the SML is very shallow, with a depth of around 75m (Weeding and Trull, 2014).

As wind-speeds pick up, there is a significant deepening of the SML, which can reach depths greater than 500 m in mid-winter. This deepening of the surface mixed layer results in convective mixing of the water layers above and below the pycnocline, forming a body of water known as Subantarctic Mode Water (Shadwick et al., 2015). This system is of global importance, as coastal upwelling in the Southern Ocean has been shown to be a key process driving upwelling in the Atlantic Meridional Overturning Circulation (AMOC) (Marshall and Speer, 2012), and thereby it has an important role in modulating the oceanic uptake of heat (Kostov et al., 2014) and carbon (Frolicher et al., 2015) into the world's oceans.

It is also this upwelling system which produces the seasonal cycle of N_2O fluxes from the Southern Ocean. N_2O concentrations in the SML are close to equilibrium with the atmosphere, as there is little surface N_2O production due to the inhibition of nitrification by light in the photic zone. In contrast, water below the pycnocline is supersaturated with N_2O. This is because N_2O is primarily produced by microbial respiration in the subsurface waters below the SML, and this water may not have been in contact with the atmosphere for some time, allowing for an accumulation of N_2O. This provides the SML with water supersaturated with N_2O, which then fluxes into the atmosphere (Nevison et al., 2004). Current best estimates of the total marine N_2O signal emitted from the Southern Ocean are that this region is responsible for approximately 10% of the global marine N_2O source (Nevison et al., 2003; Nevison et al. ,2005).

Seasonal variations in the depth of the surface mixed layer are primarily caused by variations in the Southern Annular Mode (SAM) index, which describes the pressure difference between 40°S and 65°S. This pressure difference affects the strength of the westerly winds blowing over the Southern Ocean, with a positive SAM index value (characterised by high pressure anomalies in the low latitudes over Antarctica) being associated with higher westerly winds between 50-70°S, and a negative SAM index (indicating high pressure anomalies in the mid latitudes), resulting in stronger westerlies between 30-50°S (Swart et al., 2015). Recently the SAM index values have experienced a trend towards more positive values since around 1970 (Marshall, 2003).

1.4 Air-sea gas exchange of N_2O

The two-layer boundary model

The exchange of gases between the atmosphere and the ocean is a key process in the regulation of the global climate system, because of its role in the cycling and modulation of several environmentally important gases, including CO_2 and N_2O. The oceans are a net source of several important gases to the atmosphere apart from N_2O, including DMS, CH_4 and other none-methane hydrocarbons, which have important roles in atmospheric chemistry and climate regulation (Frost and Upstill-Goddard, 1999). The oceans also absorb approximately one third of the CO_2 emitted by anthropogenic activities, which aside from tempering the warming effects of human CO_2 emissions also has knock on effects for marine ecosystems *via* ocean acidification.

Gas exchange across the air-sea boundary is generally presented using a simplified two-layer boundary model, with the transfer of gases across the boundary layer being controlled by molecular diffusion (Witman 1923; Liss and Slater, 1974). Away from the boundary layer, turbulent mixing dominates the transport of gases on both sides. As you approach the air-sea boundary, at distances within a few 10s of µm, the viscous properties of the air-sea interface cause the turbulent mixing processes to weaken, so that molecular diffusion becomes the primary transport mechanism. This produces a stagnant film on both sides of the interface, a few 10s of µm across, over which the exchange of gases occurs (figure 1O). A sharp concentration gradient across the surface film develops on both sides, as you move towards the film towards the boundary the gas concentration becomes closer to the concentration on the other side of the boundary layer.

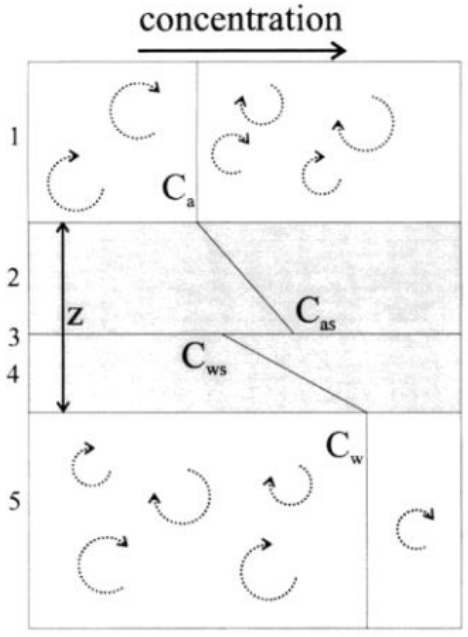

Figure 1O: Diagram of the air-sea water interface. Zone 1 indicates air, zones 2-4 are the surface film, and zone 5 is the ocean. Ca and Cw stand for concentration of a gas in air and water respectively, Cas and Cws indicate the concentrations in the air-sea boundary layer (Frost and Upstill-Goddard, 1999).

As the primary mechanism responsible for air-sea gas exchange is believed to be molecular diffusion, the transport of gases across the boundary layer is generally assumed to be proportional to the difference in concentrations of a gas in the atmosphere and ocean. Fick's law of diffusion (equation 7) can be used to calculate the transport of gases across a boundary layer, however, the equation

requires knowledge of the direct concentration gradients across the boundary layer (d_c) and the size of the boundary layer (d_z).

$$F = -D\frac{d_c}{d_z} \qquad (7)$$

Due to the very small size of the boundary layer, practical measurements of either of these parameters is impossible in the ocean. Therefore, equation 7 is restated as equations 8 and 9, where F is the rate of flux across the air-sea interface ($mol^{-2}\ s^{-1}$), k is the gas transfer velocity ($m\ s^{-1}$), C_w is the gas concentration in the water mass ($mol\ m^{-3}$), C_a is the concentration of the gas in air ($mol\ m^{-3}$) and α is the Otswald solubility coefficient of the individual gas (Wanninkhov et al., 2009). The addition of α is necessary because different gases have different solubilities in water, and the solubility of a gas in water will affect the transfer of that gas across the air-sea boundary. The k parameter incorporates both the molecular diffusivity coefficient (D) and the depth of the surface boundary layer (Z).

$$F = k(C_w - \alpha C_a) \qquad (8)$$

$$k = \frac{D}{Z} \qquad (9)$$

Estimating the gas transfer velocity (*k*), is therefore the focus of researchers attempting to better understand the process of air-sea gas exchange. The k parameter can itself be separated into k_w (gas transfer velocity in water) and k_a (gas transfer velocity in air. Liss and Slater (1974) conceptualise this in terms of resistance, with the total resistance to gas exchange being provided by the sum of the air-side and water-side resistance to exchange. N_2O is a chemically unreactive gas, and because of this the majority of the resistance to exchange is due to water-side resistance. Therefore, k_a can be ignored and k_w can be substituted for k into equation 8.

The initial two-layer boundary model was developed by Whitman (1923), however this was a simple model with significant limitations, most significant of which was that the depth of the boundary layer (Z) was assumed to be spatially and temporally invariant. This assumption is true only under very low wind conditions, with low associated turbulence values. As wind speeds increase wave turbulence influences exchange processes in the boundary layer, and laboratory and field experiments (see Frost and Upstil-Goddard, 1999, Table 1, for a synopsis) have generally found that D is proportional to between $D^{1/2}$ and $D^{1/3}$ rather than the D^1 proposed by equation 7, when turbulence is influencing gas exchange processes. This has resulted in the development of various other models, including the boundary layer model (Deacon, 1977) and the surface renewal model, first proposed by Higbie (1935), which model the boundary layer as a dynamic environment, producing results closer to those observed in field and laboratory studies.

Although there are some conceptual differences between the models, what all parameterisations of the boundary layer have in common is that they express k using a molecular diffusivity term (D), and a function incorporating a velocity component (Q), a length component (Z) and the kinematic viscosity of water (v)[9] (Wanninkhov et al., 2009). D describes the rate of diffusion of a gas through water, Q describing physical mixing processes driven by the input of kinetic energy into the surface layer through wind stress and Z represents the distance over which the mixing processes are occurring.

$$k_w = aD^n f(Q, Z, v) \qquad (10)$$

[9] The resistance to flow of a fluid.

For practical purposes equation 10 is rewritten as equation 11, with the Schmidt number (Sc) replacing the molecular diffusivity term. The reason for this is that equations 8 and 9 show that if k_w is known for one gas, then it can be inferred for any unreactive gas providing the molecular diffusivity coefficients for both gases are known. In practice, converting between gases does not work when Z is variable, due to limitations in the accuracy of measurements. The Schmidt number provides a mechanism to convert the k_w calculated for one gas into any other unreactive gas, provided that the molecular diffusivity coefficient is known for both gases, through equation 13.

$$k_w = aSc^{-n} f(Q, Z, v) \qquad (11)$$

$$Sc = \frac{v}{D} \qquad (12)$$

$$\frac{k_{w1}}{k_{w2}} = \frac{(Sc_2)^n}{(Sc_1)^n} \qquad (13)$$

Towards a parameterisation of air-sea gas exchange

The endeavour to create a global parameterisation for air-sea gas exchange was provided with unlikely assistance through the Nuclear Bomb tests conducted by USA during the 1950s and 1960s. These tests produced a very large rise in the atmospheric concentration of ^{14}C, known as "bomb ^{14}C", by the academic community (Krakaur et al., 2006). By 1964, atmospheric concentrations of ^{14}C had increased by 800% above pre-test levels, and then declined to +65% by 2004, due to the uptake of ^{14}C by the marine and terrestrial biospheres.

The natural cycle of ^{14}C begins in the upper atmosphere, where it is produced at an approximately stable rate through reactions involving cosmic rays and solar protons (Lingenfelter, 1963). It is transported into the lower atmosphere as $^{14}CO_2$, where it is then taken up by the marine and terrestrial biospheres. The isotopic abundance of ^{14}C is generally stated as its abundance relative to the more common carbon isotope of ^{12}C, using the notation $\Delta^{14}C$.

Uptake of ^{14}C by the oceans is a very slow process, it can take a mixed layer with a depth of 50 m approximately 10 years to reach equilibrium with the atmosphere following a change in the isotope composition of atmospheric CO_2. This is much longer than the typical residence time of water in the surface mixed layer, so large $\Delta^{14}C$ gradients persist between the abundance of ^{14}C in the atmosphere and the surface of the oceans. The very long equilibrium timescale across the air-sea interface, means that gas exchange processes are the primary factor limiting the marine uptake of the bomb ^{14}C.

The first comprehensive dataset of $\Delta^{14}C$ was compiled during the Geochemical Ocean Sections (GEOSECS), which took place between 1972 and 1978. The studies of Broeker et al. (1985, 1986) and Broeker and Peng (1982) used the $\Delta^{14}C$ data inventory to calculate a global estimate for the gas transfer velocity. Broeker (1986), estimated the gas transfer velocity by calculating the uptake rate of bomb $\Delta^{14}C$, while Broeker and Peng (1982) used the difference between the estimated bomb $\Delta^{14}C$ from the observed $\Delta^{14}C$ to estimate pre-industrial $\Delta^{14}C$ in the marine environment, and thus the difference between natural $\Delta^{14}C$ atmosphere and natural $\Delta^{14}C$ ocean, from which the gas exchange transfer velocity was calculated.

Both methods produced similar results, and the mean gas exchange velocities calculated by these experiments have been used to set the constant *a* in equations 10 and 11 (e.g. Wanninkhov, 1992; Wanninkhov and McGillis, 1999). Perhaps the most widely used gas exchange parameterisation is Wanninkhov (1992). To parameterise air-sea gas exchange, Wanninkhov (1992) used the results of

several field experiments to investigate the relationship between the surface forcing provided by wind speed and gas exchange, and concluded that gas exchange scales to the wind speed squared. He then scaled the results so that they matched the analysis of the $\Delta^{14}C$ data.

This parameterisation, is provided in equation 14, where k_0 is the constant calculated from the bomb ^{14}C, u^2 is the wind speed squared, (Sc/660) uses the Schmidt number calculated for CO_2 to convert between different gases (see equation 13) and -0.5 is the exponent deemed to be most realistic for the gas diffusivity coefficient by laboratory and field experiments (please refer to the two-layer boundary model discussion for more details). The value of k_0 was chosen so that the global mean gas transfer velocity was consistent with the results of the GEOSECS analysis of natural and bomb $\Delta^{14}C$.

$$k_w = k_0 \cdot u^2 \cdot \left(\frac{Sc}{660}\right)^{-0.5} \qquad (14)$$

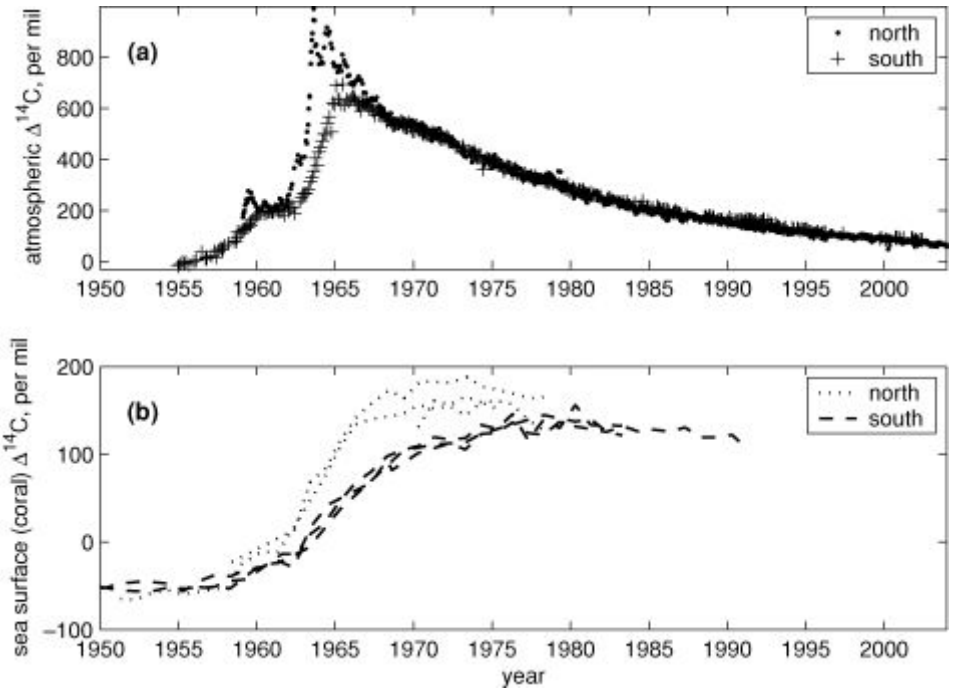

Figure 1P: $\Delta^{14}C$ in the atmosphere (top) and oceans (bottom) between 1950 and 2000 (Krakaur, 2006). The $\Delta^{14}C$ starts as negative in the ocean graph, because $\Delta^{14}C$ is defined relative to the pre-industrial atmospheric $^{14}CO_2$, and due to the disequilibria which exists between the atmosphere and oceans, even under natural conditions, the pre-industrial $\Delta^{14}C$ in the oceans was approximately -50%.

Wanninkov parameterised gas exchange with gas exchange scaling to the square of the wind speed, however linear (Broeker et al., 1995), piecewise linear (Liss and Merlivat, 1986) and cubic (Wanninkhov and McGillis, 1999) relationships have also been suggested (also see Knightingale et al. (2000)). While the published literature contains a wide range of proposed parameterisations for air-sea gas exchange, what all parameterisations have in common is that they assume that the input of kinetic energy into the water surface layer from the wind stress is the fundamental process driving air-water exchange.

The empirical relationship between wind speed and gas exchange developed by Liss and Merlivat (1986) suggests a three-stage relationship between wind speed and gas exchange. Under low wind conditions, the surface of the ocean is smooth and there is low turbulence in the water column. As the wind speed increases, friction between the air and the surface of the water generates

turbulence, which increases the rate at which gas is transported across the thin boundary layer at the sea surface. As wind speeds increase still further, surface waves begin to break. Breaking waves can introduce large amounts of turbulence into the surface layer of the water column promoting gas exchange, and various studies (e.g. Wallace and Wrick, 1992; Farmer et al., 1993; McNeill and D'Asaro, 2007) have also shown large increases in air-sea gas exchange due to the injection of bubbles into the surface layer through breaking waves. Exchange driven by this last process is believed to be significant, however, it is an extremely difficult process to solve, and as of yet no reliable parameterisation exists (Wanninkhov et al., 2009).

In addition to the above processes, the exchange of gases across the boundary layer can also be affected by other environmental variables including rainfall, buoyancy fluxes, surfactants and surface films. Rainfall increases air-sea gas exchange, with the majority of the increase being due to increased turbulence in the surface layer, and some contribution (0-20%) due to rain-generated bubbles (Ho et al., 2000). Changes in sea-surface temperature can generate buoyancy-generated turbulent mixing processes which can enhance air-sea gas exchange, which can be the dominant mixing process affecting exchange in low-wind environments (McGillis et al., 2004). The presence of both surfactants (Wei and Wu, 1992) and surface films (Schmidt and Schneider, 2011) can reduce transport of gases across the boundary layer by reducing turbulence, and surface films can further reduce gas exchange by providing an impermeable layer over the ocean surface that hiders the transport of molecules across the boundary layer.

Although the problem of air-gas exchange is quite complex, common parameterisations such as Wanninkhov (1992) use simple linear, cubic or quadratic functions of the wind speed, with coefficients calibrated using the available data. These methods ignore many of the additional environmental influences on upper ocean turbulence and gas exchange mentioned above, although in his review of the field, Wanninkhov (2009) stated that "there has been little evidence that incorporation of comprehensive surface forcing provides a better flux field than simple wind speed algorithms".

The large variety of different conflicting formulas for air-sea gas exchange in the published literature has resulted in several re-analyses of the bomb ^{14}C data (Krakaur et al., 2006; Sweeney et al., 2007). As well as the GEOSECS data, the Krakaur et al. analysis used data from World Ocean Circulation Experiment (WOCE), mainly collected in the 1990s, as well as an ocean circulation model, to re-evaluate the relationship between wind speed and the ^{14}C bomb uptake.

This re-analysis found that the latitudinal gradients in the mean gas exchange velocity were not large enough to support a quadratic or cubic dependence of wind on gas exchange, instead concluding that the relationship was approximately linear, with an exponent of 0.5 ± 0.4. Wind speeds are highest in the higher latitudes around the northern and southern poles, and thus weaker latitudinal gradients support a weaker influence of wind speed on air-sea gas exchange.

This global ocean modelling approach holds some advantages over the Wanninkhov (1992) method of scaling up the results of a few field studies to a global estimate, as this approach can introduce significant uncertainty due to the complicated nature of air-sea gas exchange discussed above. However, a much weaker relationship between air-sea gas exchange, as implied by the Krakaur (2006) analysis, does question the conceptual model of how wind speed affects air-sea gas exchange introduced in Liss and Merlivat (1986), which has been widely believed to be the correct functional relationship between the two ever since.

1.5 Modelling the atmospheric transport of trace gases in the atmosphere

Atmospheric observations in conjunction with atmospheric transport models have long been used as a method to estimate the net sources and sinks of N_2O and other trace gases from both the marine and terrestrial biospheres. The atmospheric datasets utilised by these studies have a much greater temporal coverage than marine datasets which are more sporadic, and by combining these with

atmospheric transport models it is possible to calculate top down estimates of the total N_2O source that are not possible through the more experimental process driven studies, due to the increased temporal and spatial coverage that long-term atmospheric trace gas datasets provide. Inversion modelling studies utilising these data are often used to calculate global, regional and country specific emissions inventories for various greenhouse gasses (e.g. Huang, 2008; Manning et al, 2011; Thompson et al., 2014).

The NAME (Numerical Atmospheric Modelling Enivronment) particle dispersion model is one atmospheric transport model utilised by studies such as Manning et al, 2011 to estimate sources and sinks of greenhouse gasses. This model was developed by the UK Met Office following the Chernobyl nuclear disaster in order to predict the dispersion of particulates in the atmosphere for use in emergency response to similar disasters in the future. Trace gas modelling studies run this model in reverse mode, so that instead of predicting where particles will be dispersed to from a point emissions source, the model generates an air history map showing the recent history of the air being measured at an observation site. The air history map is a 30-day integrated estimate of the contribution of potential fluxes from each grid cell to the observed concentration at a particular site and time.

The air being released from the observation site are driven by meteorology from the Met Office Unified Model (UM), with a random walk technique being used to simulate turbulence (Morrison and Webster, 2005). Air parcels are able to move from the surface to altitudes above 10 km and back again, however only air parcels which are within 100 m of the ground are recorded in the air history maps. The dosage of each grid box (g s^{-1} m^{-3}) is divided by the total mass of particles emitted and multiplied by the area of the grid box to calculate a continuous emissions value (measured in s m^{-1}), to calculate a dilution matrix. Each grid cell of the dilution matrix represents the contribution of surface fluxes over the previous 30 days to the total air concentration at an observation site for a three-hour period (i.e. for each three-hour period, this model will create a gridded dataset estimating the proportion of the total air concentration at an observation site which has originated from emissions in each grid cell, by modelling particle movements over the previous 30 days).

An estimate for the predicted concentration of a trace gas at an observation site can be calculated from the product of a gridded dataset of predicted gas fluxes and the dilution matrix (also known as a footprint). It is then possible to analyse the temporal and spatial distribution of greenhouse gas fluxes by comparing the predicted N_2O concentrations with the observed concentrations using various statistical methods. Before analysing the result, it is necessary to calculate the baseline concentration for the gas in question as well as the boundary conditions for the grid which is being modelled.

Estimating the background N_2O mole fraction

The modelling techniques mentioned above can be used to account for changes to the atmospheric mole fractions of N_2O due to physical processes within the model domain, however, they do not account for the background atmospheric concentration of N_2O. To include the remainder of the atmospheric N_2O concentration, this study has used the Eulerian Model for OZone and Related

Tracers (MOZART) (van der Werf et al., 2010; Lunt et al., 2016). The model is run for a period of years before to generate a realistic 3-D dataset for the atmospheric distribution of global N_2O concentrations, using a global anthropological emissions dataset obtained from the Emissions Database for Global Atmospheric Research (EDGAR).

The results from the MOZART model runs were used to create a box around the model domain, varying by height and longitude along the east and west boundaries and by height and latitude along the north and west boundaries. This dataset is then used to estimate the time-varying contribution of the total mole fractions of N_2O from each edge of the model domain.

1.6 Measuring N_2O in the atmosphere

Following scientific concerns regarding the environmental impacts of several anthropogenically generated gases on the ozone layer and on the global climate, a global network of atmospheric observation stations was developed first through the Atmospheric Lifetime Experiment (ALE) in 1978. The ALE comprised four globally distributed sites measuring chloroflurocarbons, chlorocarbons, hydrochloroflurocarbons and N_2O. The ALE was followed by the Global Atmospheric Gases experiment (GAGE) which lasted between 1981 and 1985; culminating in the Advanced Global Atmospheric Gases experiment (AGAGE), which has run since 1985 to the present day.

The global AGAGE network comprises 13 active observation sites, including the four original ones at Mace Head, Ireland (the original Adrigole site was replaced by Mace Head in 1987); Ragged Point, Barbados; Cape Matatula, American Samoa; and Cape Grim, Tasmania; from the ALE experiment. Each iteration of the global network responsible for measuring trace atmospheric gasses, the time resolution, instrumentation and number of atmospheric compounds observed were improved, with the result being a comprehensive long-term global dataset of unparralled importance in understanding the long term trends in the concentration of anthropologically produced greenhouse gasses in our atmosphere (Prinn et al., 2000).

2. Methodology

2.1. Research questions

Currently there are no published global modelling studies of the N_2O source which have integrated Nevison et al.'s (2003) new parameterisation of N_2O production into their model equations, as both Sunatharalingam and Sarmiento (2000) and Manizza et al. (2012) use the old parameterisation which estimates N_2O production using AOU directly. Therefore, a new global dataset of N_2O production has been produced by Manizza (unpublished), which estimates N_2O production using the Nevison et al. (2003) parameterisation.

Research hypothesis

The hypothesis of this study is that *the biogeochemical model used in this study, when used in conjunction with the NAME partical dispersion model, is able to accurately predict changes in the atmospheric concentration of N_2O at our measurement site in Cape Grim.*

Research objectives

In order to test my hypothesis, I have formulated a series of research objectives

1. An orthogonal distance regression analysis will be performed of predicted atmospheric N_2O against observed atmospheric N_2O in order to analyse the performance of the model predicted N_2O in predicting the marine N_2O source.
2. Scaling factors will be calculated for each month of data, to scale up or down the predicted N_2O source taking into account atmospheric observations.
3. Two different gas exchange parameterisations will be used, to assess how much uncertainty in our understanding of ocean-atmosphere gas exchange may be contributing to the overall uncertainty in the analysis.
4. Mixed layer depths generated by the Argo ocean observation program will be compared with mixed layer depths generated by the biogeochemical model to investigate how well the biogeochemical model is estimating vertical mixing within the Southern Ocean.

The rationale for including objectives three and four in this analysis, is that while N_2O production in the marine environment is a biological process, some of the most important factors affecting the rate of exchange of N_2O between atmosphere and sea in the Southern Ocean are physical in nature (see sections 1.3 and 1.4, and especially the subsection entitled *Coastal Upwelling in the Southern Ocean*, at the end of section 1.3). The importance of vertical mixing in the seasonal pattern of the Southern Ocean N_2O source, and the high wind speeds experienced over the Southern Ocean, especially during the winter months, mean that it is important to understand how uncertainties in these processes may be affecting the overall estimate of the N_2O source, and also means the Southern Ocean is a good region to investigate how these processes affect air-sea gas exchange and the N_2O marine source.

Gaps in our knowledge

This study will take advantage of the long continuous timeseries of N_2O measurements made by the AGAGE tall tower at Cape Grim. This site is an ideal location to test the capabilities of the model, because approximately 40% of the air-mass sampled at this station has passed over the Southern Ocean, which is responsible for significant marine fluxes of N_2O into the atmosphere.

In addition to investigating the performance of the biogeochemical model, this study will build on the work of Nevison et al. (2003), and attempt to use a biogeochemical flux model in combination with an atmospheric transport model to investigate Southern Ocean fluxes of N_2O. The study will utilise the atmospheric transport model to filter the data so that periods where terrestrial emissions of N_2O are predicted to make up a significant component of the measured variations in N_2O are excluded from the analysis. In this way, we will attempt to exclude terrestrial emissions from the analysis, a key uncertainty in Nevison et al. (2003).

This study will utilise the third incarnation of an atmospheric transport model produced by the Met-Office known as the Numerical Atmospheric Modelling Enivronment (NAME (III)) in conjunction with the output of Manizza's (unpublished) new biogeochemical model and the EDGAR inventory of terrestrial N_2O fluxes to generate timeseries of terrestrial and marine fluxes at Cape Grim, Tasmania. These timeseries will be used to filter the atmospheric observations to include only periods where the air history at Cape Grim indicates the marine source predominates.

An orthogonal distance regression analysis will then be carried out between the filtered observations and the concurrent predicted N_2O concentration derived from the biogeochemical ocean flux model, in order to determine whether the biogeochemical model and atmospheric transport model can accurately predict variations in N_2O observations at Cape Grim.

Finally, this study will perform the analysis using an N_2O marine source estimated using two different gas exchange parameterisations, the one devised by Wanninkhov (1992) and the re-analysis conducted by Krakauer et al. (2006).

The significance of this research is that currently N_2O is the largest contributor to uncertainty in regional and global greenhouse gas estimates. The marine source is a significant component of the total uncertainty in N_2O emissions estimates. Additionally, by comparing the results of two different gas exchange parameterisations, the study will seek to investigate whether this method may be able to say something about the underlying physical processes which are responsible for the fluxes of important greenhouse gasses into the atmosphere. As mentioned earlier in the introduction section, there are significant gaps in our knowledge and understanding of key marine processes responsible for the vertical mixing and gas exchange processes which are key to predicting air-sea fluxes of N_2O, and an understanding of these processes is important because it affects how the ocean will respond to future change in marine conditions.

2.2 Models and datasets

Air-Sea flux model

The work presented on both air-sea flux in the Southern Ocean and the UK N_2O budget make use of an ocean model generated air-sea flux predictions developed by the Scripps Institution of Oceanography (Manizza et al. unpublished, based on Mainzza et al. 2012 but using the ECCO2-Darwin model and updated parameterisations). To model N_2O production in the global oceans the model used the ECCO2-Darwin model, which is a new ocean biogeochemistry general circulation model. The ECCO2-Darwin model combines an ocean biogeochemical general circulation model (MITgcm) with a state estimate of ocean circulation from the Estimating the Circulation and Climate of the Ocean Phase II (ECCO2) project and the MIT Darwin ecosystem model (Brix et al., 2015). To generate the N_2O fluxes the model was modified to include add N_2O tracers, and to add terms for total N_2O and thermal N_2O to separate N_2O fluxes due to ventilation and thermal components. Vertical mixing has been parameterised using the KPP vertical mixing scheme. Two separate gridded outputs were provided, one computed using the Wanninkhov (1992) gas exchange parameterisation and one using the Krakaur (2006) parameterisation.

The data was provided on a 1° by 1° grid as monthly mean values between 2006 and 2013, and was regridded to the target domain and resolution.

Advanced Global Atmospheric Gases Experiment (AGAGE) dataset

Atmospheric observations of N_2O concentration were obtained from the AGAGE monitoring site at Cape Grim, Tasmania (40.683 S, 144.689 E). Air was collected from a tall tower at a height of 70m (164m above sea level) and sampled for N_2O every 40 minutes using a GC-ECD electron capture detector. Measurement errors are typically very small at ~0.15ppb (Prinn et al., 2000).

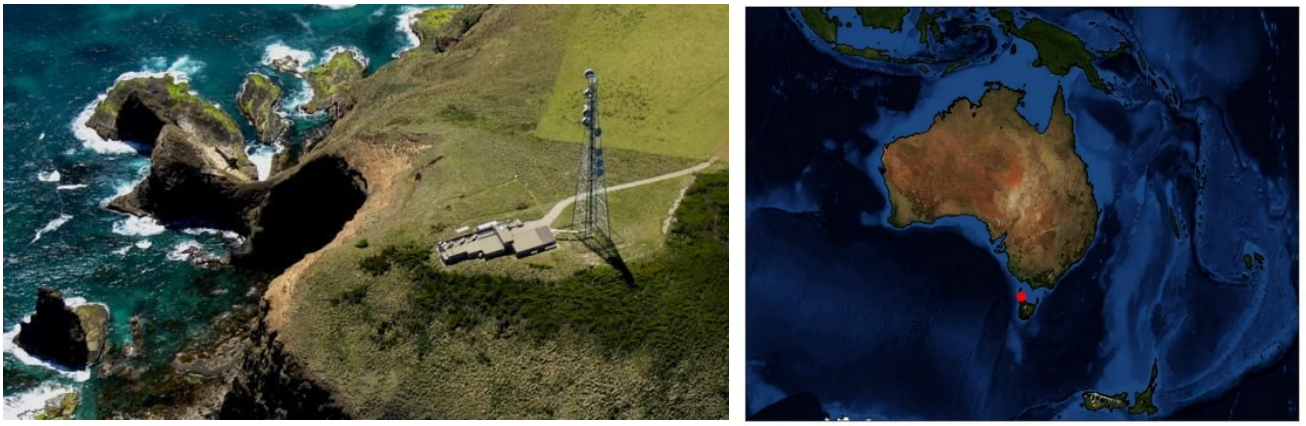

Figure 2A: Left: Cape Grim site. Image taken from the AGAGE website. Right: map of Australia with Cape Grim location marked with red dot.

Numerical Atmospheric Dispersion Modelling Environment (NAME) model output

For the purpose of this study the model was run in 'reverse' mode, where atmospheric particles are tracked backwards in time from our observation site, with the model calculating every interaction with surface regions, where air may pick up N_2O, over a period of 30 days before the measurement (Manning et al., 2011).

The stored output is a two-dimensional grid-map called a footprint (e.g. Figure 2B) demonstrating the sensitivity of the mole fractions measured at the observation site, to fluxes of N_2O into the atmosphere, from each grid-cell within the domain. One map is produced every two hours, enabling a time-evolving picture of how the atmospheric data being measured at Cape Grim is being affected

by emissions from different sources, to be produced. Since particles are only tracked for 30 days, assumptions must also be made about mole fractions that exist at the boundary to the NAME domain. In this work, we used mole fraction estimates generated using the global Model for Ozone and Related Tracers (MOZART, Emmons et al. 2010).

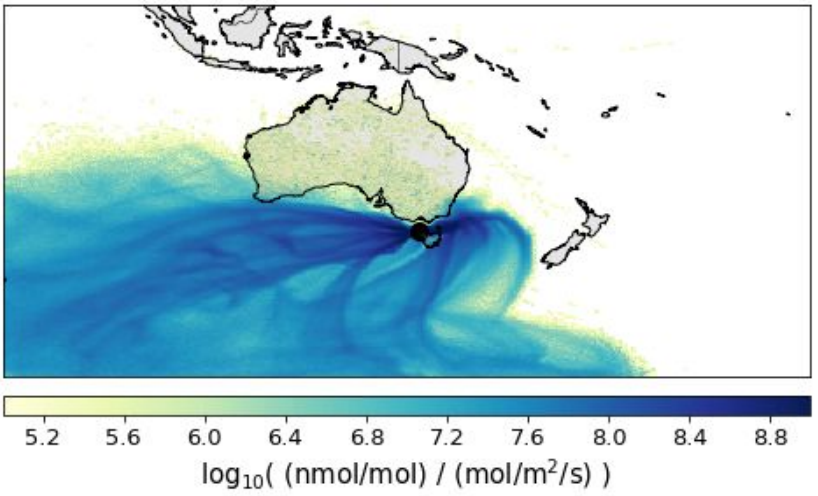

Figure 2B: Example footprint generated by the NAME model (average footprint for July 2008).

Argo dataset of marine vertical profiles

The Argo project is a large international project which has been deploying and running autonomous drifting profiling floats since 2000, collecting vertical profiles of the world's oceans. The current Argo fleet numbers approximately 4,000 floats measuring temperature, conductivity (from which it is possible to calculate salinity) and more recently sensors for other parameters such as oxygen have been added to floats. The floats are designed to conduct one vertical profile of the ocean every 10 days.

An Argo mixed layer climatology has been acquired from Holte et al. (2017). The algorithm used to compute the mixed layer depths was the density algorithm (Holte and Talley, 2009), which is currently the best automated mixed layer detection algorithm. The average mixed layer depths calculated using the density algorithm method were mapped onto a 1° x 1° grid, and then the mean MLD of each grid, for each month, was used to calculate the Argo climatology for this period. The biogeochemical model climatology was calculated by averaging the model estimated MLD of each grid cell, for each month.

The Argo climatology was regridded onto the 0.234 x 0.352 grid used in the analysis.

2.3. Methodology

N_2O fluxes generated by the biogeochemical model were regridded onto 0.234 (latitude) x 0.352 (longitude) grid centred on Australia. This dataset was then combined with an EDGAR emissions inventory for land fluxes of N_2O to enable a between-site comparison of how possible it would be to isolate the marine components of atmospheric N_2O measurements made at the three sites.

Site selection

After comparing the sensitivity of various AGAGE sites, the study site at Cape Grim, Tasmania, was selected for the analysis. This site was selected because it was the only location with close proximity to a significant N_2O marine source, whereby it was also possible to filter the data for periods where land influence on measured N_2O was low, due to its location and the prevailing wind conditions.

Calculating predicted N_2O concentrations

The predicted atmospheric mole fractions of N_2O due to atmospheric fluxes at an observation site are derived by using equation (15), where fp is a two-dimensional array of footprint values derived from the NAME model and flux is either the land-based (EDGAR) or ocean model flux estimates. If this is done for every footprint then a timeseries of predicted atmospheric mole-fractions due to surface fluxes of N_2O can be generated. If the land and ocean model fluxes perfectly represented fluxes of N_2O into the atmosphere and the NAME model perfectly represented the atmospheric transport of N_2O once in the atmosphere, then you would expect the predicted atmospheric mole-fractions to perfectly match measured N_2O once the baseline N_2O concentration was subtracted from atmospheric measurements. An example timeseries of measured N_2O and predicted N_2O concentrations, separated into atmosphere and ocean components, has been provided in figure 6A.

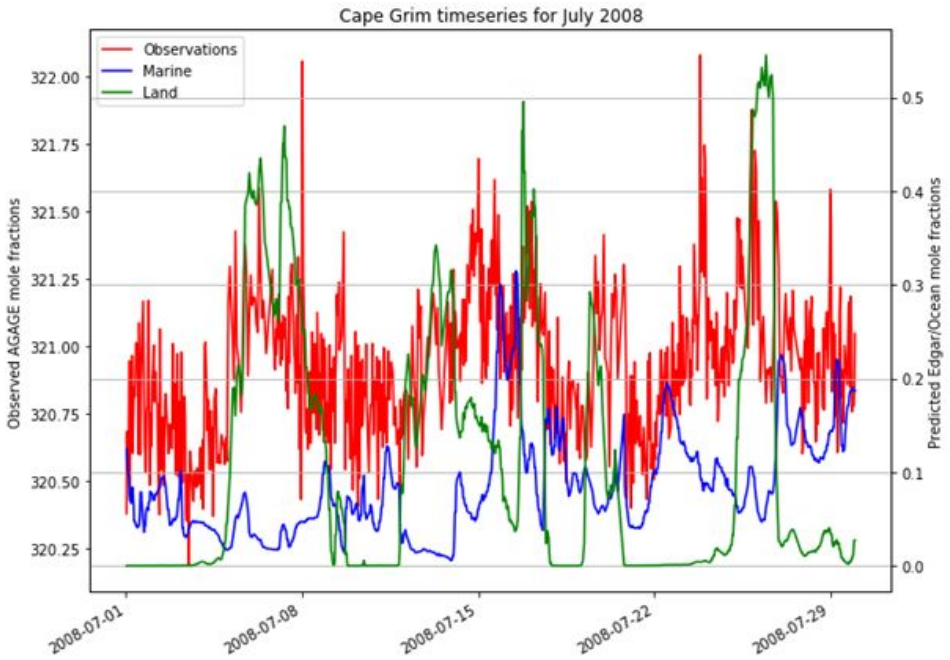

Figure 2C: Timeseries showing observed atmospheric N_2O (red line, left axis), predicted atmospheric N_2O concentrations derived from marine (blue line, right axis) and land (green line, right axis) sources.

$$N_2O_{atmos} = \sum_{i=1,\ j=1}^{n} fp_{(i,j)} \cdot flux_{(i,j)} \qquad (15)$$

To isolate the mole fractions that were most strongly influenced by the ocean the data was first filtered, so that only periods when >95% of the footprint was over ocean were retained. For example, in figure 6A, data from four periods centred on the 2nd, 10th, 19th and 22nd of July would have been included in the analysis. A second filter was then applied, excluding data recorded during periods of high local influence. This was performed because footprints with high local influence is a sign of low wind conditions. The uncertainty of the footprint is thought to be much higher under low winds, and land-based sources close to the monitoring site may have an significant influence on the observation under stagnant conditions (e.g. Manning et al., 2011).

After filtering, the north, south, east and west boundary N_2O concentrations calculated by the NAME model were subtracted from the measured N_2O concentrations to remove the baseline N_2O concentration variability. The predicted atmospheric N_2O concentration due to surface fluxes at each filtered time point was calculated using equation 15.

For each month of the ocean model simulation, an orthogonal distance regression analysis was then used to evaluate the predicted atmospheric mole-fractions of N_2O against the atmospheric observations (see following section). An orthogonal distance regression was chosen for the analysis because it is able to consider errors in both the predictor and response variable (Mandansky, 1959). As both the predicted atmospheric mole-fractions and the measured N_2O concentration are subject to error, this is a necessary requirement for this analysis.

Orthogonal distance regression

In a standard linear regression analysis, the relationship between a predictor variable (X) and the value of the response variable (Y) for a given value of X, is given by equation 16. Here, the relationship between a predictor variable and its response variable are calculated by minimising the sum of the square vertical distances (termed residuals) between data points and a line of best fit (equation 17). In this situation, the measured value of Y is assumed to be equal to the true value of Y plus an error term (ε), which has a mean of 0 and a variance of σ^2. The assumption is that if the measurement error in Y was reduced sufficiently then the relationship between X and Y would fall on a straight line (equation 18). Equation 19 displays the equation calculating the sum of the squared differences. It is this equation which is minimised by the linear regression.

$$Y|X = \alpha + \beta X \qquad (16)$$

$$Y_i = \alpha + \beta X_i + \varepsilon_i \qquad (17)$$

$$Y_{measured} = Y_{true} + \varepsilon \qquad (18)$$

$$J = \sum_{i=1}^{n} (Y_i - \alpha - \beta X_i)^2 \qquad (19)$$

Equation 16 is only designed to minimise the vertical distance between values of the response variable and the regression line. It makes no attempt to account for errors which may exist in the X variable. When errors in both variables occur, this method is not appropriate and it is necessary to use the orthogonal distance regression method, which takes into account errors in both the X and Y variables. In addition to equation 4, a second error term is required for errors in X (equation 20), which is incorporated into the least-squares model in equation 21 (Carroll and Rupert, 1995). U is

another error term with a mean of 0 and a variance of σ^2, and η represents the error variance ratio (equation 22).

The error variance ratio describes the ratio between the errors in the X and Y variables, and thus it is necessary to provide the regression with error terms for the X and Y variables. The green lines in figure 2C display the vertical errors which are minimised in a typical linear regression. The dashed turquoise lines represent the perpendicular distance from the regression line which the orthogonal distance regression also attempts to minimise in addition to the green lines. The relative weighting between the vertical and perpendicular distances which are minimised by the regression are calculated using the ratio between the error terms in the two variables.

$$W = X_{measured} + U \tag{20}$$

$$J = \sum_{i=1}^{n} \{(Y_i - \alpha - \beta X_i)^2 / \eta + (W_i - X_i)^2\} \tag{21}$$

$$\eta = \frac{var(Y|X)}{var(W|X)} = \frac{\sigma_\varepsilon^2}{\sigma_U^2} \tag{22}$$

The error used in this regression analysis for the N_2O observations (the Y variable) was taken as the measurement precision (Prinn et al., 2018), which is typically between ~0.15. The error for each value of predicted atmospheric N_2O (X value) was estimated by calculating the standard deviation of the value (X_i) and the two values before and two values after X_i. Standard deviation was chosen as the error term for the predictor variable, as it provided a measure of how much variation there was in the footprint and flux estimate at the time of the measurement. Periods with high variation signify variable or changing wind conditions, which could increase the uncertainty of the predictor variable. The standard deviation was calculated before the filtering was applied to the data.

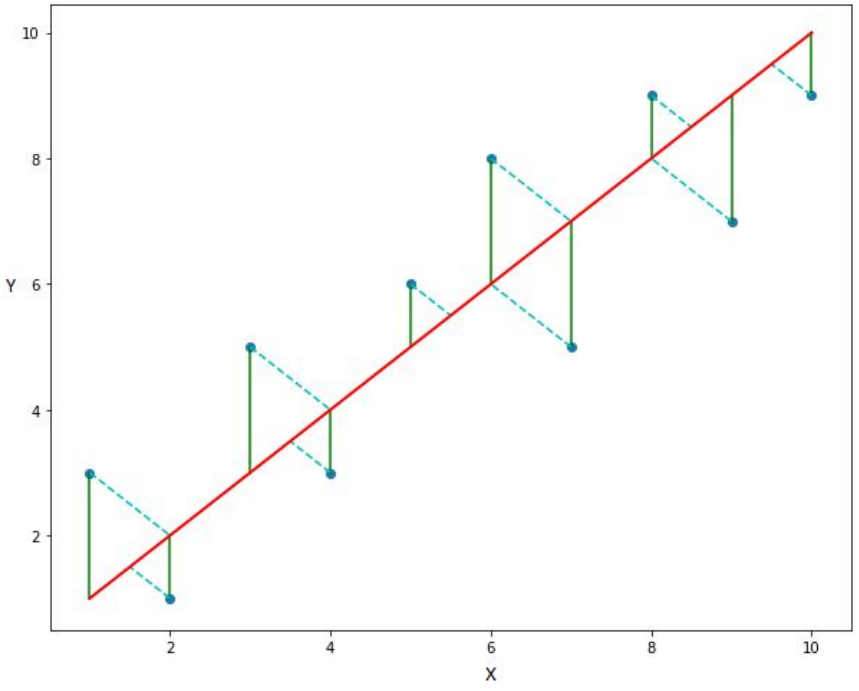

Figure 2D: An example orthogonal distance regression displaying the vertical distances (green) and perpendicular distances (dashed turquoise) which the orthogonal distance regression solves for.

Scaling the N_2O source

One regression was performed for each month of data, resulting in 72 regressions. The regression slope was used to scale up or down the model predicted N_2O fluxes using the atmospheric observations. Assuming no errors in either the method, observations, biogeochemical model or atmospheric transport model, the slope of each regression would be one. Slopes smaller than one indicate that the biogeochemical model is overestimating the N_2O source, whereas slopes greater one indicates that it is underestimating the N_2O source. By scaling the N_2O source we are modifying the predicted values to account for atmospheric observations, in order to calculate the actual N_2O source estimated by this analysis.

3. Results

This section discusses the comparison of N_2O flux estimates generated by the new biogeochemical model and atmospheric observations at Cape Grim. Two different gas exchange parameterisations were used, with the primary objective being to calculate scaling factors for each month of data and use these to scale the predicted fluxes up or down, in order to calculate new flux estimates for each region which are consistent with the atmospheric observations. Figure 3A shows the predicted N_2O source, as well as how this is split between thermal and ventilation components, by the biogeochemical model, with the inset showing the geographical area used in this analysis (on top of a representative footprint displaying where the air measured at our observation site will have picked up surface fluxes of N_2O calculated by our atmospheric transport model), which was within the black box.

Although the biogeochemical model dataset ran from 2006 to 2013, the years 2006 and 2007 were excluded from the analysis after a problem with the model was identified for these years. Some data was excluded from the analysis due to errors with the model output which were not resolved before completion of the analysis. These periods were between 2012-06-15 23:38:35 and 2012-06-16 22:19:35 and between 2013-11-18 00:00:00 and 2013-11-29 23:59:59.

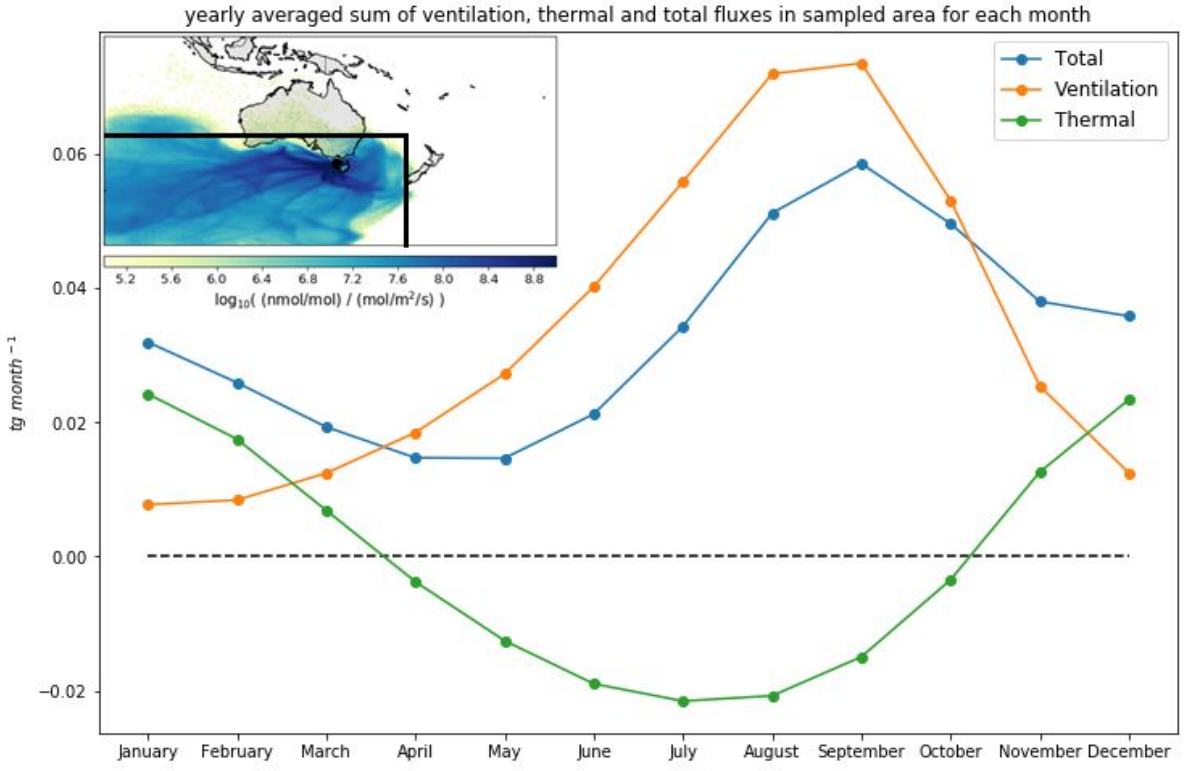

Figure 3A: Ventilation, thermal and total N_2O flux (mean fluxes from 2008-2013) from the marine environment in the sampled area (black box in insert) as predicted by the biogeochemical model using the Krakaur parameterisation.

3.1 The seasonal cycle of the nitrous oxide source in the Southern Ocean

A summary of the scaling factors calculated by this analysis for both the Wanninkhov 92 and Krakaur gas exchange parameterisations has been presented as a box and whisker plot in figures 3B and 3C. The orange lines indicate the median scaling factors, with the box indicating the upper and lower quartiles (50% of values fall within this range) and the whiskers indicate the range of values outside these quartiles.

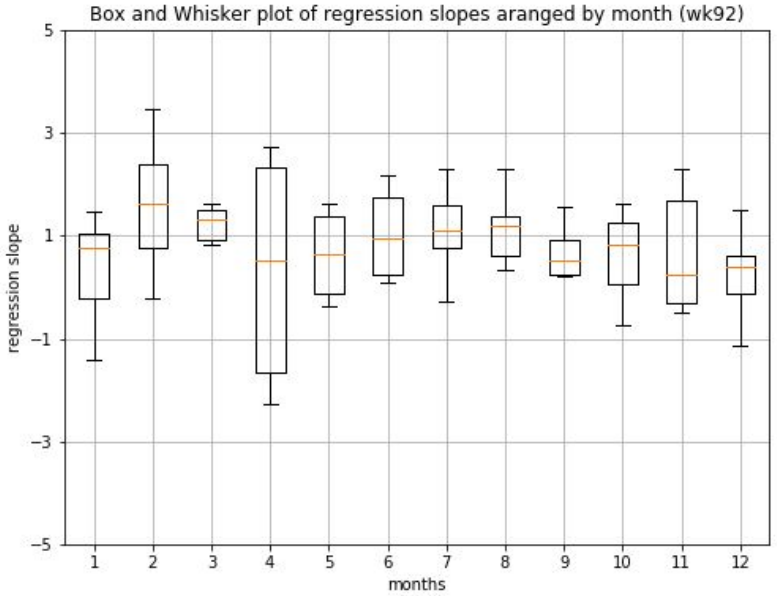

Figure 3B: Box and whisker plot of the gradient of the regression lines (2008-2013 inclusive) for each month (Wanninkhov 92).

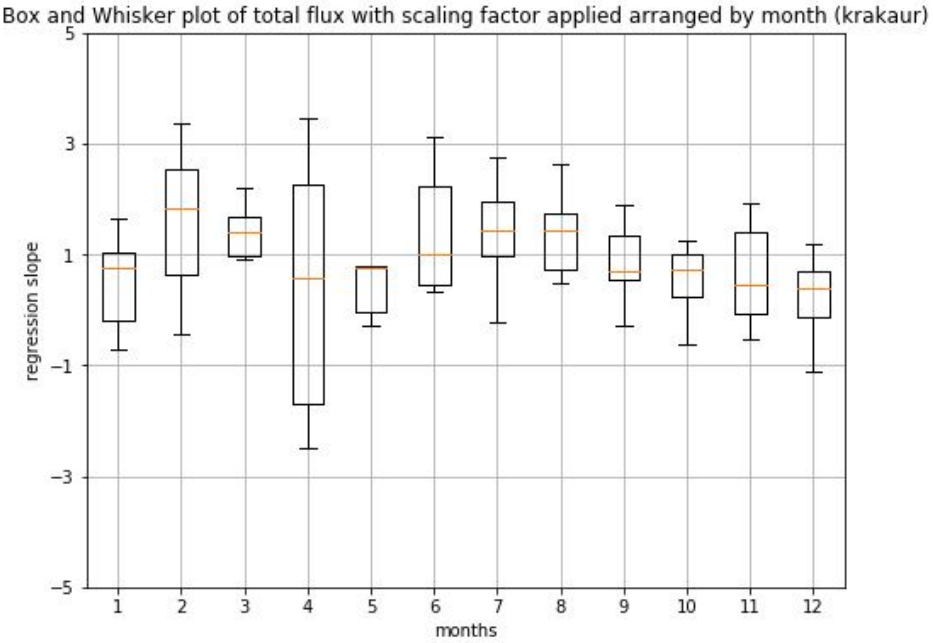

Figure 3C: Box and whisker plot of the gradient of the regression lines (2008-2013 inclusive) for each month (Krakaur).

The scaling factors have then been applied to the model predicted fluxes, with a summary of the results presented in table 3A, as well a figures 3D and 3E.

Table 3A: Median adjusted (predicted total flux in the sampled area with the scaling factor applied) marine source in sampled area alongside associated uncertainties.

Average adjusted N_2O marine source (flux units in Tg N_2O $month^{-1}$)								
	Lower 95 (WK92)	Median (WK92)	Upper 95 (WK92)	Uncertainty (WK92) (%)	Lower 95 (Krakaur)	Median (Krakaur)	Upper 95 (Krakaur)	Uncertainty (Krakaur) (%)
January	-0.032	0.0014	0.035	148	0.005	0.013	0.025	152
February	0.012	0.021	0.034	102	0.015	0.025	0.037	87
March	-0.003	0.013	0.023	198	-0.001	0.014	0.025	182
April	-0.003	0.004	0.009	342	-0.005	0.004	0.012	377
May	-0.001	0.006	0.011	209	-0.003	0.006	0.013	282
June	-0.004	0.011	0.021	226	-0.001	0.013	0.027	220
July	0.014	0.023	0.036	96	0.015	0.027	0.041	96
August	0.015	0.038	0.052	97	0.017	0.039	0.050	84
September	0.000	0.020	0.043	215	0.010	0.023	0.047	157
October	0.008	0.024	0.038	124	0.008	0.020	0.030	110
November	-0.008	0.005	0.018	501	-0.006	0.0010	0.025	318
December	-0.003	0.007	0.017	271	-0.003	0.008	0.017	256
Total	0.033	0.186	0.327	210	0.053	0.201	0.349	193

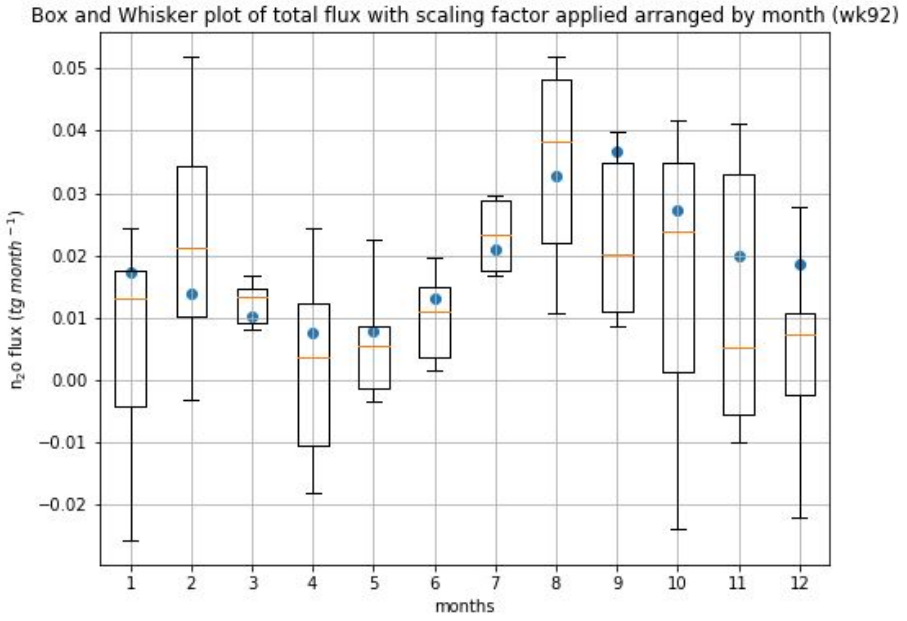

Figure 3D: Box and whisker plot of new flux values after scaling factors have been applied (sum of fluxes calculated in box region shown in figure 3A), with the mean total flux from all years provided as blue dots (Wanninkhov 92 gas exchange parameterisation).

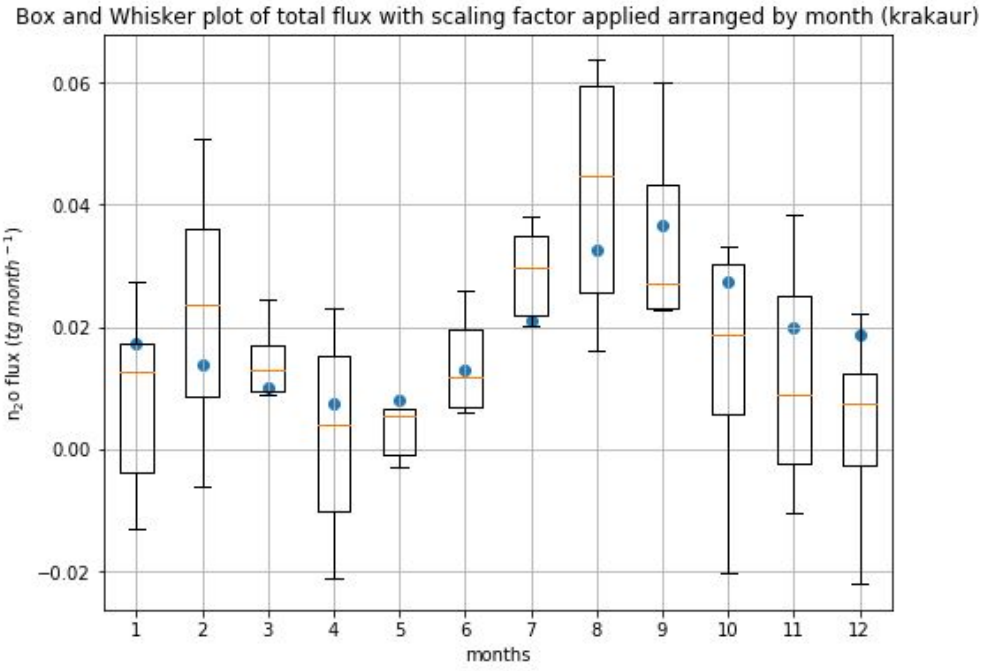

Figure 3E: Box and whisker plot of new flux values after scaling factors have been applied (sum of fluxes calculated in box region shown in figure 3A), with the mean total flux from all years provided as blue dots (Wanninkhov 92 gas exchange parameterisation).

When applied to the model predicted fluxes, the seasonal cycle inferred from the regression analysis is broadly similar to that predicted by the biogeochemical model with two exceptions. Taking the mean of the two gas exchange parameterisations produces a total marine N_2O source of 0.1935 Tg N_2O, with a difference of around 10% between the total fluxes calculated by the two gas exchange parameterisations. The Krakaur gas exchange parameterisation had a lower total uncertainty of approximately 17%.

Uncertainties are high in all months, with the lowest uncertainties in both gas exchange parameterisations seen in the winter months of peak Southern Ocean N_2O flux. The total uncertainty is slightly smaller with the Krakaur gas exchange parameterisation than with the Wanninkhov 92 parameterision. The analysis performed on both gas exchange parameterisations suggests emissions peak in August, rather than in September as predicted by the model, and the analysis predicts almost zero net flux in November and January. However, apart from this there is a good match between the seasonal cycle of the biogeochemical model predicted and median adjusted fluxes as calculated by this analysis.

For each month, the upper and lower 95% confidence intervals have been calculated using the standard errors calculated during the regression analysis. These have then been applied to the sum of the flux estimated by the biogeochemical model in the sampled area (box in insert of figure 3A) for each individual month, and provided the plots in figures 3F to 3K. The adjusted fluxes (dots) have been presented alongside the original values (bars). The results have been split so that they are presented as three groups of four. The first graphs cover the period from June to September, where the marine N_2O source is at its peak. The second four graphs cover the October to January period, where the N_2O source is decreasing as the climate moves into the Australian summer, whereas the final four graphs cover the February to June period where the N_2O source begins to increase due to the strengthening of the westerly winds from February.

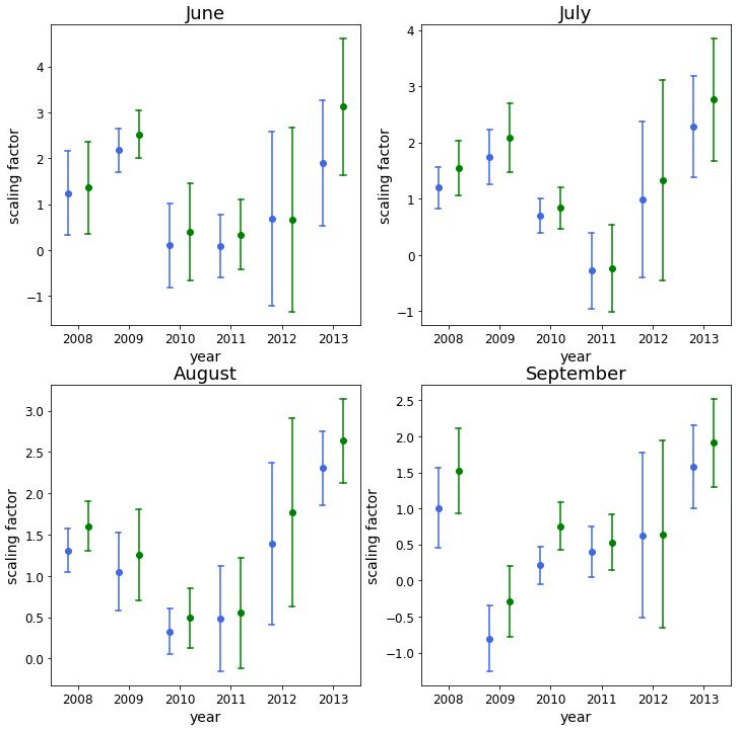

Figure 3F: Scaling factors, upper and lower confidence intervals for each year between July and October. Blue dots are Wanninkov 92 and green dots are Krakaur.

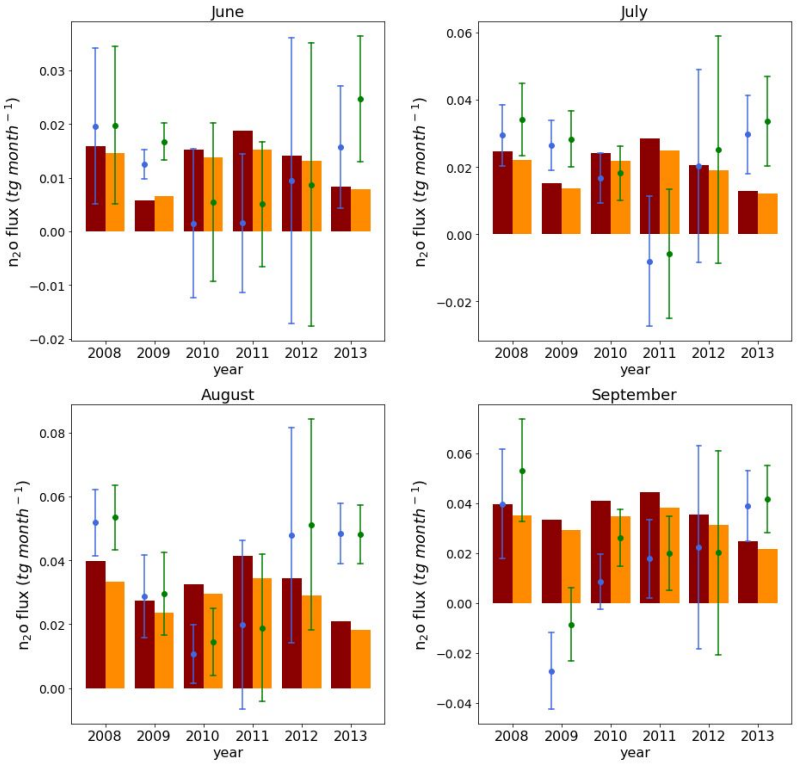

Figure 3G: Applied scaling factors with 95% confidence intervals are provided as the blue (Wanninkhov 92) and green (Krakaur) dots. The biogeochemical model predicted total fluxes for the sampled area are provided as the dark red (Wanninkhov 92) and orange (Krakaur) bars. Plots show the June to September period.

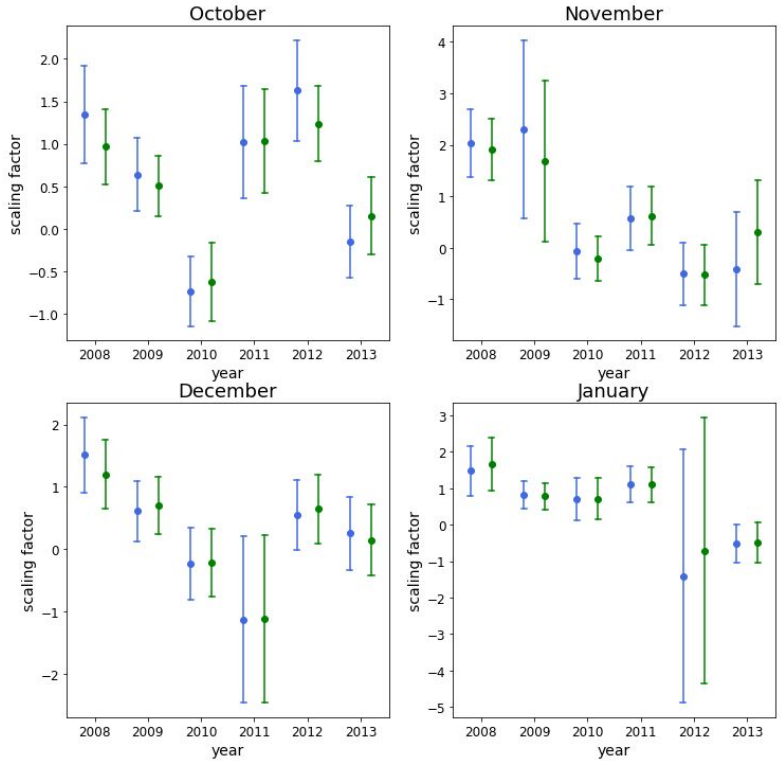

Figure 3H: Scaling factors, upper and lower confidence intervals for each year between October and January. Blue dots are Wanninkov 92 and green dots are Krakaur.

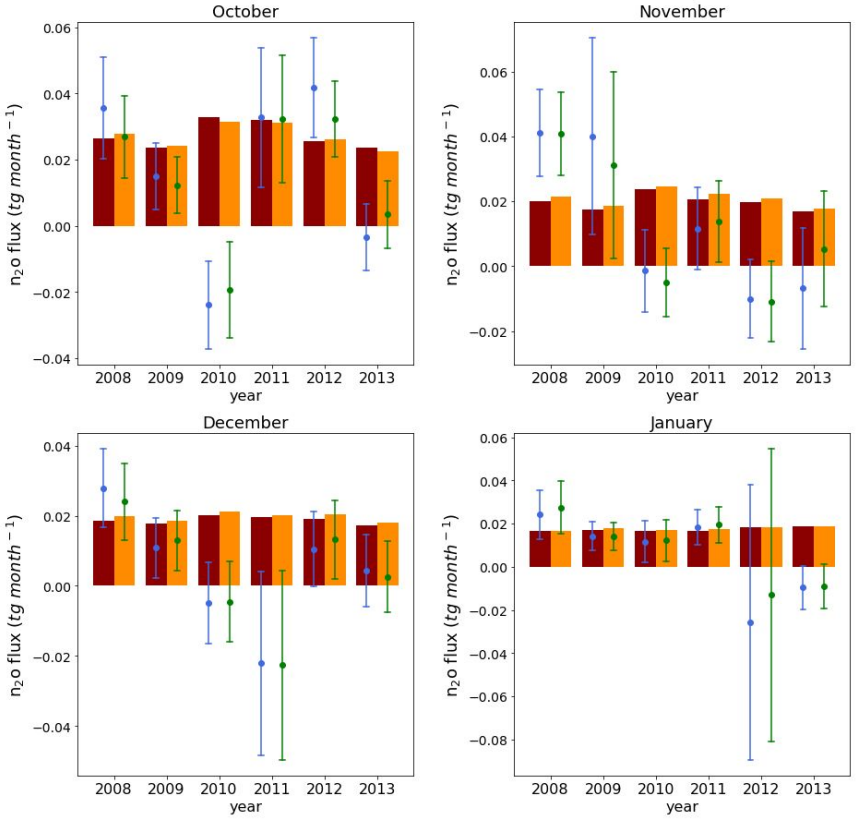

Figure 3I: Applied scaling factors with 95% confidence intervals are provided as the blue (Wanninkhov 92) and green (Krakaur) dots. The biogeochemical model predicted total fluxes for the sampled area are provided as the dark red (Wanninkhov 92) and orange (Krakaur) bars. Plots show the October to January period.

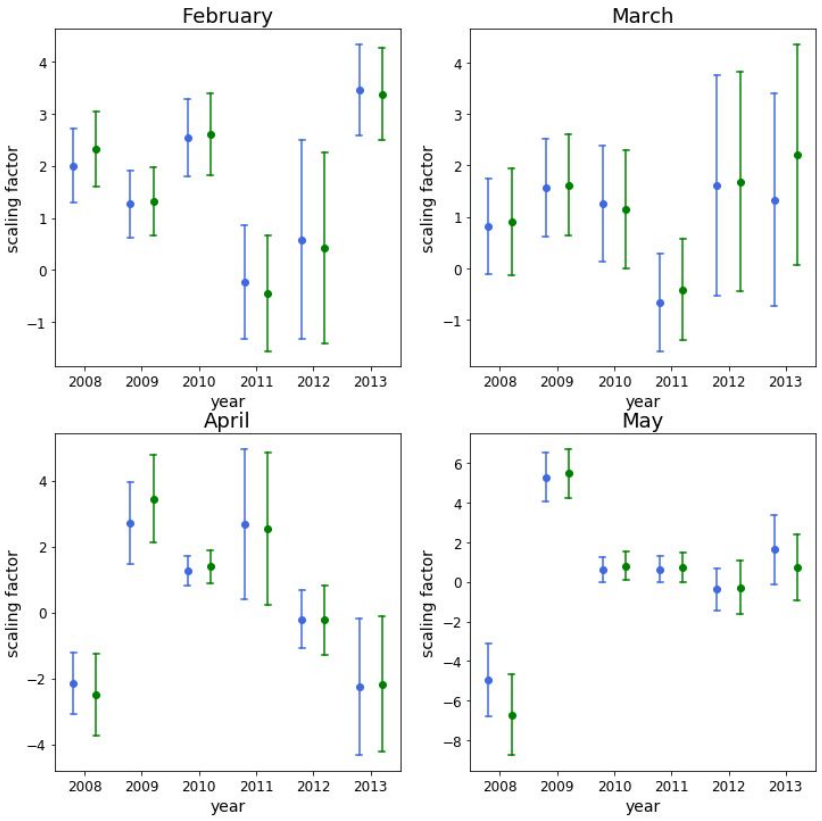

Figure 3J: Scaling factors, upper and lower confidence intervals for each year between February and May. Blue dots are Wanninkov 92 and green dots are Krakaur.

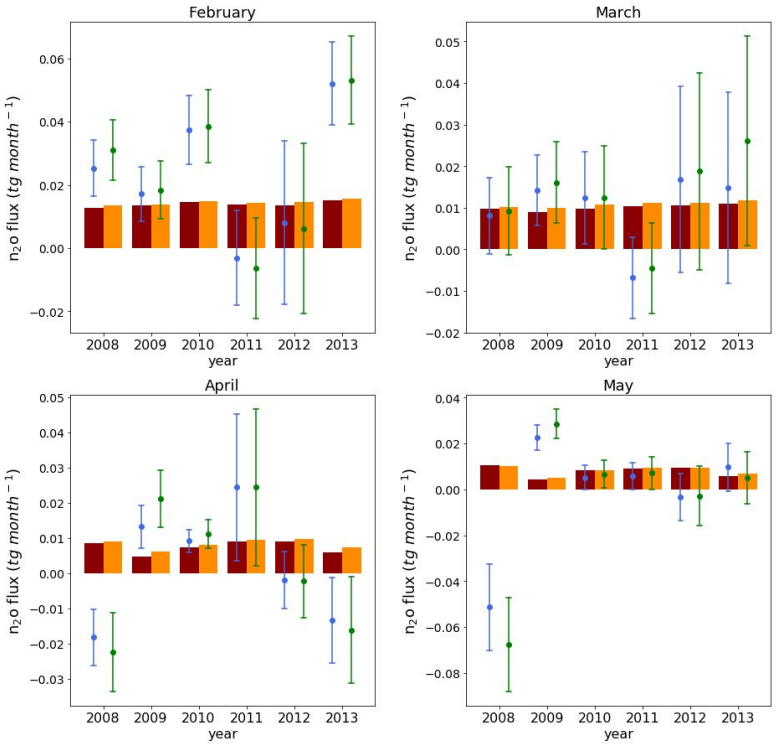

Figure 3K: Applied scaling factors with 95% confidence intervals are provided as the blue (Wanninkhov 92) and green (Krakaur) dots. The biogeochemical model predicted total fluxes for the sampled area are provided as the dark red (Wanninkhov 92) and orange (Krakaur) bars. Plots show the February to May period.

Looking at the results between June and September, there appears to be a similar annual pattern in the four months, with the total marine N_2O source after applying the scaling factors being lowest in 2010 and 2011 (excluding the September 2009 result), and very high uncertainty values in 2012 in all months. Outside of this period there is a lot of variability in the scaling factors calculated between different months. The annual variability in the adjusted N_2O source appears to bear little relationship with the annual variations in the N_2O source as predicted by the biogeochemical model.

3.2. Interannual variations

Tables 3B-3C and figures 3L-3M display the adjusted marine source against the original N_2O source in the sampled area as predicted by the biogeochemical model, by each individual month. The results of the analysis suggest that the biogeochemical model using both gas exchange parameterisations is slightly overestimating the N_2O source from the Southern Ocean. If the results are extrapolated over the all the southern oceans (south of -20°) then the results would be a Southern Ocean marine N_2O source 1.187 Tg N_2O yr^{-1} (instead of 1.429 Tg N_2O yr^{-1} as originally predicted) using the Wanninkhov 92 gas exchange parameterisation, or 1.329 Tg N_2O yr^{-1} (instead of 1.397 Tg N_2O yr^{-1} as originally predicted) using the Krakaur parameterisation.

When looking at the results by year (figures 7M-N), there is a close match in the total yearly N_2O source in 2008, 2009 and 2010, but a significant divergence between 2009 and 2011, with the data showing a decrease of approximately 0.1 Tg $year^{-1}$ compared with the average flux outside this period, whereas the model predicts a smaller increase in the total flux of approximately 0.05 Tg $year^{-1}$. $year^{-1}$.

Table 3B: Median adjusted marine source alongside original N_2O source in sampled area for Wanninkhov 92 gas exchange parameterisation.

	Jan	Feb	Mar	Apr	May	Jun	Jul	Aug	Sep	Oct	Nov	Dec	Total
Original WK92	0.017	0.014	0.010	0.008	0.009	0.015	0.022	0.034	0.038	0.026	0.020	0.019	0.232
Adjusted WK92	0.013	0.021	0.013	0.004	0.006	0.011	0.023	0.038	0.020	0.024	0.005	0.007	0.186

Table 3C: Median adjusted marine source alongside original N_2O source in sampled area for Krakaur gas exchange parameterisation.

	Jan	Feb	Mar	Apr	May	Jun	Jul	Aug	Sep	Oct	Nov	Dec	Total
Original Krakaur	0.018	0.015	0.011	0.009	0.009	0.014	0.020	0.029	0.033	0.027	0.021	0.020	0.226
Adjusted Krakaur	0.013	0.025	0.014	0.004	0.006	0.013	0.027	0.039	0.023	0.020	0.010	0.008	0.201

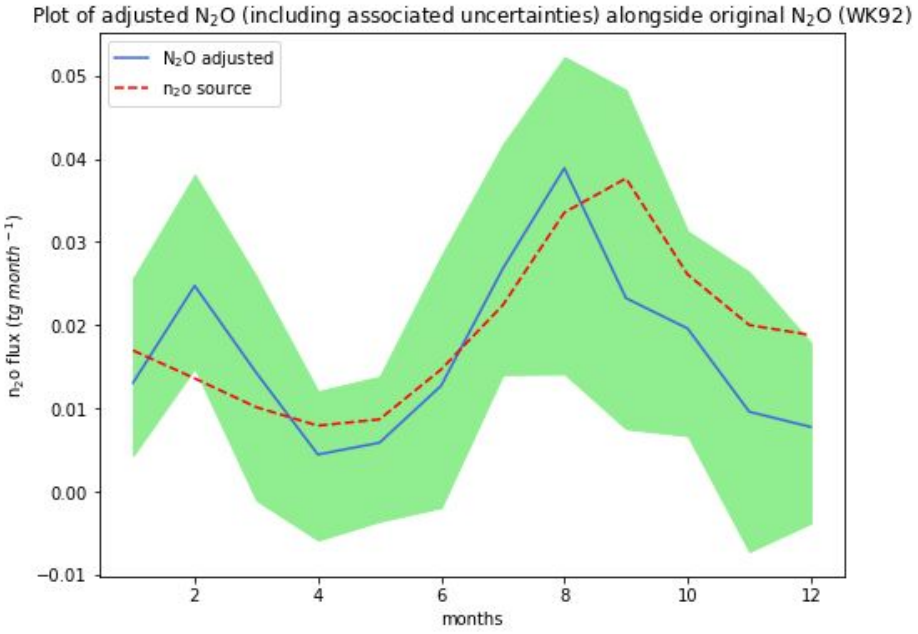

Figure 3L: Median original N_2O as predicted by the biogeochemical model (sum of total flux in sampled area) (red dashed line) alongside the median N_2O adjusted (sum of total flux in sampled area with scaling factor applied to each month) (blue line, green shading shows 95% confidence intervals) for the Wanninkhov 92 gas exchange parameterisation.

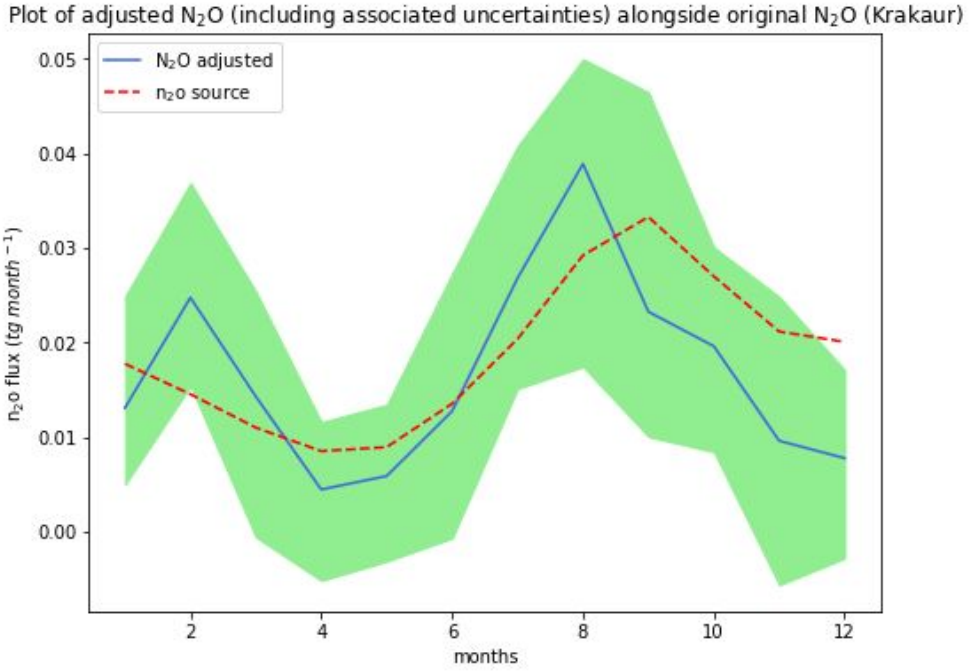

Figure 3M: Median original N_2O as predicted by the biogeochemical model (sum of total flux in sampled area) (red dashed line) alongside the median N_2O adjusted (sum of total flux in sampled area with scaling factor applied to each month) (blue line, green shading shows 95% confidence intervals) for the Krakaur gas exchange parameterisation.

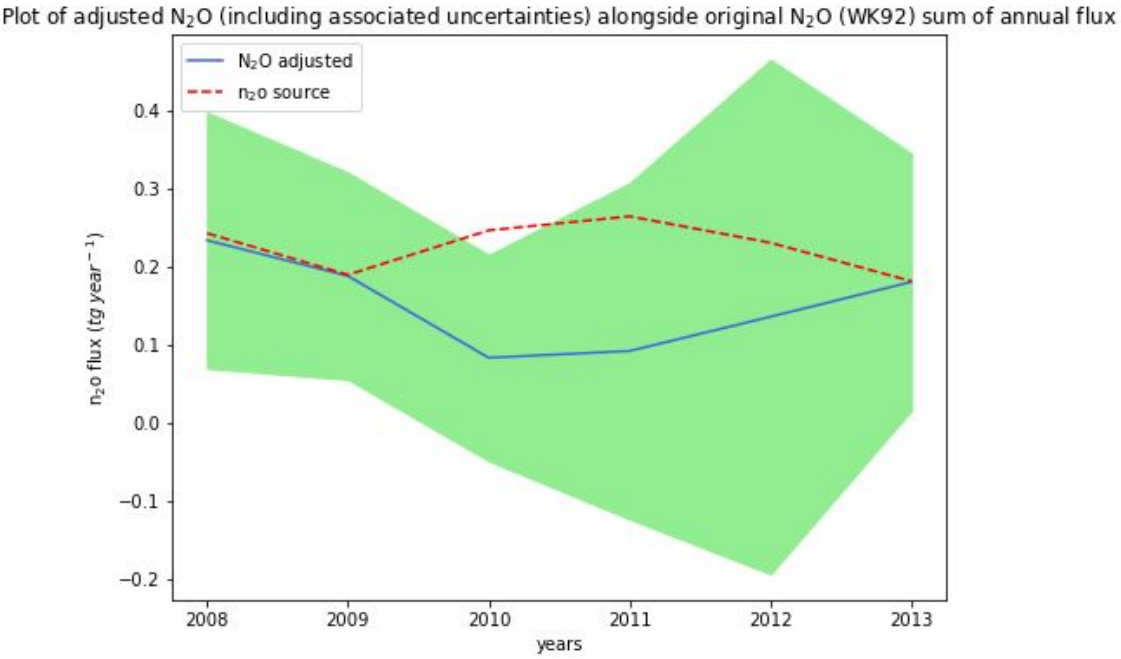

Figure 3N: Sum of original N_2O as predicted by the biogeochemical model (sum of total flux in sampled area) (red dashed line) alongside the sum of the N_2O adjusted (sum of total flux in sampled area with scaling factor applied to each month) (blue line, green shading shows 95% confidence intervals) for the Wanninkhov 92 gas exchange parameterisation.

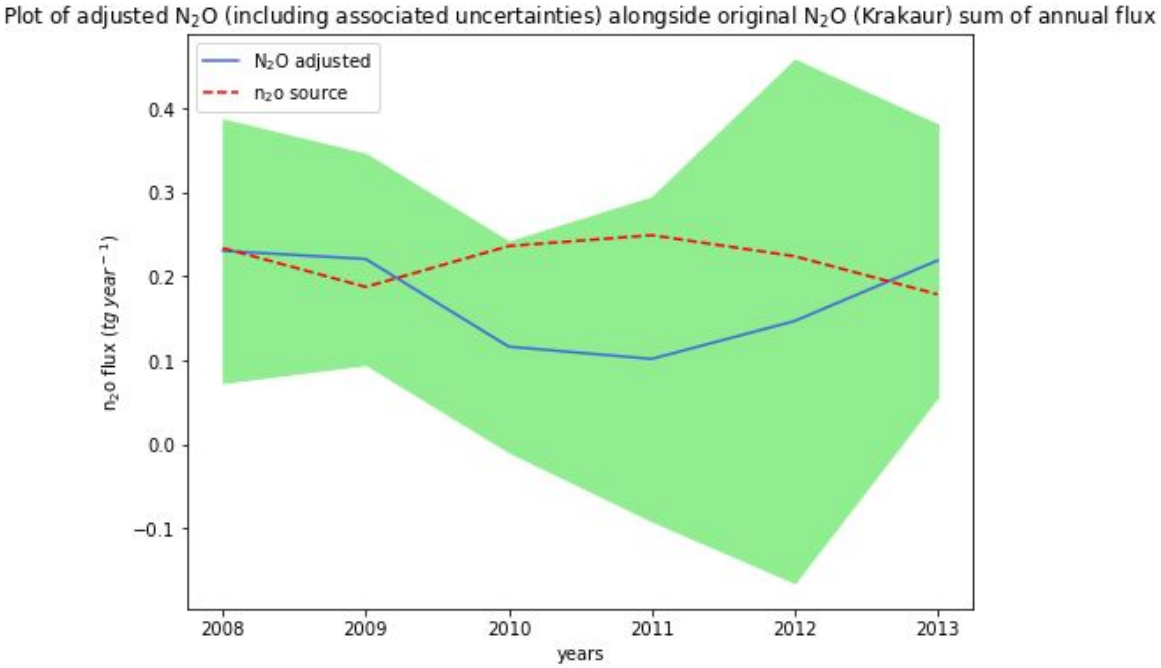

Figure 3O: Sum of original N_2O as predicted by the biogeochemical model (sum of total flux in sampled area) (red dashed line) alongside the sum of the N_2O adjusted (sum of total flux in sampled area with scaling factor applied to each month) (blue line, green shading shows 95% confidence intervals) for the Krakaur gas exchange parameterisation

A comparison of the mixed layer depths calculated by the biogeochemical model and from Argo profiling floats has been provided in the appendix. An example plot for August has been provided below (figure 3P). A climatology was calculated for the mixed layer depths estimated by the

biogeochemical model and then compared to the MLD climatology generated from Argo profiling floats. There is a plan to integrate Argo profiling data into the ECCO2-Darwin model although this has not been done in the dataset used in the analysis, so it is a useful comparison to see how well the model is estimating changes to the mixed layer depths which are responsible for the ventilation component of the mixing.

The colour axes in the Argo and model mixed layer depth plots vary from one month to the next, in order to better demonstrate the spatial patterns in the MLD in each month. The colour axes in plots which show the Argo – biogeochemical model MLD difference and the N_2O source are fixed in all months, in order to better display how the difference in MLD and the N_2O source varies between each month.

Comparing the Argo climatology with the biogeochemical model climatology reveals two interesting features. The biogeochemical model appears to be overestimating the mixed layer depths in higher latitudes north of -50°S and underestimating mixed layer depths in the lower latitudes south of -50°S. The MLD estimated by the biogeochemical model using the KPP vertical mixing parameterisation results in significant overestimations of the winter MLD, with the majority of cells south of the Australian coast having a mixed layer depth overestimated by over 200 m, when compared to the Argo MLD.

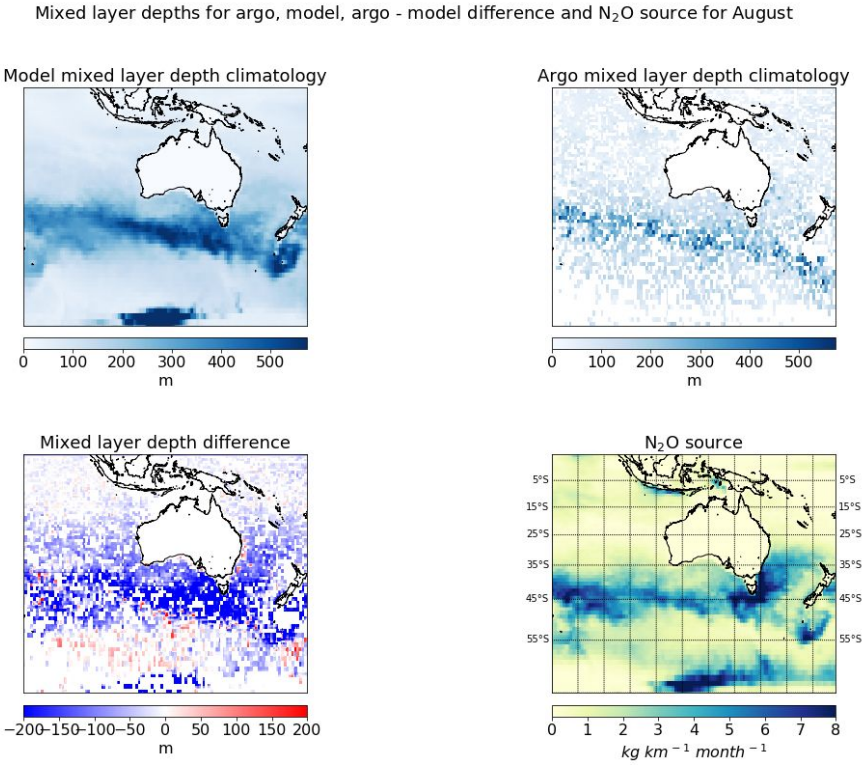

Figure 3P: Model predicted mixed layer depth (top left), Argo measured mix layer depth (top right), Argo MLD – Model MLD (bottom right), biogeochemical model estimated N_2O source (bottom right), for August

4. Discussion

4.1 Main conclusions

An atmospheric transport model was used to estimate how marine N_2O fluxes generated by an ocean-circulation model linked to a biogeochemical model would be observed up by an atmospheric monitoring site located at Cape Grim, Australia. A regression analysis of predicted atmospheric N_2O concentrations against observed concentrations was performed in order to assess the ability of the biogeochemical model to predict variations of atmospheric N_2O at Cape Grim using two different gas exchange parameterisations. The purpose of this study was to evaluate the ability to predict the marine N_2O source, to calculate scaling factors to upscale or downscale the N_2O fluxes predicted by the biogeochemical model and to assess whether there was a clear difference in the performance of two different gas exchange parameterisations.

On the whole the biogeochemical model performed reasonably, with the model estimated N_2O flux being within the 95% confidence intervals in all months but January, in both gas exchange parameterisations. However, the results have a high level of uncertainty in all months, with the biogeochemical model predicted N_2O source being within the range of uncertainty in all months except December of the Krakaur gas exchange parameterisation and February of the Wanninkhov 92 parameterisation.

The comparison between the two different gas exchange parameterisations yielded some interesting results, with the differences in the total flux calculated between the two methods being approximately 10% of the total flux, and the Krakaur gas exchange parameterisation producing a total uncertainty which was 17% less than the Wanninkhov 92 gas exchange parameterisation. The analysis performed using the Krakaur parameterisation produced uncertainties which were consistently equal to or smaller than the Wanninkhov 92 parameterisation in all months except April and May, where the uncertainties in Wanninkhov 92 were smaller. Due to the complicated nature of gas exchange dynamics, with the processes outlined in the introduction, it is possible that the performance of each gas exchange parameterisation may perform differently under certain wind regimes, and this could be worth further investigation.

However, not enough data was collected to perform a comprehensive analysis of the uncertainties in the various marine processes that contribute to the N_2O source, and it is difficult to draw strong conclusions with the available data. What is needed, is a more comprehensive examination of the uncertainties within the range of physical and biological factors that contribute to the marine N_2O source within the Southern Ocean, especially with regards to ocean circulation processes but possibly also taking into account biogeochemical production and uncertainties in the atmospheric transport model, in order to draw strong conclusions regarding the relative contribution of uncertainties in the different processes that are being examined by this analysis.

This study builds on the work of Nevison et al. (2005), who used the mean N_2O signal measured at Cape Grim, in combination with the O_2/N_2 ratio, to infer the seasonal cycle and total N_2O source for the Southern Ocean. One significant limitation of their analysis was that the effect of land observations were not accounted for. Our use the NAME atmospheric transport model shows that land emissions have a significant effect on the atmospheric N_2O mole fractions measured at Cape Grim, and thus the mean atmospheric N_2O at Cape Grim may not be a reliable signal of the marine N_2O source. Nevertheless, the results of this study are in broad agreement with the main conclusions of Nevison et al. (2005), in demonstrating that the Southern Ocean ventilation N_2O source is one

component of the atmospheric observations site, and in finding a similar seasonal cycle and total net Southern Ocean N_2O source to the 2005 study.

The N_2O source estimated for the all southern oceans south of 20° (1.187 Tg N_2O yr^{-1} WK92, 1.329 Tg N_2O yr^{-1} Kraur) was slightly smaller than the estimate provided in the global inversion study conducted by Thompson et al. (2014), which estimated the marine N_2O source in southern oceans south of 20° S to be 1.58 Tg N_2O yr^{-1}, however it was comfortably in the range of this estimate and other estimates of the Southern Ocean marine source, especially considering the large uncertainties present in the analysis. This study also found significant inter-annual variation in the Southern Ocean N_2O source in concurrence with the Thompson et al. (2014) study, as well as a stronger seasonal cycle than that predicted by the model, another feature of the global inversion study.

One surprising feature of the analysis was the divergence between the observed and predicted marine N_2O source between 2009 and 2011. This was especially surprising, because these were the months where the model predicted higher than average N_2O fluxes, whereas the regression analysis suggests that, especially in 2010 and 2011, the N_2O source is significantly lower than predicted by the model. This change is mainly driven by lower than expected adjusted fluxes in the winter months, between June and September, where N_2O fluxes are highest. A second unexpected result is the many negative scaling factors calculated in certain months, especially during periods where N_2O fluxes are low. These are unrealistic, and are probably due to the various errors and uncertainties which were unaccounted for in the analysis. The following section explores the errors and uncertainties in the analysis, before going on to discuss the key processes which may explain some of the these uncertainties.

4.2 Sources of error and uncertainty

Atmospheric transport modelling errors

Although several papers have conducted validation experiments on the NAME III model (Jones et al., 2007) and its predecessor, the NAME II model (Ryall and Meryon, 2006; 2008), and found it does well at predicting the spatial/temporal spread of the footprint and observed atmospheric concentrations of dispersion events, the model is not perfect and will introduce some error into the analysis.

These will affect both the predicted concentration of N_2O at Cape Grim, and also the estimated percentage of the N_2O fluxes measured at Cape Grim which originated from land sources. Regarding the second point, as Cape Grim is a coastal site close to terrestrial areas which are large sources of N_2O into the atmosphere, any errors in the spatial spread of the NAME generated footprint, which result in including data which has a significant terrestrial source could potentially add large amounts of error to the results. This analysis attempted to account for this by filtering the data so that periods where significant proportion of the total footprint was close to Cape Grim were excluded from the analysis. Footprints with high local influence are more often than not caused by low wind conditions, which increases the uncertainty of the footprint, so excluding data where the local influence is high has the double benefit of removing potentially inaccurate data from the analysis and excluding data which is more likely to have influence from localised terrestrial N_2O sources. Nevertheless, even after local filtering has been applied, uncertainty within the NAME model will still add some uncertainty to this analysis.

Observation errors

The measurement precision of the observations (Prinn et al., 2018) are approximately ~0.15 ppb (0.05%). While these are low compared to the baseline N_2O concentration of approximately 325 ppb, they are a significant proportion of the predicted atmospheric N_2O concentration measured at Cape Grim at any one-time due to marine sources. Even in peak months, predicted N_2O at Cape Grim due to air-sea flux rarely exceeded 0.5 ppb and thus the measurement error is a significant contributor to overall error. In most months, the largest predicted atmospheric N_2O concentrations were around 0.25 ppb, which would mean measurement error is approximately 50% of the observed maximum. The problem is even more significant in summer months where predicted N_2O rarely exceeded 0.15 ppb. This is a problem for lots of top-down estimates of N_2O from both marine and terrestrial sources, where the signals are small in comparison to the errors in the models and observations.

Errors introduced by the analysis

The orthogonal distance regression analysis depends primarily on the ratio between the errors in the data and the errors in the model. As no accurate assessment of the errors in the NAME and biogeochemical models exists, the standard deviation of the model-predicted N_2O concentrations was used to estimate model error. However, this is a relatively subjective measure of the uncertainty. The quality of the analysis could be improved if a better estimate of the errors related to the model predicted N_2O was available.

A second error introduced by the analysis is that the biogeochemical model dataset used to estimate the N_2O source was provided in a monthly resolution. As the underlying physical processes which are responsible for the Southern Ocean N_2O source are driven primarily by wind strength, which varies quite significantly over the course of a month, the loss of temporal resolution will undoubtedly have some impact on the results. Additionally, as wind speed and direction is also a key component in the atmospheric transport model, it is possible that the filtering, both by local influence and by percentage of footprint over land, may add some bias to the results by discriminating against certain wind regimes over others.

For this study higher resolution data was not available, however it would be a useful follow up study to perform this analysis with higher resolution model predicted fluxes, and see how that effects the total uncertainty and N_2O source estimated by this analysis.

4.3 Implications for our understanding of biological and physical processes leading to N2O emissions from the ocean

Gas exchange

This study found that the total uncertainty calculated using the Krakaur gas exchange parameterisation was lower than that calculated by the Wanninkhov 92 parameterisation, perhaps suggesting that the Krakaur model produces a better estimate of air-sea gas exchange. However, there were some interesting features within the results, such as the Wanninkhov 92 parameterisation having a smaller uncertainty in the months of April and May, perhaps suggesting that the performance of Krakaur is not better than the Wanninkhov 92 parametrisation under all wind regimes.

The two gas exchange parameterisations used in this study were calculated via completely different methods, and came up with two quite different relationships between wind speed and gas exchange, however the differences in the uncertainties of the two methods were only a small percentage of the total uncertainty, suggesting that a better understanding of air-sea gas exchange is not a priority when attempting to reduce the overall uncertainty of top down estimates of the

marine N_2O source. As the Southern Ocean experiences the fastest wind speeds on earth, as well as a great range of wind speeds with the large difference between winter and summer wind regimes, there is not a better place on the planet to investigate the effect that uncertainties in wind driven gas exchange has on the uncertainty of N_2O flux estimates, so I am confident that if this is true here, then it is also true elsewhere.

As mentioned earlier in this discussion, an extended analysis looking into the uncertainties of other processes, especially ocean mixing processes, is necessary to have a complete understanding of the relative importance uncertainties in air-sea gas exchange are to the total estimate of the marine N_2O source. Also, because of the important uncertainties and errors not taken into account by this analysis, especially the coarse resolution used to estimate a very temporarily variable process, more insight into the contribution of uncertainties with air-sea gas exchange could be gained by a follow up study which estimated the N_2O source at a finer resolution than was used in this analysis. However, this thesis represents an important first step, in demonstrating how a future analysis of this nature may be carried out.

Vertical mixing

Comparisons between a climatology of the modelled mixed layer depth and one created for Argo floats produced two interesting features. The first was that the biogeochemical model climatology was predicting deeper mixed layers than observed in the Argo dataset north of 50°S, and shallower mixed layer depths south of 50°S. The second was the large overestimation of the surface mixed layer north of 50°S in the winter months between June and October.

One plausible explanation could be due to buoyancy term in the KPP scheme parameterisation of vertical mixing. The buoyancy term will be affected by surface water temperatures in the surface mixed layer, which will change as you move from mid to high latitudes. Therefore, it is plausible to imagine a scenario where the KPP mixing scheme could underestimate the critical Richardson number in some areas and over estimate it in others, depending on surface temperatures. A third explanation could be the effects of other vertical mixing processes such as Langmuir circulation or the more controversial none-breaking wave induced turbulence.

The large overestimation in part is also interesting, partially because it does not seem to be having a significant effect on the N_2O flux estimates. There are a couple of potential explanations for this. One is that, in areas where there has already been a large deepening of the surface mixed layer, the difference between a mixed layer depth of 400 m and 600+ m may not have such a large effect on the N_2O concentration of the surface mixed layer. Another is that, if other turbulence driven processes are affecting the mixed layer depth, then even if the average mixed layer depth is being overestimated, there may still be more mixing. The effects on the mixed layer of turbulence driven processes are more instantaneous than with vertical shear instability, which requires the generation of horizontal currents at the base of the mixed layer. If more instantaneous processes are affecting the mixed layer depth, then the mixed layer depth may fluctuate more and induce a similar amount of mixing even if the average mixed layer depth is less.

Thermal air-sea flux

One process which has not been explored much in this thesis is the uncertainties in the thermal component of the N_2O source. Further investigation of this area is worthwhile as this does have a large impact on the net air-sea flux in some months.

4.4 Directions for further research

The processes of air-sea gas exchange and vertical mixing together have a big influence on the Southern Ocean N_2O source. Both these processes are influenced to a large extent by wind forcing, which is a temporally variable process. Therefore, using a single monthly value for each grid location will increase the errors in the analysis. Increasing the temporal resolution of the flux dataset could reduce these errors. There are a wide variety of different sources for high resolution wind speeds available, so increasing the temporal resolution for physical processes affected by wind forcing should be feasible.

Increasing our understanding of the key marine processes which affect the Southern Ocean N_2O source would help to reduce some of the uncertainty in our current understanding of the N_2O source in this region. Regarding the parameterisation of marine N_2O production, Nevison et al. (2003) identified the spatial variability in the abundances of nitrifying bacteria and the availability and composition of oxidizable organic matter, isopycnal mixing of water masses and N_2O transport from regions of high production into the wider ocean as being the three largest sources of uncertainty in the ΔN_2O/AOU ratio.

In investigating the physical processes responsible for driving the mixing of marine N_2O into the atmosphere, two quite different gas exchange parameterisations were utilised in this analysis, with the total uncertainty Krakaur parameterisation 17% less than with the Wanninkhov 92 parameterisation. This difference is only a small portion of the total uncertainty in the analysis, however both still used a simply parameterisation linked to wind speed, and thus do not represent the functional model of gas exchange discussed in Wanninkhov et al. (2009). Extending the analysis of gas exchange to use a functional model could be an interesting extension of this analysis.

A comparison of the mixed layer depths generated by the biogeochemical model and the Argo dataset (using the Holte et al. (2009) algorithm) found some large differences between the Argo mixed layer depths and those computed by the biogeochemical model in winter months. A better understanding of the physical mechanisms by which wind forcing affects mixing between the surface mixed layer and the underlying water would yield a more reliable N_2O source estimate. Additionally, this thesis has not investigated in great detail the uncertainties in the thermal contribution to net air-sea flux. One potential avenue could be to conduct a sensitivity study, where different gas exchange, thermal mixing and vertical mixing parameterisations are compared to see which combination of parameterisations yields the most reliable flux estimate and surface mixed layer depth.

An analysis that incorporates all of the above could build on the work presented in this analysis, and yield useful insights into how the various factors that affect top down estimates of the marine N_2O source contribute to the total uncertainty of current estimates. This study has attempted use atmospheric modelling in combination to investigate how atmospheric modelling can be used to constrain a marine biogeochemical model with atmospheric observations, comparing the results obtained using different parametrisations of some of the physical processes effecting the N_2O source. One strength of this thesis, is that there are not that many studies which use atmospheric modelling methodologies such as those used in this analysis to investigate uncertainties in the

parameterisations of processes responsible for the marine N_2O source. This study demonstrates that such a study could have potential to yield important insights into uncertainties surrounding the N_2O source, if it incorporates the improvements outlined above.

Finally, it would also be interesting to extend this analysis to other sites. Investigations into the AGAGE sites at Mace Head, Trinidad Head and Ragged Point found these sites to be unsuitable for an investigation of the N_2O source using this method, due to the prevailing wind conditions and N_2O source spatial distribution (in the case of Mace Head and Trinidad Head), or due to their lack of proximity to any significant N_2O source (Ragged Point). The AGAGE measurement site at Samoa may be more suitable for analysis, as it is far away from any significant landmass and reasonably close to an area of high predicted N_2O source in the Pacific Ocean. Furthermore, the N_2O source near this station may be subject to the influence of El Nino / La Nina cycles. Apart from AGAGE sites, the area off the coast of Peru could be an interesting location for further analysis, due to its proximity to a strong N_2O source, which will also be strongly influenced by the El Nino / La Nina cycles.

Appendix

Here is presented a comparison between the Argo mixed layer depths climatology (Holte et al., 2017) and the mixed layer depths calculated by the biogeochemical model. Vertical mixing of N_2O is the main factor influencing the seasonal cycle of N_2O, so a correct estimation of the mixed layer depth is very important for a correct estimation of the N_2O flux. The model mixed layer depth climatology was calculated as an average mixed layer depth over all years (as was the N_2O source).

Figure A1: Model predicted mixed layer depth (top left), Argo measured mix layer depth (top right), Argo MLD – Model MLD (bottom right), biogeochemical model estimated N_2O source (bottom right), for January.

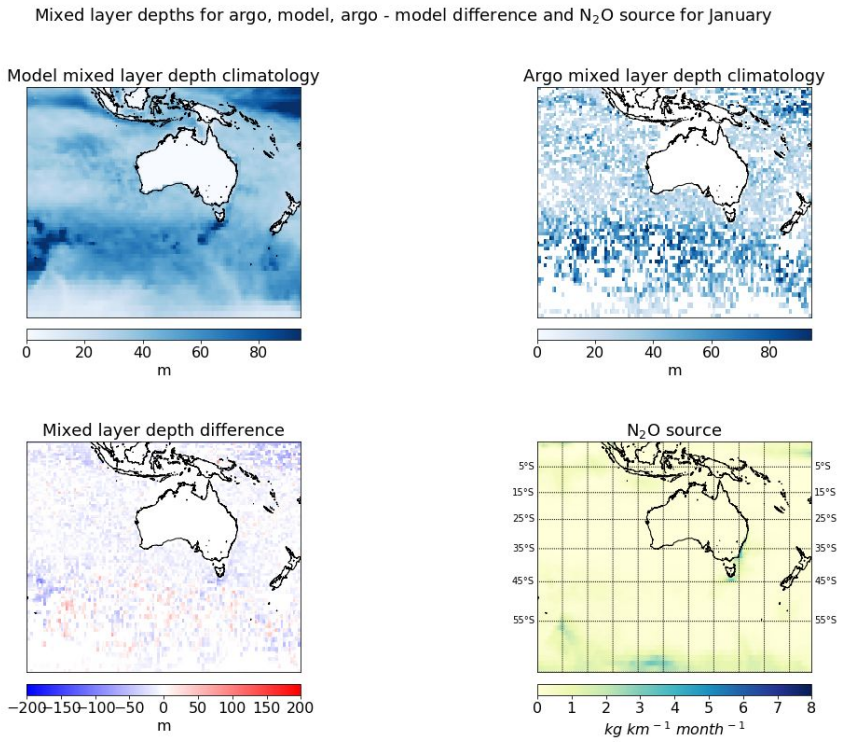

.

Figure A2: Model predicted mixed layer depth (top left), Argo measured mix layer depth (top right), Argo MLD – Model MLD (bottom right), biogeochemical model estimated N_2O source (bottom right), for February.

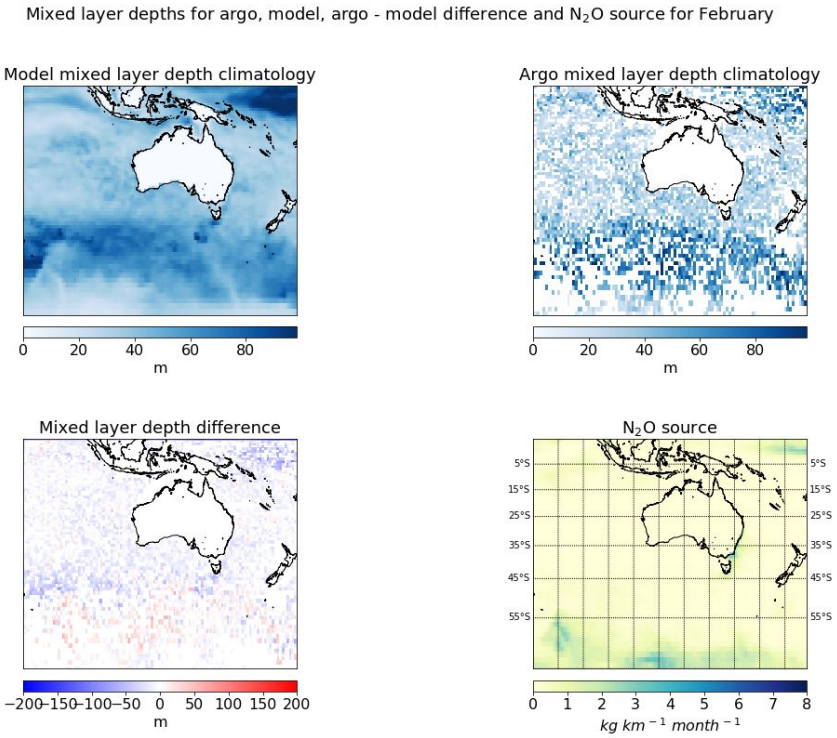

Figure A3 Model predicted mixed layer depth (top left), Argo measured mix layer depth (top right), Argo MLD – Model MLD (bottom right), biogeochemical model estimated N_2O source (bottom right), for March.

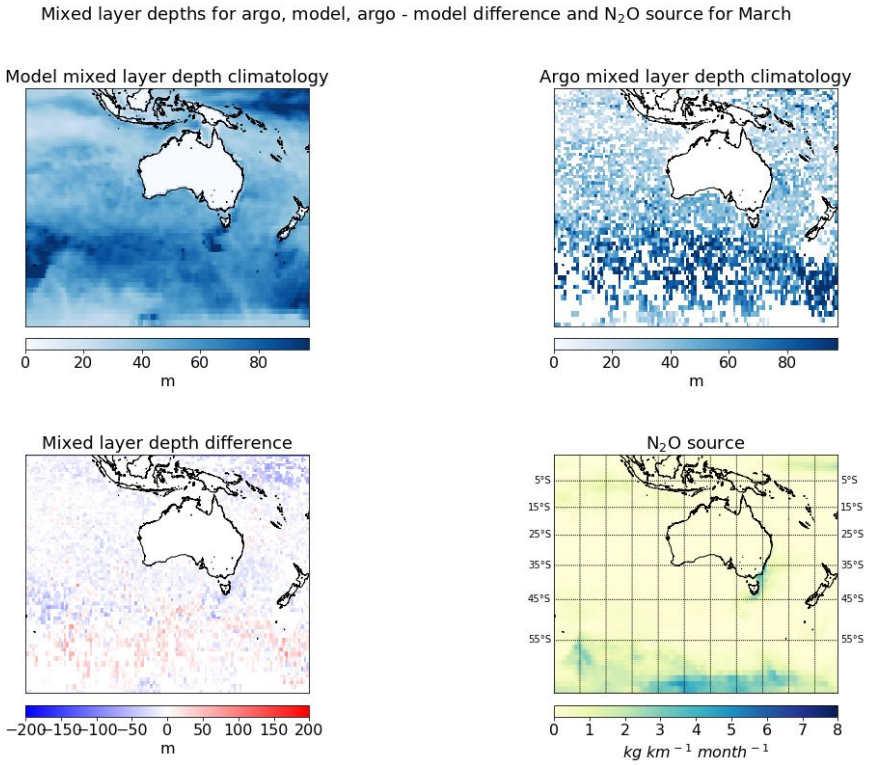

Figure A4: Model predicted mixed layer depth (top left), Argo measured mix layer depth (top right), Argo MLD – Model MLD (bottom right), biogeochemical model estimated N_2O source (bottom right), for April.

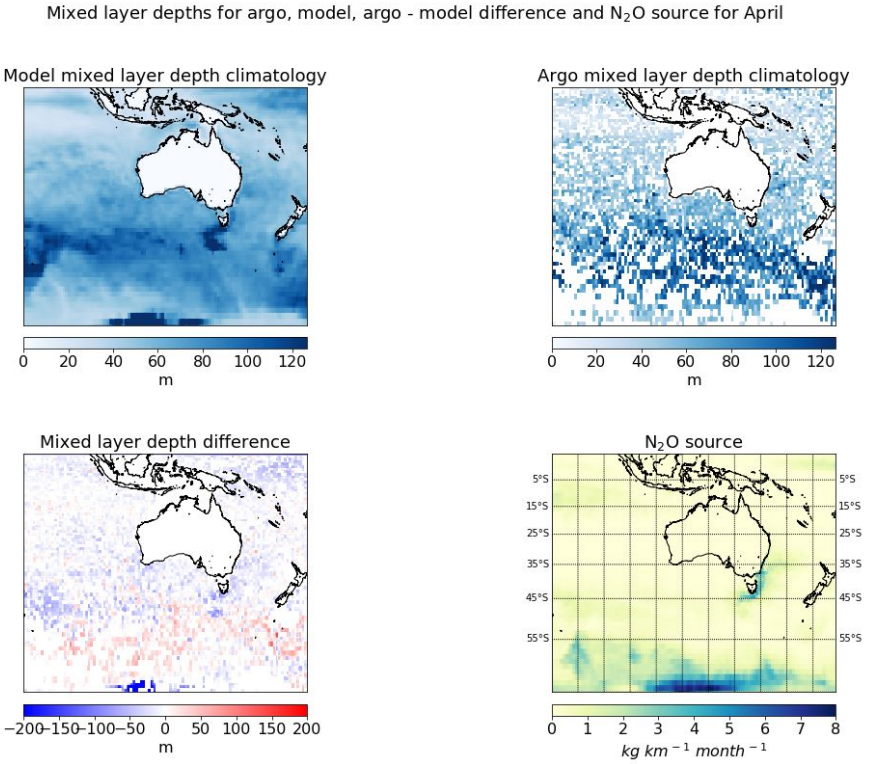

Figure A5: Model predicted mixed layer depth (top left), Argo measured mix layer depth (top right), Model MLD – Argo MLD (bottom right), biogeochemical model estimated N_2O source (bottom right), for May.

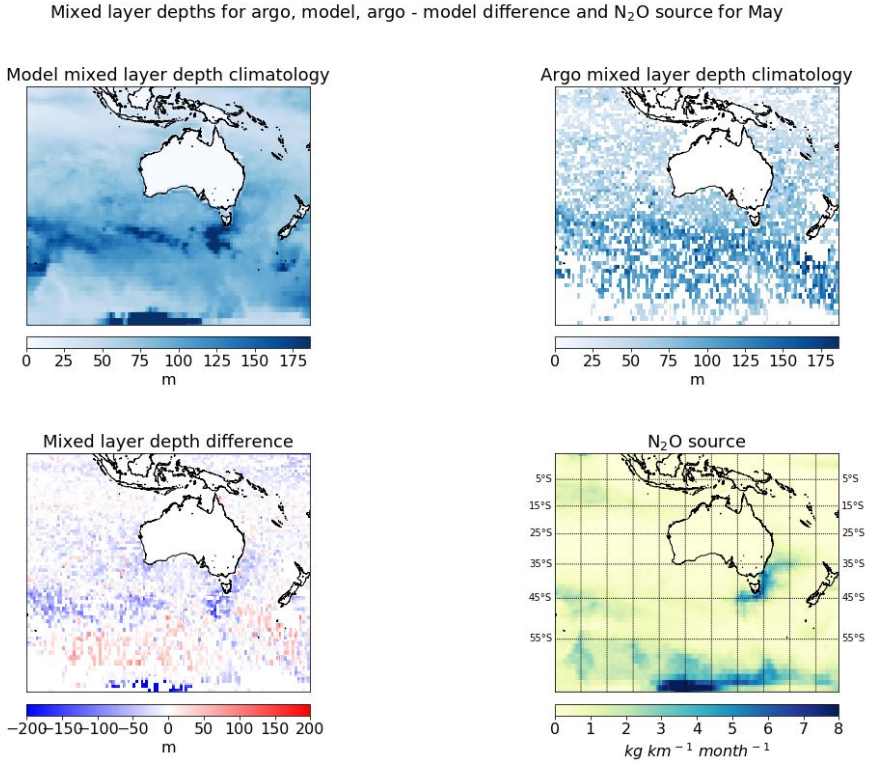

Figure A6: Model predicted mixed layer depth (top left), Argo measured mix layer depth (top right), Argo MLD – Model MLD (bottom right), biogeochemical model estimated N_2O source (bottom right), for June.

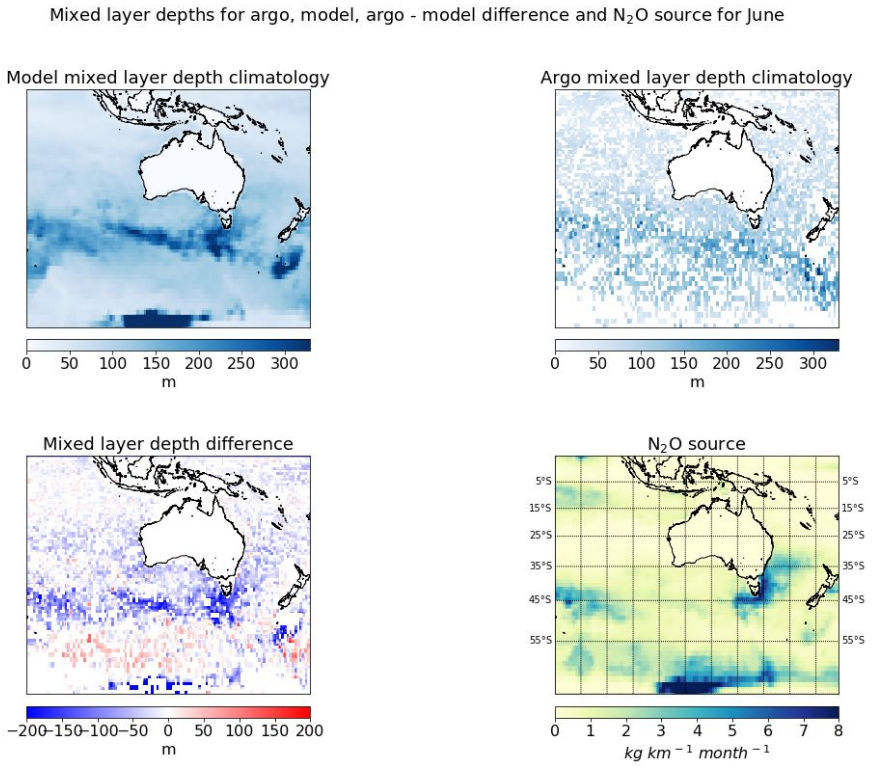

Figure A7: Model predicted mixed layer depth (top left), Argo measured mix layer depth (top right), Argo MLD – Model MLD (bottom right), biogeochemical model estimated N_2O source (bottom right), for July.

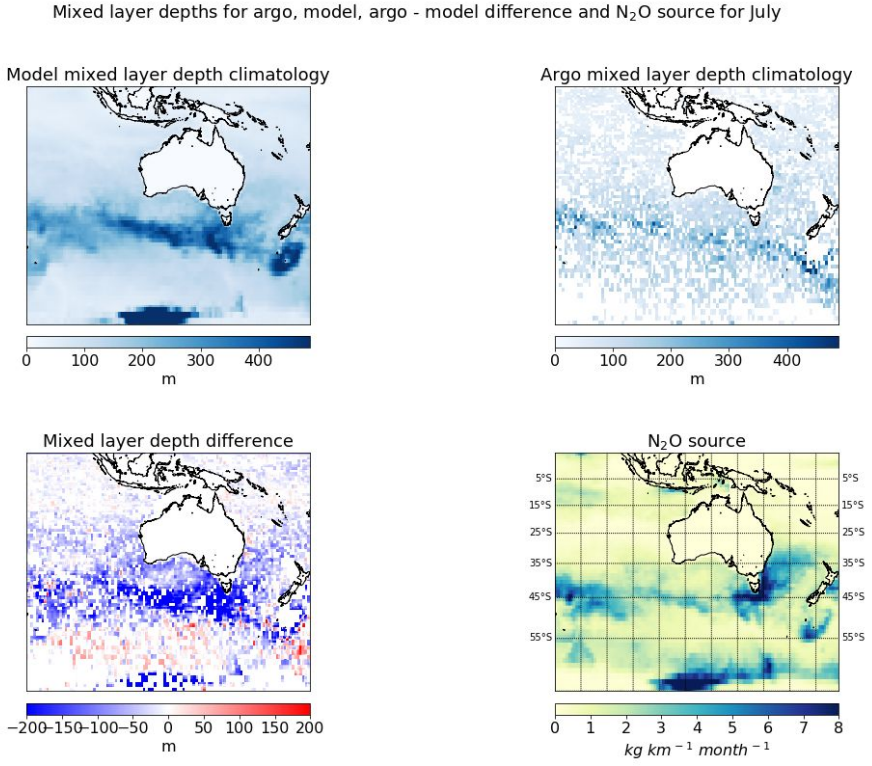

Figure A8: Model predicted mixed layer depth (top left), Argo measured mix layer depth (top right), Argo MLD – Model MLD (bottom right), biogeochemical model estimated N_2O source (bottom right), for August

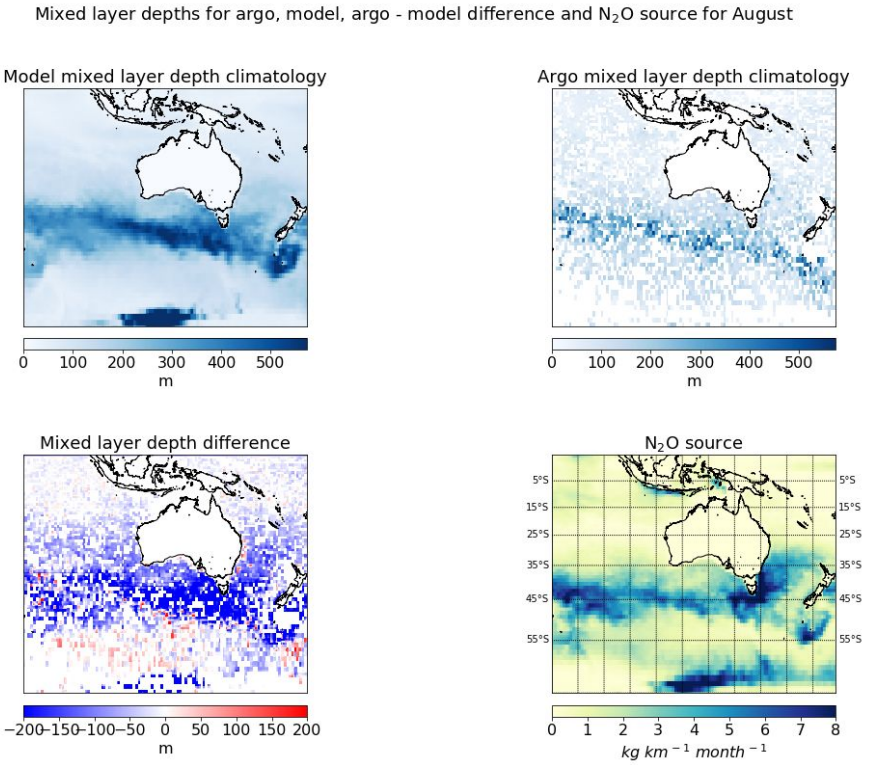

Figure A9: Model predicted mixed layer depth (top left), Argo measured mix layer depth (top right), Argo MLD – Model MLD (bottom right), biogeochemical model estimated N_2O source (bottom right), for September

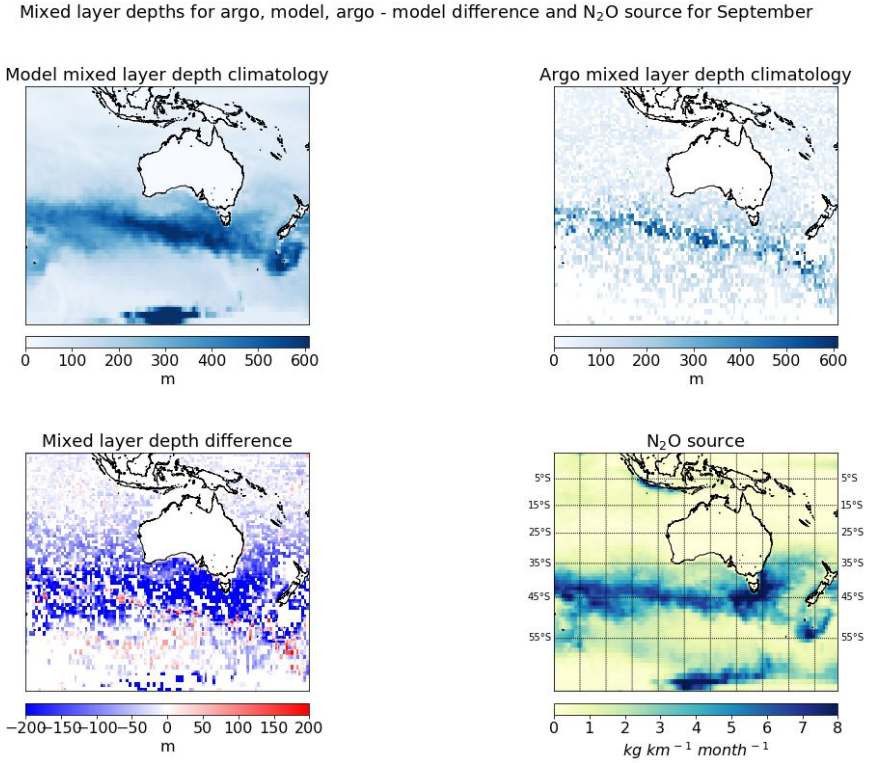

Figure A10: Model predicted mixed layer depth (top left), Argo measured mix layer depth (top right), Argo MLD – Model MLD (bottom right), biogeochemical model estimated N_2O source (bottom right), for October

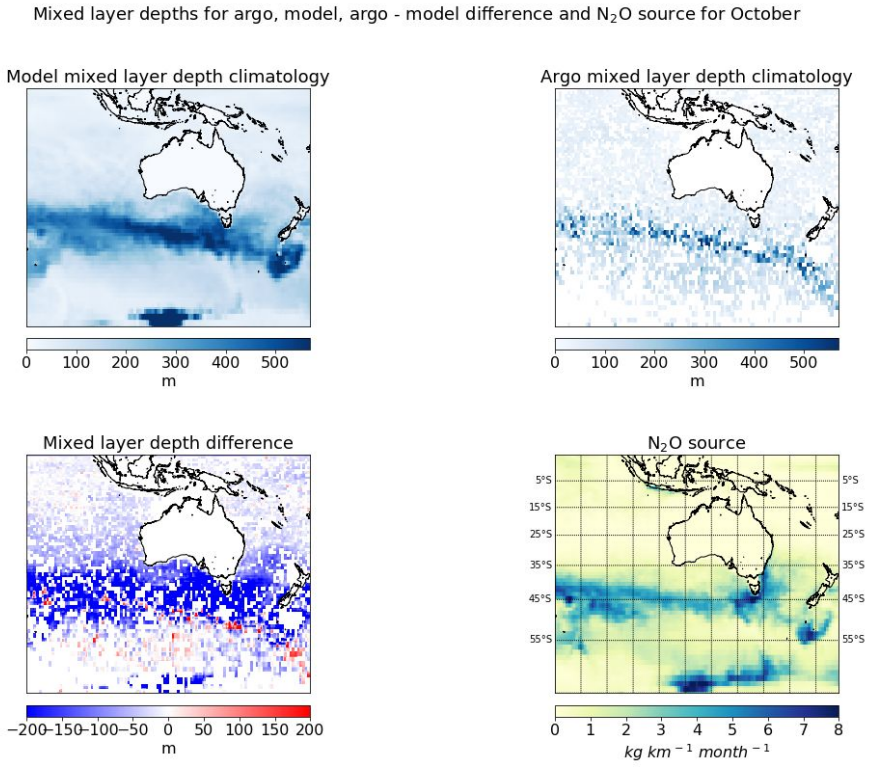

Figure A11: Model predicted mixed layer depth (top left), Argo measured mix layer depth (top right), Argo MLD – Model MLD (bottom right), biogeochemical model estimated N_2O source (bottom right), for November

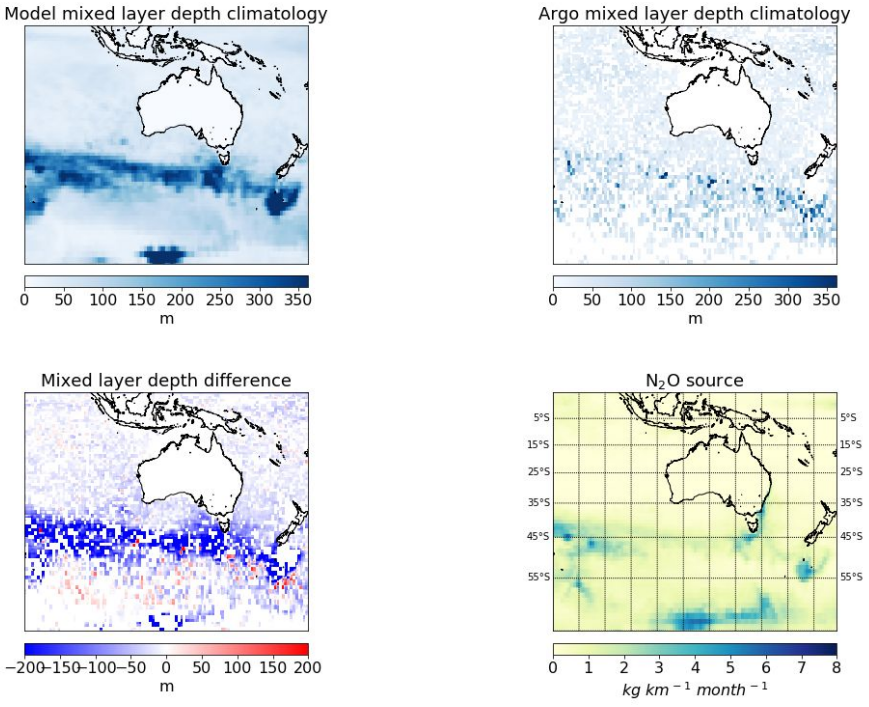

Figure A12: Model predicted mixed layer depth (top left), Argo measured mix layer depth (top right), Argo MLD – Model MLD (bottom right), biogeochemical model estimated N_2O source (bottom right), for December

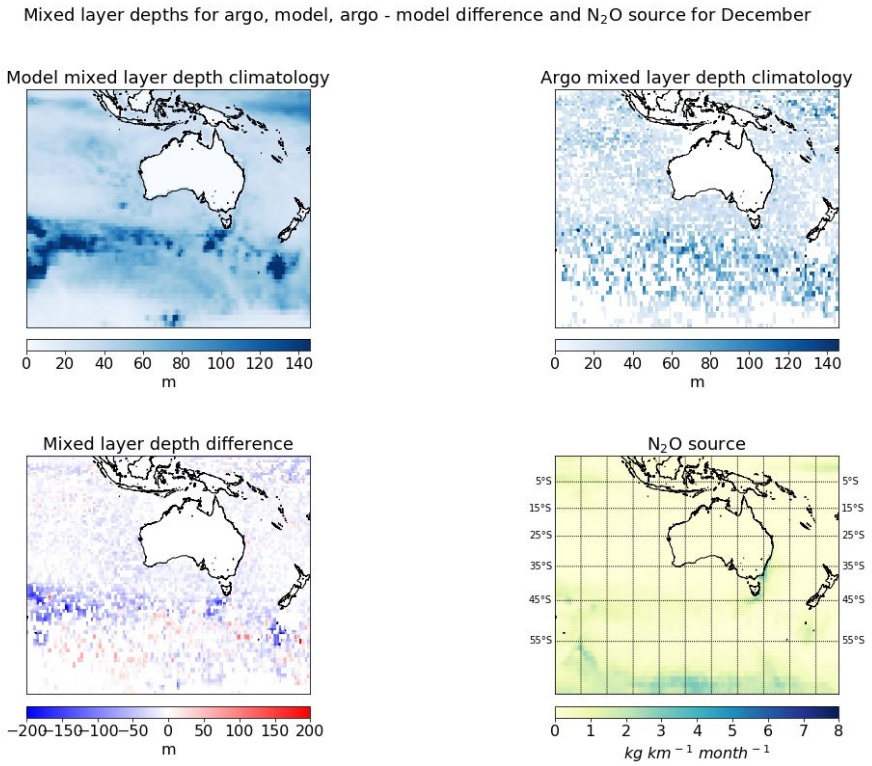

References

ANDERSON, L. A. & SARMIENTO, J. L. 1994. REDFIELD RATIOS OF REMINERALIZATION DETERMINED BY NUTRIENT DATA-ANALYSIS. *Global Biogeochemical Cycles,* 8**,** 65-80.

BABANIN, A. V. & HAUS, B. K. 2009. On the Existence of Water Turbulence Induced by Nonbreaking Surface Waves. *Journal of Physical Oceanography,* 39**,** 2675-2679.

BAGGS, E. M. 2008. A review of stable isotope techniques for N 2 O source partitioning in soils: recent progress, remaining challenges and future considerations. *Rapid Communications in Mass Spectrometry,* 22**,** 1664-1672.

BANGE, H. W. 2006a. New Directions: The importance of oceanic nitrous oxide emissions.

BANGE, H. W. 2006b. Nitrous oxide and methane in European coastal waters. *Estuarine, Coastal and Shelf Science,* 70**,** 361-374.

BANGE, H. W. 2008. Gaseous nitrogen compounds (NO, N₂O, N₂, NH₃) in the ocean. *In:* CAPONE, D. G., BRONK, D. A., MULHOLLAND, M. R. & CARPENTER, E. J. (eds.) *Nitrogen in the Marine Environment.* Amsterdam: Elsevier.

BANGE, H. W. & ANDREAE, M. O. 1999. Nitrous oxide in the deep waters of the world's oceans. *Global Biogeochemical Cycles,* 13**,** 1127-1135.

BEYA, J. F., PEIRSON, W. L. & BANNER, M. L. 2012. Turbulence beneath finite amplitude water waves. *Experiments in Fluids,* 52**,** 1319-1330.

BRIX, H., MENEMENLIS, D., HILL, C., DUTKIEWICZ, S., JAHN, O., WANG, D., BOWMAN, K. & ZHANG, H. 2015. Using Green's Functions to initialize and adjust a global, eddying ocean biogeochemistry general circulation model. *Ocean Modelling,* 95**,** 1-14.

BROECKER, W. S., LEDWELL, J. R., TAKAHASHI, T., WEISS, R., MERLIVAT, L., MEMERY, L., PENG, T. H., JAHNE, B. & MUNNICH, K. O. 1986. ISOTOPIC VERSUS MICROMETEOROLOGICAL OCEAN CO2 FLUXES - A SERIOUS CONFLICT. *Journal of Geophysical Research-Oceans,* 91**,** 517-527.

BROECKER, W. S. & PENG, T.-H. (1982) *Tracers in the Sea*, Palisades, NY, Eldigio Press: Lamont-Doherty Geological Observatory.

BROECKER, W. S., PENG, T. H., OSTLUND, G. & STUIVER, M. 1985. THE DISTRIBUTION OF BOMB RADIOCARBON IN THE OCEAN. *Journal of Geophysical Research-Oceans,* 90**,** 6953-6970.

CODISPOTI, L. A., ELKINS, J. W., YOSHINARI, T., FRIEDERICH, G. E., SAKAMOTO, C. M. & PACKARD, T. T. 1993. ON THE NITROUS-OXIDE FLUX FROM PRODUCTIVE REGIONS THAT CONTAIN LOW OXYGEN WATERS. *Oceanography of the Indian Ocean***,** 271-284.

CRAIK, A. D. D. & LEIBOVICH, S. 1976. RATIONAL MODEL FOR LANGMUIR CIRCULATIONS. *Journal of Fluid Mechanics,* 73**,** 401-426.

D'ASARO, E. A. 2014. Turbulence in the Upper-Ocean Mixed Layer. *In:* CARLSON, C. A. & GIOVANNONI, S. J. (eds.) *Annual Review of Marine Science, Vol 6.* Palo Alto: Annual Reviews.

DAI, D. J., QIAO, F. L., SULISZ, W., HAN, L. & BABANIN, A. 2010. An Experiment on the Nonbreaking Surface-Wave-Induced Vertical Mixing. *Journal of Physical Oceanography,* 40**,** 2180-2188.

DASARO, E. A. & DAIRIKI, G. T. 1997. Turbulence intensity measurements in a wind-driven mixed layer. *Journal of Physical Oceanography,* 27**,** 2009-2022.

DEACON, E. L. 1977. GAS TRANSFER TO AND ACROSS AN AIR-WATER-INTERFACE. *Tellus,* 29**,** 363-374.
FAIRAILL, C. W., HARE, J. E., EDSON, J. B. & MCGILLIS, W. 2000. Parameterization and micrometeorological measurement of air-sea gas transfer. *Boundary-Layer Meteorology,* 96**,** 63-105.
FALLER, A. J. 1978. EXPERIMENTS WITH CONTROLLED LANGMUIR CIRCULATIONS. *Science,* 201**,** 618-620.
FARMER, D. M., MCNEIL, C. L. & JOHNSON, B. D. 1993. EVIDENCE FOR THE IMPORTANCE OF BUBBLES IN INCREASING AIR SEA GAS FLUX. *Nature,* 361**,** 620-623.
FROLICHER, T. L., SARMIENTO, J. L., PAYNTER, D. J., DUNNE, J. P., KRASTING, J. P. & WINTON, M. 2015. Dominance of the Southern Ocean in Anthropogenic Carbon and Heat Uptake in CMIP5 Models. *Journal of Climate,* 28**,** 862-886.
FROST, T. & UPSTILL-GODDARD, R. C. 1999. Air-sea gas exchange into the millennium: Progress and uncertainties. *Oceanography and Marine Biology, Vol 37,* 37**,** 1-45.
FUHRMAN, J. A. & CAPONE, D. G. 1991. POSSIBLE BIOGEOCHEMICAL CONSEQUENCES OF OCEAN FERTILIZATION. *Limnology and Oceanography,* 36**,** 1951-1959.
GALLOWAY, J. N., ABER, J. D., ERISMAN, J. W., SEITZINGER, S. P., HOWARTH, R. W., COWLING, E. B. & COSBY, B. J. 2003. The nitrogen cascade. *Bioscience,* 53**,** 341-356.
GARBE, C. S., SCHIMPF, U. & JAHNE, B. 2004. A surface renewal model to analyze infrared image sequences of the ocean surface for the study of air-sea heat and gas exchange. *Journal of Geophysical Research-Oceans,* 109**,** 18.
GARCIA, R. R. & SOLOMON, S. 1994. A NEW NUMERICAL-MODEL OF THE MIDDLE ATMOSPHERE .2. OZONE AND RELATED SPECIES. *Journal of Geophysical Research-Atmospheres,* 99**,** 12937-12951.
GENT, P. R., BRYAN, F. O., DANABASOGLU, G., DONEY, S. C., HOLLAND, W. R., LARGE, W. G. & MCWILLIAMS, J. C. 1998. The NCAR Climate System Model global ocean component. *Journal of Climate,* 11**,** 1287-1306.
GERBI, G. P., TROWBRIDGE, J. H., EDSON, J. B., PLUEDDEMANN, A. J., TERRAY, E. A. & FREDERICKS, J. J. 2008. Measurements of momentum and heat transfer across the air-sea interface. *Journal of Physical Oceanography,* 38**,** 1054-1072.
GHANTOUS, M. & BABANIN, A. V. 2014. One-dimensional modelling of upper ocean mixing by turbulence due to wave orbital motion. *Nonlinear Processes in Geophysics,* 21**,** 325-338.
HIGBIE, R. 1935. The rate of absorption of a pure gas into a still liquid during short periods of exposure. *Transactions of the American Institute of Chemical Engineers,* 31**,** 365-389.
HO, D. T., ASHER, W. E., BLIVEN, L. F., SCHLOSSER, P. & GORDAN, E. L. 2000. On mechanisms of rain-induced air-water gas exchange. *Journal of Geophysical Research-Oceans,* 105**,** 24045-24057.
HOLTE, J. & TALLEY, L. 2009. A New Algorithm for Finding Mixed Layer Depths with Applications to Argo Data and Subantarctic Mode Water Formation. *Journal of Atmospheric and Oceanic Technology,* 26**,** 1920-1939.
HOLTE, J., TALLEY, L. D., GILSON, J. & ROEMMICH, D. 2017. An Argo mixed layer climatology and database. *Geophysical Research Letters,* 44**,** 5618-5626.
HORRIGAN, S. G., CARLUCCI, A. F. & WILLIAMS, P. M. 1981. LIGHT INHIBITION

OF NITRIFICATION IN SEA-SURFACE FILMS. *Journal of Marine Research,* 39**,** 557-565.

HUANG, C. J., QIAO, F. L., SONG, Z. Y. & EZER, T. 2011. Improving simulations of the upper ocean by inclusion of surface waves in the Mellor-Yamada turbulence scheme. *Journal of Geophysical Research-Oceans,* 116**,** 13.

HUANG, J., GOLOMBEK, A., PRINN, R., WEISS, R., FRASER, P., SIMMONDS, P., DLUGOKENCKY, E. J., HALL, B., ELKINS, J., STEELE, P., LANGENFELDS, R., KRUMMEL, P., DUTTON, G. & PORTER, L. 2008. Estimation of regional emissions of nitrous oxide from 1997 to 2005 using multinetwork measurements, a chemical transport model, and an inverse method. *Journal of Geophysical Research-Atmospheres,* 113**,** 19.

ISHIJIMA, K., SUGAWARA, S., KAWAMURA, K., HASHIDA, G., MORIMOTO, S., MURAYAMA, S., AOKI, S. & NAKAZAWA, T. 2007. Temporal variations of the atmospheric nitrous oxide concentration and its δ 15 N and δ 18 O for the latter half of the 20th century reconstructed from firn air analyses. *Journal of Geophysical Research: Atmospheres,* 112**,** n/a-n/a.

JIN, X. & GRUBER, N. 2003. Offsetting the radiative benefit of ocean iron fertilization by enhancing N2O emissions. *Geophysical Research Letters,* 30**,** n/a-n/a.

JOOS, F., ROTH, R., FUGLESTVEDT, J. S., PETERS, G. P., ENTING, I. G., BLOH, W. V., BROVKIN, V., BURKE, E. J., EBY, M., EDWARDS, N. R., FRIEDRICH, T., FRÖLICHER, T. L., HALLORAN, P. R., HOLDEN, P. B., JONES, C., KLEINEN, T., MACKENZIE, F. T., MATSUMOTO, K., MEINSHAUSEN, M., PLATTNER, G. K., REISINGER, A., SEGSCHNEIDER, J., SHAFFER, G., STEINACHER, M., STRASSMANN, K., TANAKA, K., TIMMERMANN, A. & WEAVER, A. J. 2013. Carbon dioxide and climate impulse response functions for the computation of greenhouse gas metrics: a multi-model analysis. *Atmospheric Chemistry and Physics,* 13**,** 2793-2825.

JORGENSEN, K. S., JENSEN, H. B. & SORENSEN, J. 1984. NITROUS-OXIDE PRODUCTION FROM NITRIFICATION AND DENITRIFICATION IN MARINE SEDIMENT AT LOW OXYGEN CONCENTRATIONS. *Canadian Journal of Microbiology,* 30**,** 1073-1078.

KOSTOV, Y., ARMOUR, K. C. & MARSHALL, J. 2014. Impact of the Atlanticmeridional overturning circulation on ocean heat storage and transient climate change. *Geophysical Research Letters,* 41**,** 2108-2116.

KRAKAUER, N. Y., RANDERSON, J. T., PRIMEAU, F. W., GRUBER, N. & MENEMENLIS, D. 2006. Carbon isotope evidence for the latitudinal distribution and wind speed dependence of the air-sea gas transfer velocity. *Tellus Series B-Chemical and Physical Meteorology,* 58**,** 390-417.

LANGMUIR, I. 1938. Surface motion of water induced by wind. *Science,* 87**,** 119-123.

LARGE, W. G. & CRAWFORD, G. B. 1995. OBSERVATIONS AND SIMULATIONS OF UPPER-OCEAN RESPONSE TO WIND EVENTS DURING THE OCEAN STORMS EXPERIMENT. *Journal of Physical Oceanography,* 25**,** 2831-2852.

LARGE, W. G., DANABASOGLU, G., DONEY, S. C. & MCWILLIAMS, J. C. 1997. Sensitivity to surface forcing and boundary layer mixing in a global ocean model: Annual-mean climatology. *Journal of Physical Oceanography,* 27**,** 2418-2447.

LARGE, W. G., MCWILLIAMS, J. C. & DONEY, S. C. 1994. OCEANIC VERTICAL MIXING - A REVIEW AND A MODEL WITH A NONLOCAL BOUNDARY-LAYER PARAMETERIZATION. *Reviews of Geophysics,* 32**,**

363-403.
LARGE, W. G. G. & GENT, P. R. 1999. Validation of vertical mixing in an equatorial ocean model using large eddy simulations and observations. *Journal of Physical Oceanography,* 29**,** 449-464.
LAW, C. S., REES, A. P. & OWENS, N. J. P. 1991. Temporal variability of denitrification in estuarine sediments. *Estuarine, Coastal and Shelf Science,* 33**,** 37-56.
LI, Q., WEBB, A., FOX-KEMPER, B., CRAIG, A., DANABASOGLU, G., LARGE, W. G. & VERTENSTEIN, M. 2016. Langmuir mixing effects on global climate: WAVEWATCH III in CESM. *Ocean Modelling,* 103**,** 145-160.
LINGENFELTER, R. E. 1963. PRODUCTION OF CARBON-14 BY COSMIC-RAY NEUTRONS. *Reviews of Geophysics,* 1**,** 35-55.
LINICK, T. W. 1980. BOMB-PRODUCED C-14 IN THE SURFACE-WATER OF THE PACIFIC OCEAN. *Radiocarbon,* 22**,** 599-606.
LISS, P. S. & L., M. 1986. Air-sea gas exchange rates: introduction and synthesis . *In:* BUAT-MÉNARD, P. (ed.) *The Role of Air-Sea Exchange in Geochemical Cycling.* D. Reidel, Dordrecht.
LISS, P. S. & SLATER, P. G. 1974. FLUX OF GASES ACROSS AIR-SEA INTERFACE. *Nature,* 247**,** 181-184.
LUEKER, T. J., WALKER, S. J., VOLLMER, M. K., KEELING, R. F., NEVISON, C. D., WEISS, R. F. & GARCIA, H. E. 2003. Coastal upwelling air-sea fluxes revealed in atmospheric observations of O-2/N-2, CO2 and N2O. *Geophysical Research Letters,* 30**,** 4.
LUNT, M. F., RIGBY, M., GANESAN, A. J. & MANNING, A. J. 2016. Estimation of trace gas fluxes with objectively determined basis functions using reversible-jump Markov chain Monte Carlo. *Geosci. Model Dev.,* 9**,** 3213-3229.
MACFARLING MEURE, C., ETHERIDGE, D., TRUDINGER, C., STEELE, P., LANGENFELDS, R., VAN OMMEN, T., SMITH, A. & ELKINS, J. 2006. Law Dome CO2, CH4 and N2O ice core records extended to 2000 years BP. *Geophysical Research Letters,* 33**,** 4.
MACK, S. A. & SCHOEBERLEIN, H. C. 2004. Richardson number and ocean mixing: Towed chain observations. *Journal of Physical Oceanography,* 34**,** 736-754.
MANIZZA, M., KEELING, R. F. & NEVISON, C. D. 2012. On the processes controlling the seasonal cycles of the air-sea fluxes of O-2 and N2O: A modelling study. *Tellus Series B-Chemical and Physical Meteorology,* 64**,** 18.
MARSHALL, G. J. 2003. Trends in the southern annular mode from observations and reanalyses. *Journal of Climate,* 16**,** 4134-4143.
MARSHALL, J., ADCROFT, A., HILL, C., PERELMAN, L. & HEISEY, C. 1997. A finite-volume, incompressible Navier Stokes model for studies of the ocean on parallel computers. *Journal of Geophysical Research-Oceans,* 102**,** 5753-5766.
MARSHALL, J. & SPEER, K. 2012. Closure of the meridional overturning circulation through Southern Ocean upwelling. *Nature Geoscience,* 5**,** 171-180.
MCGILLIS, W. R., EDSON, J. B., ZAPPA, C. J., WARE, J. D., MCKENNA, S. P., TERRAY, E. A., HARE, J. E., FAIRALL, C. W., DRENNAN, W., DONELAN, M., DEGRANDPRE, M. D., WANNINKHOF, R. & FEELY, R. A. 2004. Air-sea CO2 exchange in the equatorial Pacific. *Journal of Geophysical Research-Oceans,* 109**,** 17.
MCNEIL, C. & D'ASARO, E. 2007. Parameterization of air-sea gas fluxes at extreme wind speeds. *Journal of Marine Systems,* 66**,** 110-121.
MELLOR, G. L. & DURBIN, P. A. 1975. STRUCTURE AND DYNAMICS OF OCEAN

SURFACE MIXED LAYER. *Journal of Physical Oceanography,* 5**,** 718-728.
MIDDELBURG, J. J., KLAVER, G., NIEUWENHUIZE, J., MARKUSSE, R. M., VLUG, T. & VAN DER NAT, F. J. W. A. 1995. Nitrous oxide emissions from estuarine intertidal sediments. *Hydrobiologia,* 311**,** 43-55.
MILES, J. W. 1961. ON THE STABILITY OF HETEROGENEOUS SHEAR FLOWS. *Journal of Fluid Mechanics,* 10**,** 496-508.
MILES, J. W. 1963. ON THE STABILITY OF HETEROGENEOUS SHEAR FLOWS .2. *Journal of Fluid Mechanics,* 16**,** 209-227.
NAQVI, S. W. A., YOSHINARI, T., JAYAKUMAR, D. A., ALTABET, M. A., NARVEKAR, P. V., DEVOL, A. H., BRANDES, J. A. & CODISPOTI, L. A. 1998. Budgetary and biogeochemical implications of N2O isotope signatures in the Arabian Sea. *Nature,* 394**,** 462-464.
NEVISON, C., BUTLER, J. H. & ELKINS, J. W. 2003. Global distribution of N2O and the Delta N2O-AOU yield in the subsurface ocean. *Global Biogeochemical Cycles,* 17**,** 18.
NEVISON, C., LUECKER, J. & ELKINS, J. 1995. Global oceanic emissions of nitrous oxide. *Journal of Geophysical Research: Oceans,* 100**,** 15809-15820.
NEVISON, C. D., KEELING, R. F., WEISS, R. F., POPP, B. N., JIN, X., FRASER, P. J., PORTER, L. W. & HESS, P. G. 2005. Southern Ocean ventilation inferred from seasonal cycles of atmospheric N(2)O and O(2)/N(2) at Cape Grim, Tasmania. *Tellus Series B-Chemical and Physical Meteorology,* 57**,** 218-229.
NEVISON, C. D., LUEKER, T. J. & WEISS, R. F. 2004. Quantifying the nitrous oxide source from coastal upwelling. *Global Biogeochemical Cycles,* 18**,** 24.
NIGHTINGALE, P. D., MALIN, G., LAW, C. S., WATSON, A. J., LISS, P. S., LIDDICOAT, M. I., BOUTIN, J. & UPSTILL-GODDARD, R. C. 2000. In situ evaluation of air-sea gas exchange parameterizations using novel conservative and volatile tracers. *Global Biogeochemical Cycles,* 14**,** 373-387.
OPEN UNIVERSITY. 2001. Ocean Circulation. Butterworth-Heinemann. 1-242.
PLESKACHEVSKY, A., DOBRYNIN, M., BABANIN, A. V., GUNTHER, H. & STANEV, E. 2011. Turbulent Mixing due to Surface Waves Indicated by Remote Sensing of Suspended Particulate Matter and Its Implementation into Coupled Modelling of Waves, Turbulence, and Circulation. *Journal of Physical Oceanography,* 41**,** 708-724.
PORTMANN, R. W., DANIEL, J. S. & RAVISHANKARA, A. R. 2012. Stratospheric ozone depletion due to nitrous oxide: influences of other gases. *Philosophical Transactions of the Royal Society B-Biological Sciences,* 367**,** 1256-1264.
PRATHER, M. J. 1998. Time scales in atmospheric chemistry: Coupled perturbations to N2O, NOy, and O-3. *Science,* 279**,** 1339-1341.
PRATHER, M. J., HOLMES, C. D. & HSU, J. 2012. Reactive greenhouse gas scenarios: Systematic exploration of uncertainties and the role of atmospheric chemistry. *Geophysical Research Letters,* 39**,** n/a-n/a.
PRINN, R. G., WEISS, R. F., FRASER, P. J., SIMMONDS, P. G., CUNNOLD, D. M., ALYEA, F. N., O'DOHERTY, S., SALAMEH, P., MILLER, B. R., HUANG, J., WANG, R. H. J., HARTLEY, D. E., HARTH, C., STEELE, L. P., STURROCK, G., MIDGLEY, P. M. & MCCULLOCH, A. 2000. A history of chemically and radiatively important gases in air deduced from ALE/GAGE/AGAGE. 105**,** 17751-17792.
PRINN, R.G., WEISS, R.F., ARDUINI J., ARNOLD, T., DEWITT, H. L., FRASER, P.J., GANESAN, A.L., GASORE, J. HARH, C. M., HERMANSEN, O., KIM, J., KRUMMEL, P.

B., LI, S., LOH, Z. M., LUNDER, C. R., MAIONE, M., MANNING, A.J., MILLER, B. R., MITREVSKI, B., MUHLE, J., O'DOHERTY, S., PARK, S., REIMANN, S., RIGBY, M., SAITO, T., SALAMEH, P. K., SCHMIDT, R., SIMMONDS, P. G., STEELE, L., P., VOLLMER, M., K., WANG, R. H., YAO, B., YOKOUCHI, Y., YOUNG, D., ZHOU, L., ET AL. 2018. History of chemically and radiatively important atmospheric gases from the Advanced Global Atmospheric Gases Experiment (AGAGE). *Earth Syst. Sci. Data*, 10, 985–1018.

QIAO, F. L. & HUANG, C. J. 2012. Comparison between vertical shear mixing and surface wave-induced mixing in the extratropical ocean. *Journal of Geophysical Research-Oceans,* 117**,** 9.

QIAO, F. L., YUAN, Y. L., YANG, Y. Z., ZHENG, Q. N., XIA, C. S. & MA, J. A. 2004. Wave-induced mixing in the upper ocean: Distribution and application to a global ocean circulation model. *Geophysical Research Letters,* 31**,** 4.

RAVISHANKARA, A. R., DANIEL, J. S. & PORTMANN, R. W. 2009. Nitrous Oxide (N2O): The Dominant Ozone-Depleting Substance Emitted in the 21st Century. *Science,* 326**,** 123-125.

RINTOUL, S. R. & TRULL, T. W. 2001. Seasonal evolution of the mixed layer in the Subantarctic Zone south of Australia. *Journal of Geophysical Research-Oceans,* 106**,** 31447-31462.

RÖCKMANN, T. & LEVIN, I. 2005. High-precision determination of the changing isotopic composition of atmospheric N 2 O from 1990 to 2002. *Journal of Geophysical Research: Atmospheres,* 110**,** n/a-n/a.

SCHMIDT, R. & SCHNEIDER, B. 2011. The effect of surface films on the air-sea gas exchange in the Baltic Sea. *Marine Chemistry,* 126**,** 56-62.

SCHROPP, S. J. & SCHWARZ, J. R. 1983. NITROUS-OXIDE PRODUCTION BY DENITRIFYING MICROORGANISMS FROM THE EASTERN TROPICAL NORTH PACIFIC AND THE CARIBBEAN SEA. *Geomicrobiology Journal,* 3**,** 17-31.

SEITZINGER, S. P. 1988a. DENITRIFICATION IN FRESH-WATER AND COASTAL MARINE ECOSYSTEMS - ECOLOGICAL AND GEOCHEMICAL SIGNIFICANCE. *Limnology and Oceanography,* 33**,** 702-724.

SEITZINGER, S. P. 1988b. Denitrification in freshwater and coastal marine ecosystems: Ecological and geochemical significance. *Limnology and Oceanography,* 33**,** 702-724.

SHADWICK, E. H., TRULL, T. W., TILBROOK, B., SUTTON, A. J., SCHULZ, E. & SABINE, C. L. 2015. Seasonality of biological and physical controls on surface ocean CO2 from hourly observations at the Southern Ocean Time Series site south of Australia. *Global Biogeochemical Cycles,* 29**,** 223-238.

SHU, Q., QIAO, F. L., SONG, Z. Y., XIA, C. S. & YANG, Y. Z. 2011. Improvement of MOM4 by including surface wave-induced vertical mixing. *Ocean Modelling,* 40**,** 42-51.

SMITH, J. A. 1992. OBSERVED GROWTH OF LANGMUIR CIRCULATION. *Journal of Geophysical Research-Oceans,* 97**,** 5651-5664.

SOLOVIEV, A. X. & SCHLUSSEL, P. 1994. PARAMETERIZATION OF THE COOL SKIN OF THE OCEAN AND OF THE AIR OCEAN GAS TRANSFER ON THE BASIS OF MODELING SURFACE RENEWAL. *Journal of Physical Oceanography,* 24**,** 1339-1346.

SPAHNI, R., CHAPPELLAZ, J., STOCKER, T. F., LOULERGUE, L., HAUSAMMANN,

G., KAWAMURA, K., FLÜCKIGER, J., SCHWANDER, J., RAYNAUD, D., MASSON-DELMOTTE, V. & JOUZEL, J. 2005. Atmospheric methane and nitrous oxide of the Late Pleistocene from Antarctic ice cores. *Science (New York, N.Y.),* 310**,** 1317.

SUNTHARALINGAM, P. & SARMIENTO, J. L. 2000. Factors governing the oceanic nitrous oxide distribution: Simulations with an ocean general circulation model. *Global Biogeochemical Cycles,* 14**,** 429-454.

SWART, N. C., FYFE, J. C., GILLETT, N. & MARSHALL, G. J. 2015. Comparing Trends in the Southern Annular Mode and Surface Westerly Jet. *Journal of Climate,* 28**,** 8840-8859.

SWEENEY, C., GLOOR, E., JACOBSON, A. R., KEY, R. M., MCKINLEY, G., SARMIENTO, J. L. & WANNINKHOF, R. 2007. Constraining global air-sea gas exchange for CO2 with recent bomb C-14 measurements. *Global Biogeochemical Cycles,* 21**,** 10.

TEJADA-MARTINEZ, A. E., AKKERMAN, I. & BAZILEVS, Y. 2012. Large-Eddy Simulation of Shallow Water Langmuir Turbulence Using Isogeometric Analysis and the Residual-Based Variational Multiscale Method. *Journal of Applied Mechanics-Transactions of the Asme,* 79**,** 12.

TERRAY, E. A., DONELAN, M. A., AGRAWAL, Y. C., DRENNAN, W. M., KAHMA, K. K., WILLIAMS, A. J., HWANG, P. A. & KITAIGORODSKII, S. A. 1996. Estimates of kinetic energy dissipation under breaking waves. *Journal of Physical Oceanography,* 26**,** 792-807.

THOMPSON, R. L., CHEVALLIER, F., CROTWELL, A. M., DUTTON, G., LANGENFELDS, R. L., PRINN, R. G., WEISS, R. F., TOHJIMA, Y., NAKAZAWA, T., KRUMMEL, P. B., STEELE, L. P., FRASER, P., O'DOHERTY, S., ISHIJIMA, K. & AOKI, S. 2014. Nitrous oxide emissions 1999 to 2009 from a global atmospheric inversion. *Atmospheric Chemistry and Physics,* 14**,** 1801-1817.

TOFFOLI, A., MCCONOCHIE, J., GHANTOUS, M., LOFFREDO, L. & BABANIN, A. V. 2012. The effect of wave-induced turbulence on the ocean mixed layer during tropical cyclones: Field observations on the Australian North-West Shelf. *Journal of Geophysical Research-Oceans,* 117**,** 8.

TOGGWEILER, J. R. & SAMUELS, B. 1995. EFFECT OF DRAKE PASSAGE ON THE GLOBAL THERMOHALINE CIRCULATION. *Deep-Sea Research Part I-Oceanographic Research Papers,* 42**,** 477-500.

WALLACE, D. W. R. & WIRICK, C. D. 1992. LARGE AIR SEA GAS FLUXES ASSOCIATED WITH BREAKING WAVES. *Nature,* 356**,** 694-696.

WANG, Y. G., QIAO, F. L., FANG, G. H. & WEI, Z. X. 2010. Application of wave-induced vertical mixing to the K profile parameterization scheme. *Journal of Geophysical Research-Oceans,* 115**,** 12.

WANNINKHOF, R. 1992. RELATIONSHIP BETWEEN WIND-SPEED AND GAS-EXCHANGE OVER THE OCEAN. *Journal of Geophysical Research-Oceans,* 97**,** 7373-7382.

WANNINKHOF, R., ASHER, W. E., HO, D. T., SWEENEY, C. & MCGILLIS, W. R. 2009. Advances in Quantifying Air-Sea Gas Exchange and Environmental Forcing. *Annual Review of Marine Science.* Palo Alto: Annual Reviews.

WANNINKHOF, R. & MCGILLIS, W. R. 1999. A cubic relationship between air-sea CO2 exchange and wind speed. *Geophysical Research Letters,* 26**,** 1889-1892.

WEEDING, B. & TRULL, T. W. 2014. Hourly oxygen and total gas tension measurements at

the Southern Ocean Time Series site reveal winter ventilation and spring net community production. *Journal of Geophysical Research-Oceans,* 119**,** 348-358.
WEI, Y. & WU, J. 1992. INSITU MEASUREMENTS OF SURFACE-TENSION, WAVE DAMPING, AND WIND PROPERTIES MODIFIED BY NATURAL FILMS. *Journal of Geophysical Research-Oceans,* 97**,** 5307-5313.
WEISS, R. F., KEELING, C. D. & CRAIG, H. 1981. The determination of tropospheric nitrous oxide. 86**,** 7197-7202.
WHITMAN, W., G 1923. The two-film theory of gas absorption. *Chem. metall. Engng.,* 29**,** 146-148.
WOLFF, E. & SPAHNI, R. 2007. Methane and Nitrous Oxide in the Ice Core Record. *Philosophical Transactions: Mathematical, Physical and Engineering Sciences,* 365**,** 1775-1792.
YOSHIDA, N., MORIMOTO, H., HIRANO, M., KOIKE, I., MATSUO, S., WADA, E., SAINO, T. & HATTORI, A. 1989. NITRIFICATION RATES AND N-15 ABUNDANCES OF N2O AND NO-3 IN THE WESTERN NORTH PACIFIC. *Nature,* 342**,** 895-897.
YOUNG, I. R. 1999. Seasonal variability of the global ocean wind and wave climate. *International Journal of Climatology,* 19**,** 931-950.
YUAN, X. J. 2004. High-wind-speed evaluation in the Southern Ocean. *Journal of Geophysical Research-Atmospheres,* 109**,** 10.